DIFFERENTIAL ABSORPTION LIDAR MEASUREMENTS OF TROPOSPHERIC OZONE IN THE ARCTIC

JEFFREY A. SEABROOK

A DISSERTATION SUBMITTED TO
THE FACULTY OF GRADUATE STUDIES
IN PARTIAL FULFILMENT OF THE REQUIREMENTS
FOR THE DEGREE OF
DOCTOR OF PHILOSOPHY

GRADUATE PROGRAM IN PHYSICS AND ASTRONOMY
YORK UNIVERSITY
TORONTO, ONTARIO
OCTOBER 2014

Abstract

A differential absorption lidar was constructed at the laboratory at York University and deployed in field campaigns to measure vertical profiles of tropospheric ozone. Profiles of ozone concentration were derived from the range-resolved simultaneous detection of backscatter from two or more wavelengths of laser radiation. By analyzing the absorption differences due to ozone between the two lidar returns, an ozone profile along the optical path of the laser was determined. This method is capable of resolving ozone concentrations between a range of 300 m to 8 km from the lidar.

During the spring in the polar region, tropospheric ozone depletion events occur due to the presence of inert halide salt ions such as Br^- in the atmosphere. After polar sunrise, this Bromine photochemistry can cause ozone concentrations near the ice surface to drop to near zero levels. Outstanding questions addressed by the lidar measurements were (a) whether significant ozone depletion occurs in layers not connected to the surface, and, (b) how local topography can influence ozone concentrations measured at land based locations such as Eureka NU.

Measurements were made during three field campaigns. The first was on the Amundsen icebreaker ship of the Canadian Coast Guard as part of the circumpolar Flow Lead study. For the second campaign the lidar was installed on the Polar-5 aircraft for flights over the sea ice north of Barrow Alaska. The third campaign involved ground based measurements from Eureka Weather Station on Ellesmere Island in the Canadian High Arctic.

All of the measured ozone depletions were connected to the surface, and no evidence of ozone depleted air detached from the boundary layer was found. The lack of free tropospheric depletions indicate that such events are likely rare, and not a significant ozone sink. While measuring tropospheric ozone from a land based location, the measured depletions were found to be mainly confined to the atmospheric boundary layer except in instances where surrounding topography enabled the transport of ozone depleted air into the free troposphere. This effect was common at the Eureka weather station on Ellesmere Island, which is surrounded by a number of mountain ranges.

Dedication

To my wonderful wife Olivia. This wouldn't have been possible without you.

Acknowledgements

I would like to express my gratitude to my supervisor Dr. James Whiteway, for his guidance, patience, and providing me with the opportunity to conduct research in such amazingly remote locations that few people get to experience. I would also like to thank Lawrence Gray with whom I spent many months in the field and on the road with. His years of field experience and wide breadth of practical knowledge made the success of these field campaigns possible. Special thanks goes to Dr. Gary Klaassen, who was willing to participate as the Chair on my final defense committee at the very last moment.

I would also like to thank my mother Donna, my father Robert, who sadly was unable to see me complete this work, and my twin brother William. They were always encouraging me with their best wishes.

Finally, I would like to thank my wife, Olivia Eckersley. Her love, support and understanding was unwavering through the good times and bad, the countless weekends that I worked, and the many months I was away from home.

Table of Contents

List of Tables

List of Figures

Preface

The following chapters of this dissertation have been adapted from previously published peer reviewed papers:

Chapter 3: Seabrook, J. A., J. Whiteway, R. M. Staebler, J. W. Bottenheim, L. Komguem, L. H. Gray, D. Barber, and M. Asplin, 2011: Lidar measurements of arctic boundary layer ozone depletion events over the frozen arctic ocean. Journal of Geophysical Research, 116.

Chapter 4: Seabrook, J. A., J. A. Whiteway, L. H. Gray, R. Staebler, and A. Herber, 2013: Airborne lidar measurements of surface ozone depletion over arctic sea ice. Atmospheric Chemistry and Physics, 13(12), 60236029.

1 Introduction

This thesis concerns the experimental investigation of surface level ozone depletion events (ODEs) during a number of field campaigns in the Arctic using a differential absorption lidar (DIAL). A compact differential absorption lidar for the measurement of ozone was developed and tested at York University in order to investigate the vertical and temporal evolution of ozone in the lower troposphere. The DIAL was deployed on a number of field campaigns to the Arctic in order to measure tropospheric ozone depletions during the spring shortly after polar sunrise.

The study of Arctic ozone depletion events has been an active field of research, but has generally relied on ground based or ozonesonde measurements from costal weather stations or research outposts. Ground based measurements provide no vertical information regarding ozone concentrations and ozonesondes are generally launched weekly, and thus do not provide continuous temporal resolution. The high vertical and temporal resolution of the DIAL measurements enabled the vertical structure of ozone during depletion events to be investigated. These type of lidar measurements of Arctic ozone are

relatively rare due to the difficulty and expense of developing a field capable DIAL, as well as the difficulty in mounting a measurement campaign over Arctic sea ice.

The ozone depletion events being investigated involve the the rapid loss of boundary layer ozone beginning during the period shortly after polar sunrise, and are the result of a photochemical process unique to the polar regions. The first reported observations of Arctic ODEs were made during the 1980s (Barrie et al. 1989, Bottenheim et al. 1986, Oltmans 1981, Oltmans and Komhyr 1986) using measurements at costal ground based monitoring stations. It was found that in the spring shortly after polar sunrise, the surface ozone mixing ratio periodically dropped from normal ($30 - 40$ ppbv) levels to near zero for periods ranging from hours to weeks at a time. Long term measurements from Arctic weather stations have shown that during the winter polar dark period, surface ozone concentrations remain nearly constant between $30 - 35$ ppbv and increasing up to 45 ppbv by April (Anlauf et al. 1994). Depletion events occur in the spring after polar sunrise, mainly between March - May (Oltmans and Komhyr 1986, Tarasick and Bottenheim 2002) and have been occurring since at least 1966 when regular ozone soundings began in the Canadian Arctic (Tarasick and Bottenheim 2002). The frequency and duration of these depletion events varies widely from year to year. Ground based measurements recorded between $1973 - 2010$ at Barrow AK show that during April the number of hours during which a depletion was recorded can vary between $70 - 360$ hours for the month (Oltmans et al. 2012).

The currently understood mechanism facilitating these depletion events is the photochemical conversion of inert halide salt ions (e.g. Br^-) into reactive halogen species (such as Br atoms) that deplete ozone in the boundary layer (McConnell et al. 1992, Ridley et al. 2003). Here it was suggested that the source of this bromide was the buildup of sea salt Br^- on the snow pack during the polar night via open leads, polynyas and cracks in the ice. Further support for this mechanism was given by Pratt et al. (2013) when it was determined experimentally that the oxidation of bromide occurs via a photochemical mechanism and that molecular bromine was detected over the snowpack only in the presence of sunlight. The rate at which active chemistry can destroy ozone is approximately 1.5 ppb/hour making it unlikely that in situ chemical destruction of ozone can explain rapid onset of depletions observed in many depletion events (Hausmann and Platt 1994).

An open question not addressed by ground based measurements or periodic soundings is the efficacy of this chemical reaction in depleting ozone in the free troposphere. McElroy et al. (1999) suggested that the presence of high concentrations (10 pptv) of BrO in the free troposphere could signify significant ozone chemical destruction occurring above the boundary layer. If free tropospheric Bromine chemistry is a significant ozone sink, ozone depleted masses of air above the boundary layer should be a frequent occurrence, and readily detectable with range resolved detection of tropospheric ozone.

The frequency and duration of ozone depletion events has largely been characterized by ozone measurements from land based high Arctic weather stations. One aspect that

3

is not clear is how ozone concentrations at land based monitoring sites are affected by surrounding topography. Routine ozone monitoring occurs at the Eureka weather station and spring time ozone depletions are common. Eureka is surrounded by a number of costal mountain ranges on Ellesmere island with vertical features exceeding 1.5 km in some places. One factor that can be investigated through high resolution vertically resolved measurements of ozone is how the beginning and end of depletion events are influenced by the topography, and how the vertical structure of the depletions are affected by the passage of air over or around the mountain ranges.

Between 2007 and 2012 the ozone lidar was used in the Arctic in a number of campaigns in order to study the structure of tropospheric ozone depletion events following polar sunrise. Chapter 2 will describe differential absorption measurement technique, the DIAL developed at York and a description of the analysis method used to obtain ozone retrievals from the lidar data. Chapter 3 will cover the results of a field campaign in which a DIAL was installed aboard the CCGS Amundsen and operated throughout March of 2008. This campaign was unique in that it allowed for the detailed vertically resolved measurement of ozone directly over the arctic sea ice for an extended period of time, allowing the vertical structure of a number of depletion events to be recorded in high temporal resolution. Chapter 4 will detail the results of a 2011 airborne measurement campaign in which a nadir oriented DIAL was operated aboard the Polar-5 research aircraft. These measurements were taken in the spring of 2011 with flights over the Arc-

tic sea ice and provided the opportunity to measure tropospheric ozone concentrations over a large area of the sea ice in a relatively short period of time. Chapter 5 will detail the results of a DIAL operated at the Eureka weather station since 2007. This is an inland weather station surrounded by a number of large mountain ranges and provides some insight into how near surface ozone concentrations are influenced by complex topography, as ozone depleted air from over the arctic sea ice interacted with mountainous terrain reaching altitudes of 2500 m above sea level. Chapter 6 will discuss the conclusions from these three unique measurement campaigns regarding the structure and origins of the ozone concentrations measured. Finally, the appendix will cover the error analysis of the DIAL measurements and some of the considerations such as choice of wavelength pairs and interference from atmospheric gasses that need to be taken into account when using the DIAL technique to obtain ozone concentrations.

2 Measurement and Analysis Methods

The differential absorption lidar (DIAL) measurement technique was first developed in the 1960's and used for the range resolved detection of water vapour (Schotland 1966). The technique was first used for stratospheric measurements of ozone in 1977 (Megie et al. 1977). Prior to the availability of powerful compact UV lasers and Raman shifting techniques, early DIAL systems were generally unwieldy and non-portable due to the need to emit multiple wavelengths at high energies.

A compact DIAL for the measurement of vertical profiles of ozone was developed and tested at York University. Two of these miniaturized DIAL systems suitable for both ground based and airborne measurements were developed at York. All have the capability to determine atmospheric profiles of O_3 to a range of $8\,km$. The compact design of the system was possible due to the use of a frequency quadrupled, high energy pulsed Nd:YAG laser (CFR-800) emitting at a wavelength of $266\,nm$, and Raman shifting in a UV Raman active medium to generate multiple wavelengths from a single source. A number of field experiments have been conducted with these ozone DIAL systems in

6

order to study the vertical structure of O_3 in the troposphere.

2.1 Lidar method

The basic light detection and ranging (lidar) technique is to emit pulses of laser light into the atmosphere and record the backscattered photons as a function of time or, equivalently, range. The elastic backscatter lidar is the simplest type of lidar and is typically used for studies of aerosols and clouds. The number of backscattered photons detected from a given range depends on the backscatter coefficient of scatterers at that range and the transmittance along the path to that range.

For an ultraviolet wavelength absorbed significantly only by ozone, within an atmosphere with no significant scattering by aerosol, the single wavelength backscatter signal can be described as

$$P_\lambda(r) = \frac{A}{r^2} C_\lambda \beta_{\pi,\lambda}(r) \exp\left[-2 \int_0^r [\sigma_\lambda\, n(r') + \alpha_\lambda(r')]\, \mathrm{d}r'\right], \qquad (2.1)$$

where $P_\lambda(r)$ is the recorded received power from range r due to backscatter. The combined backscatter coefficient, $\beta_{\pi,\lambda}(r) = \beta_{\pi,\lambda}^a(r) + \beta_{\pi,\lambda}^m(r)$, represents the fraction of light scattered backward per unit length and per unit solid angle from both aerosols and molecules. The total volume scattering extinction coefficient, $\alpha_\lambda(r) = \alpha_\lambda^a(r) + \alpha_\lambda^m(r)$, is the fractional decrease in laser pulse intensity due to scattering per unit length. The

product of the ozone molecule absorption cross section σ_λ, and ozone number density, $n(r)$, is the fractional decrease per unit length due to molecular absorption by O_3. C_λ is a range independent system constant that takes into account properties such as transmitted laser pulse energy, system optical throughput, and detector efficiency. The A/r^2 factor represents the projected solid angle of the receiver with area A as seen from a scatterer at range r. This is analogous to the Beer-Lambert relationship except that it describes the detection of backscattered photons rather than the one way transmission of light.

2.2   Differential Absorption lidar equation

A Differential Absorption lidar (DIAL) is typically used for range-resolved measurements of a particular gas in the atmosphere, such as ozone, carbon dioxide, or water vapour. The DIAL simultaneously transmits and detects multiple wavelengths of light: an "on" wavelength that is absorbed by the species of interest and an "off" wavelength that is not absorbed or absorbed to a smaller degree than the on-line wavelength. For ozone, an absorption band known as the Hartley absorption band (Fig. 2.1) exists in the UV between 200-300 nm, with peak absorption at 255 nm. Shown in Fig 2.1 are the wavelengths transmitted by the DIAL. The measured difference in the signals at the two wavelengths of light on this absorption band enables the concentration of the gas as a function of range to be determined. The possible wavelength pairs along with their differential absorption coefficients for the DIAL systems used are shown in Table 2.1.
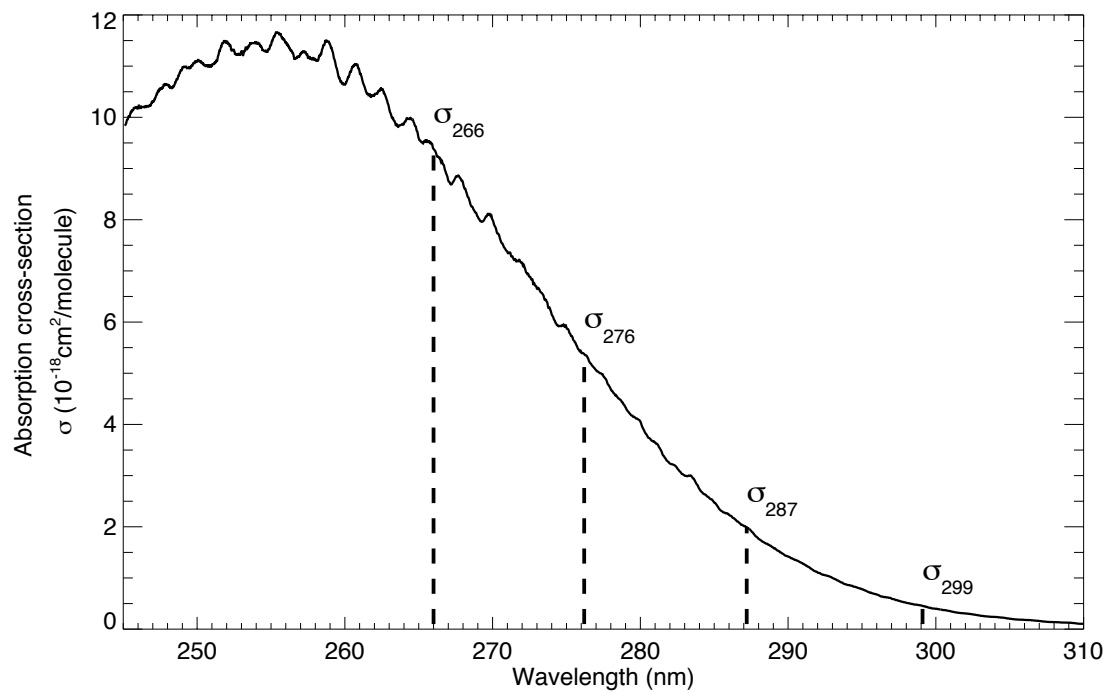
Figure 2.1: The Hartley Band - Ozone absorption cross-section at 300 K in the UV from the Hitran 2008 database (Rothman et al. 2009). The wavelengths emitted by the ozone DIAL are shown.

From the recorded backscattered photons of the "on" and "off" wavelengths, the atmospheric number density of the species of interest can be determined from the ratio of the slope of the log of the ratio of the two signals. Due to the simultaneous transmission and recording of the multiple wavelengths, this technique is self calibrating, with the unknown equipment dependent variables being eliminated from the determination of the number density. The ratio of the elastic lidar equation (Equation 2.1) for both on and off wavelengths yields

$$\frac{P_{\text{on}}(r)}{P_{\text{off}}(r)} = \frac{C_{\text{on}}}{C_{\text{off}}} \frac{\beta_{\pi,\text{on}}(r)}{\beta_{\pi,\text{off}}(r)} \exp\left\{-2 \int_0^r [\Delta\sigma\, n(r') + \Delta\alpha]\, \mathrm{d}r\right\}, \qquad (2.2)$$

where $\Delta\sigma$ is the differential ozone absorption $(\sigma_{\text{on}}(r') - \sigma_{\text{off}}(r'))$ and $\Delta\alpha$ is the differential scattering coefficient $(\alpha_{\text{on}}(r') - \alpha_{\text{off}}(r'))$ between the on and off wavelength pairs.

By taking the natural logarithm and the derivative with respect to r, the number density $n(r)$ of the target species can be extracted, and is given by

$$n(r) = n'(r) + \Delta n_{\text{b}}(r) + \Delta n_{\text{e}}(r), \qquad (2.3\text{a})$$

$$n'(r) = \frac{-1}{2\Delta\sigma}\left\{\frac{\mathrm{d}}{\mathrm{d}r}\left[\ln\frac{P_{\text{on}}(r)}{P_{\text{off}}(r)}\right]\right\}, \qquad (2.3\text{b})$$

$$\Delta n_b(r) = \frac{1}{2\Delta\sigma}\left\{\frac{\mathrm{d}}{\mathrm{d}r}\left[\ln\frac{\beta_{\pi,\text{on}}(r)}{\beta_{\pi,\text{off}}(r)}\right]\right\}, \qquad (2.3\text{c})$$

$$\Delta n_e(r) = \frac{-1}{\Delta\sigma}\Delta\alpha, \qquad (2.3\text{d})$$

where the second and third terms (2.3c, 2.3d) are correction terms for scattering and

10

absorption of interfering gas species as well as the differential extinction between the on and off wavelengths. If an appropriate choice of wavelengths is made in order to avoid interference from other species, and the wavelengths are spaced closely enough that the differential extinction is small, then these correction terms are negligible.

The second term (2.3c) takes into account the range dependent differential backscatter coefficient that exists in non-homogeneous atmospheres. Assuming a homogeneous atmosphere and closely spaced on/off wavelength pairs, this term can be safely ignored. In practice the differential extinction term in (2.3d) is not negligible, and for molecular extinction it is possible to calculate this with knowledge of local temperature and pressure. Under conditions involving heavy aerosol loading this assumption no longer applies and corrections are difficult without detailed knowledge of the aerosol properties. This is avoided by removing affected measurements from the data set before retrieving ozone concentrations.

With knowledge of the atmospheric conditions at the time of the measurement, the retrieved number densities (molecules/cm^3) can be converted into concentrations (ppbv). This is performed using atmospheric profiles from radiosonde measurements using data from a sonde launch closest in time (nominally launched within one hour of 00:00 and 12:00 UTC) to the measurement from the nearest geographical monitoring station for which radiosonde information is available.

Wavelength pair (on/off)	σ_{on} (O$_3$) $\times$ 10^{-18} (cm^2/molecule)	σ_{off} (O$_3$) $\times$ 10^{-18} (cm^2/molecule)	$\Delta\sigma$ (O$_3$) $\times$ 10^{-18} (cm^2/molecule)
266/276 nm	9.384	5.376	4.008
266/287 nm	9.384	1.994	7.390
266/299 nm	9.384	0.455	8.929
276/287 nm	5.376	1.994	3.382
276/299 nm	5.376	0.455	4.921
287/299 nm	1.994	0.455	1.539

Table 2.1: Differential ozone absorption cross-sections for the possible on/off DIAL wavelength pairs at 300 K.

2.3 DIAL Design and Construction

Two separate ozone DIAL systems were built at York University. DIAL-A was built and tested in the lab at York as part of this project in mid 2007 (Fig. 2.2) and permanently installed in the 0PAL lab at Eureka, Nunavut, Canada, in 2008. DIAL-B was constructed simultaneously and was used in all the field work excluding Eureka. In 2010 the DIAL-B system was substantially modified for the 2011 Polar 5 flight campaign. These modifications included miniaturization in order to fit into an aircraft rack, insulation and thermal control to prevent environmental temperature fluctuations from affecting the laser output, and vibrational isolation of the DIAL from the frame it was mounted in. While the optical layouts for each lidar were not exactly the same, all versions of the DIAL were built to very similar specifications and operate in an identical manner. The schematic in Figure 2.3 applies in general for each system.

All lidar systems consist of three main components: a transmitter, receiver and detection electronics. The York DIAL transmitter is based on a Quantel CFR-800 Nd:YAG laser with 4th harmonic generation in order to emit in the ultraviolet at 266 nm. The rated output of the laser was nominally 80 mJ per pulse of 266 nm radiation, with a pulse duration of 10 ns at a repetition rate of 20 Hz. Dielectric laser line mirrors (Y4 mirrors) from CVI (1" diameter, .375" thick) were used to direct the 266 nm light while simultaneously filtering out the remaining 1064 and 532 nm radiation emitted by the laser. This residual

13
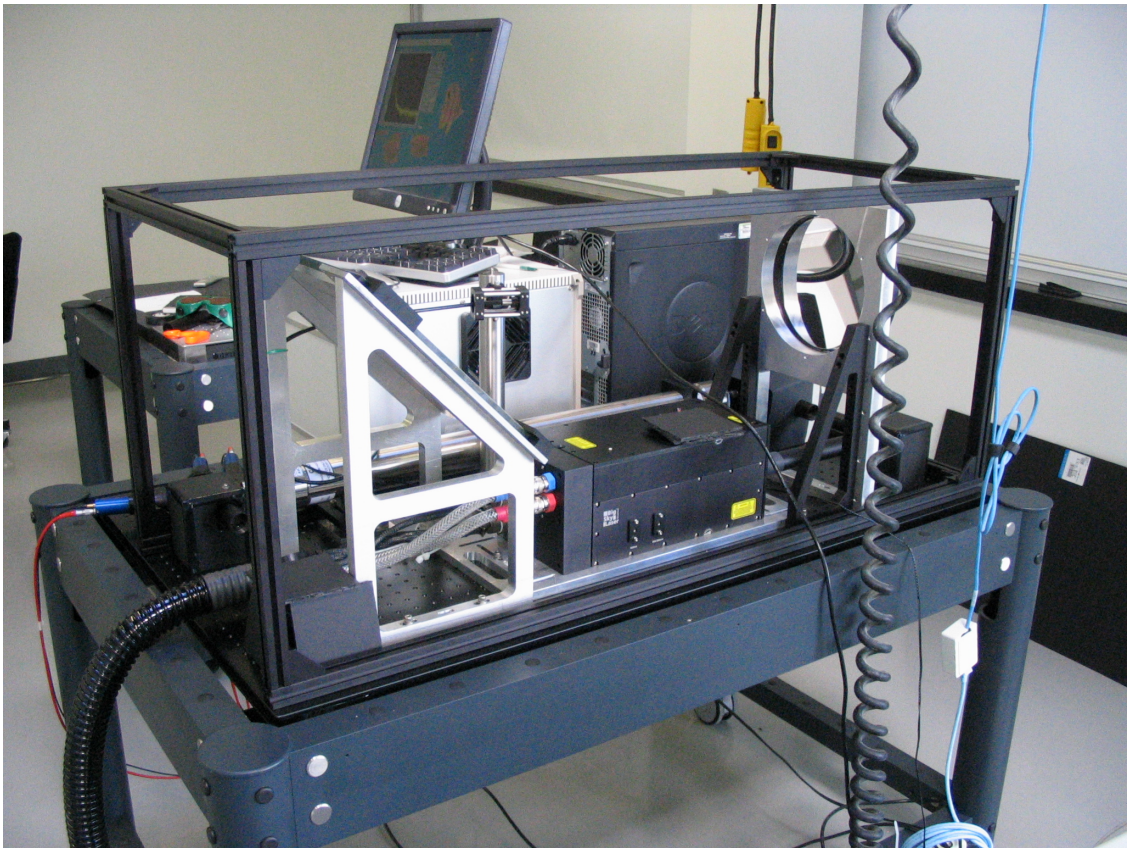
Figure 2.2: Ozone DIAL-A development at York University.

energy was collected by a beam dump located behind the first Y4 mirror.

In version-A of the DIAL, the Raman cell consisted of a stainless steel cylinder 50 cm in length (the Eureka DIAL used a 75 cm long Raman cell) filled with research grade carbon dioxide to a pressure of 140 psi. The optical entrance to the Raman cell was a 1" diameter 266 nm anti-reflective coated window made out of fused silica, the output window to the Raman cell was an anti-reflection dielectric coated fused silica window designed for broadband UV wavelengths. The 266 nm laser pulse was focused into a Raman cell filled with 140 PSI of CO_2 using a 1" diameter 266 nm anti-reflective coated plano-convex lens with a focal length of 500 mm. This focusing lens was placed approximately 250 mm from the front of the Raman cell input window with the purpose of focusing the laser pulse into the center of the Raman cell. The laser light was then re-collimated using a broadband UV AR coated 500 mm focal length plano-convex lens located 250 mm after the exit window. The Eureka DIAL used lenses with a focal length of 750 mm positioned 125 mm from the entrance and exit windows.

In version-B of the DIAL system, external lenses were removed and the input and output windows of the Raman cell were replaced with plano-convex lenses with a focal length of 250 mm. The input lens was AR coated for 266 nm light, and the output lens was broadband UV coated so that the anti reflection properties would be effective over the output wavelengths. This alteration to the Raman cell optical layout was done due to constraints on the length of the optical pathway in the updated DIAL system. A more

compact optical path length was required in order to mount the complete DIAL system into an aircraft rack.

Output from the Raman cell consisted of 266 nm, 276 nm, 287 nm and 299 nm light, which comprise the first to third Stokes lines of stimulated Raman scattering (Nakazato et al. 2007) as well as the original 266 nm pump energy. At an input pulse energy of 80 mJ at the 266 nm wavelength, output from the Raman cell was measured at 10 mJ, 8 mJ and 5 mJ pulse energy for the 276 nm, 287 nm and 299 nm output wavelengths respectively. Residual 266 nm output was measured at approximately 15 mJ per pulse. All downstream steering mirrors were 1" diameter CVI broadband coated mirrors designed to reflect light over the range of wavelengths emitted from the Raman cell. The diameter of the multi-wavelength output beam was expanded by a factor of three to reduce the divergence to about 0.2 mrad before it was directed into the atmosphere. Full overlap between the emitted laser pulse and the telescope field of view occurs at a range of approximately 300 m and the signal received from within that range was not used in the ozone analysis.

In DIAL version-A, backscattered light was collected with a 15 cm diameter off-axis parabolic mirror and a 1.5 mm diameter optical fiber positioned in the focal plane, 1 m from the mirror, to form a receiver field of view of 1.5 mrad. For version-B, in order to reduce the footprint of the telescope, an off axis parabolic mirror with a focal length of 500 mm was used. The light was collected with an identical 1.5 mm diameter optical fibre, resulting in a telescope with a field of view of 3 mrad.
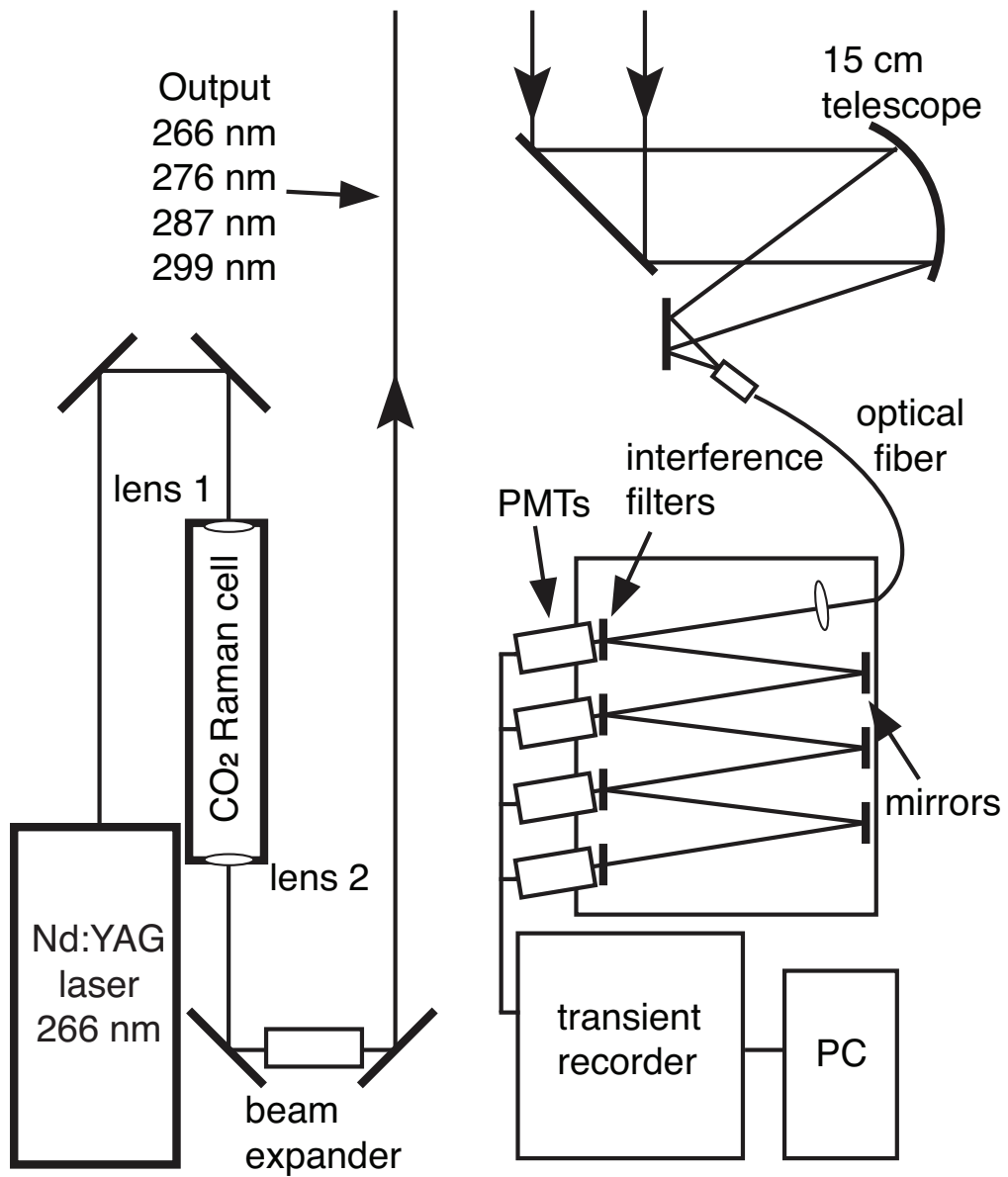
Figure 2.3: Schematic diagram of the York DIAL system.

In both versions of the DIAL, the multiple wavelengths collected by the telescope were separated in the receiver (Fig. 2.4) by the transmittance and reflectance from interference filters purchased from Barr Associates. The filters were tilted at an angle of $5°$ and had transmission bandwidths of 1 nm. Photomultiplier detectors generated electrical signals that were recorded using photon counting for the weak signals from distances greater than 1.5 km and using analog to digital conversion for the strong signals nearer to the transmitter. At a count rate of approximately 10 MHz, the photon counting statistics begin to become non-linear as pulse pile up due to the pulse-pair resolution of the photomultiplier tube occurs. The pulse-pair resolution is the minimum time interval at which each pulse can be separated and be individually counted, pulses that overlap during this time period are counted as a single pulse. The analog mode is immune to the pulse pile up issue as overlapping photons contribute to the recorded signal, but is much more susceptible to noise, making it of limited use when the received signal becomes weaker with range.

The raw data in both analog and photon counting mode, was recorded with a range gate of 7.5 m. During ground-based operation, an integration period of 1200 laser shots (1 min at 20 Hz) was typically used. When airborne measurements were taken, the integration time was reduced to 200 laser shots (10 s at 20 Hz).

During processing, these data were averaged temporally over a window ranging between 200 seconds and 60 minutes. The temporal averaging applied is dependent on

18

the maximum range for which ozone retrieval is desired. Averaging was also applied spatially over the 7.5 m bins. The amount of vertical smoothing is range dependent and increases with range. Nearest to the transmitter, a range resolution of 22.5 m was achieved, while at a range of 5 km a common achievable range resolution was 75 m. The 276/287 nm analog signals are typically used to a range of 1 km and the 287/299 nm photon counting signals are used at greater ranges.

Ozone retrieval is based on the derivative of the recorded lidar signal, which is fundamentally noisy. This noise can introduce significant errors, most significantly at longer ranges when the signal to noise ratio worsens. A certain amount of smoothing must be performed on the signal in order to extract ozone concentrations. This can be done with boxcar averaging of the signal (using a low pass filter). The amount of smoothing required depends on the signal to noise ratio of the data. Thus the boxcar window must be increased with range. It is unavoidable that sharp gradients in the ozone profile may be smoothed over due to the averaging process, particularly at longer ranges where greater smoothing must be applied. Details regarding the specific temporal and vertical smoothing and averaging, as well as the wavelength pairs used to derive ozone will be covered in each of the measurement chapters.

Figure 2.5 illustrates the ozone derived from raw lidar signals. The 276/287 nm analog recorded wavelength pair, and the 287/299 nm photon counting signal pair are shown with their resulting ozone concentration profiles. The error bars are a result of the statis-
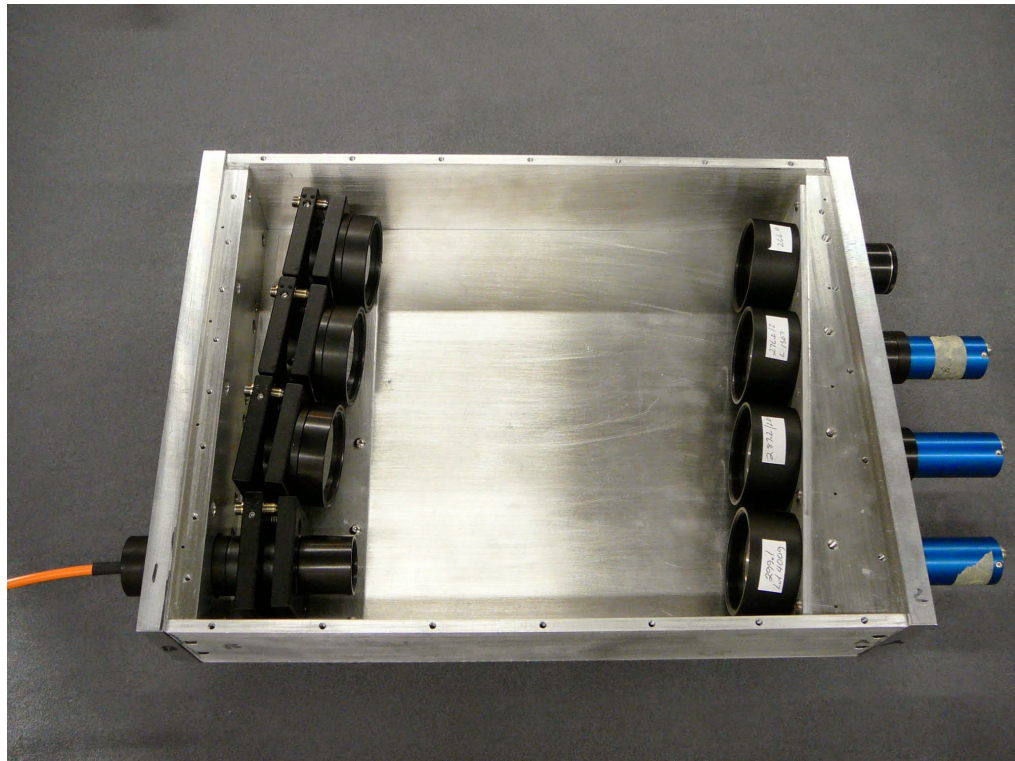
Figure 2.4: Fiber coupled spectrometer used to separate the multiple wavelengths simultaneously recorded by the lidar. Light collected by the telescope is transmitted to the spectrometer via optical fiber. A series of reflective narrow bandwidth (1 nm) interference filters (labeled in white) were used to isolate the wavelengths of interest. The filters are ordered in regards to return intensity, with the weakest intensity wavelengths selected first. Shown here in order are 299.1 nm, 287.2 nm, 276.2 nm and 266 nm. A series of three concave mirrors on the left were used to re-image the fiber output after each reflection.

tical uncertainty inherent to the photon counting process. A comparison between ozone recorded by a ozonesonde launched at Eureka in April 2012, and DIAL derived ozone measured simultaneously is shown in Figure 2.6. The lidar data was recorded for 90 minutes before and after the ozonesonde launch and averaged into the shown vertical profile.

2.3.1 Generation of DIAL wavelengths - CO_2 as a Raman Active Medium

Stimulated Raman Scattering (SRS) in carbon dioxide was employed in order to generate the multiple closely spaced wavelengths of laser light needed for the DIAL technique. Raman scattering is an inelastic process in which incident light is scattered by a molecular sample. The resulting scattered radiation is lower in energy than the incident radiation for a Stokes line, and greater then the incident radiation for an anti-Stokes line. The energy increase or decrease corresponds to vibrational energies in a Raman active vibrational state of the molecule. Multiple Raman shifts occur when the intensity of the generated Stokes wavelength becomes sufficiently high and acts as the source for a further Raman process (Fig. 2.7).

Carbon dioxide has a wave number of molecular Raman shift of $v_m = 1388.15\ \mathrm{cm}^{-1}$ due to a Raman active $C - O$ symmetric stretching mode (Shimanouchi 1972). The
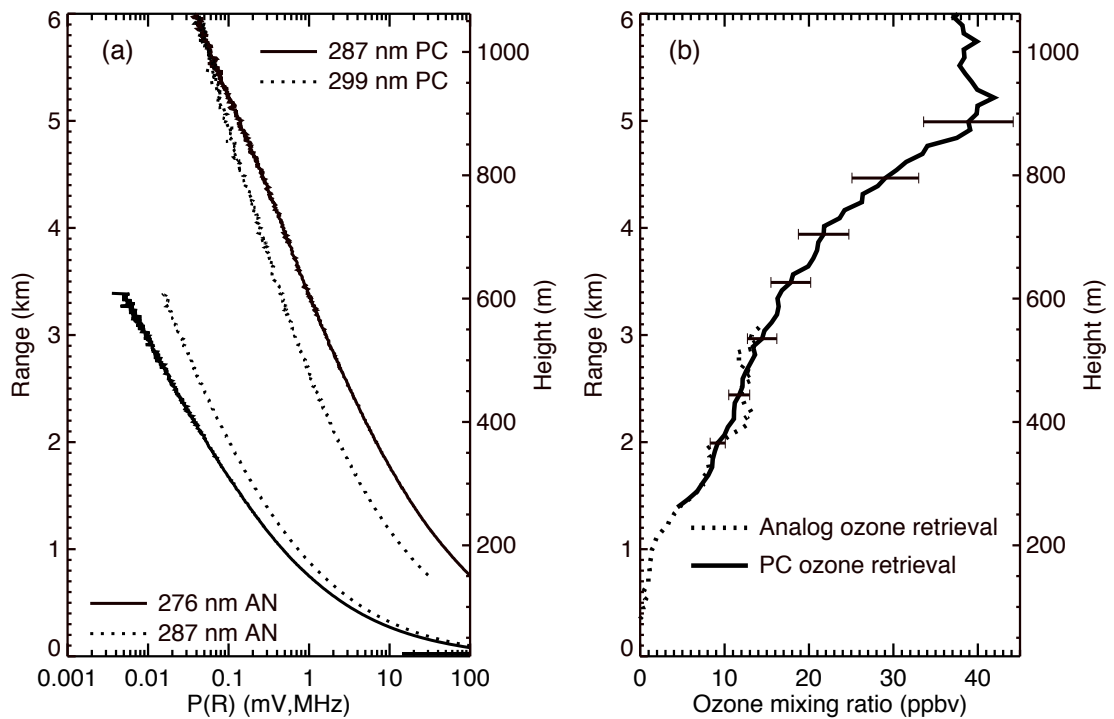
Figure 2.5: (a) Lidar analog (AN) and photon counting (PC) backscatter signals obtained from the Amundsen Icebreaker ship on 14 March 2008 at 01h GMT. (b) Ozone mixing ratio derived from the lidar signals using the analog wavelength pair 276/287 nm below range 1.8 km (height 332 m ASL) and the photon counting pair 287/299 nm above. The indicated uncertainty is one standard deviation in the photon counts, propagated through the ozone derivation.
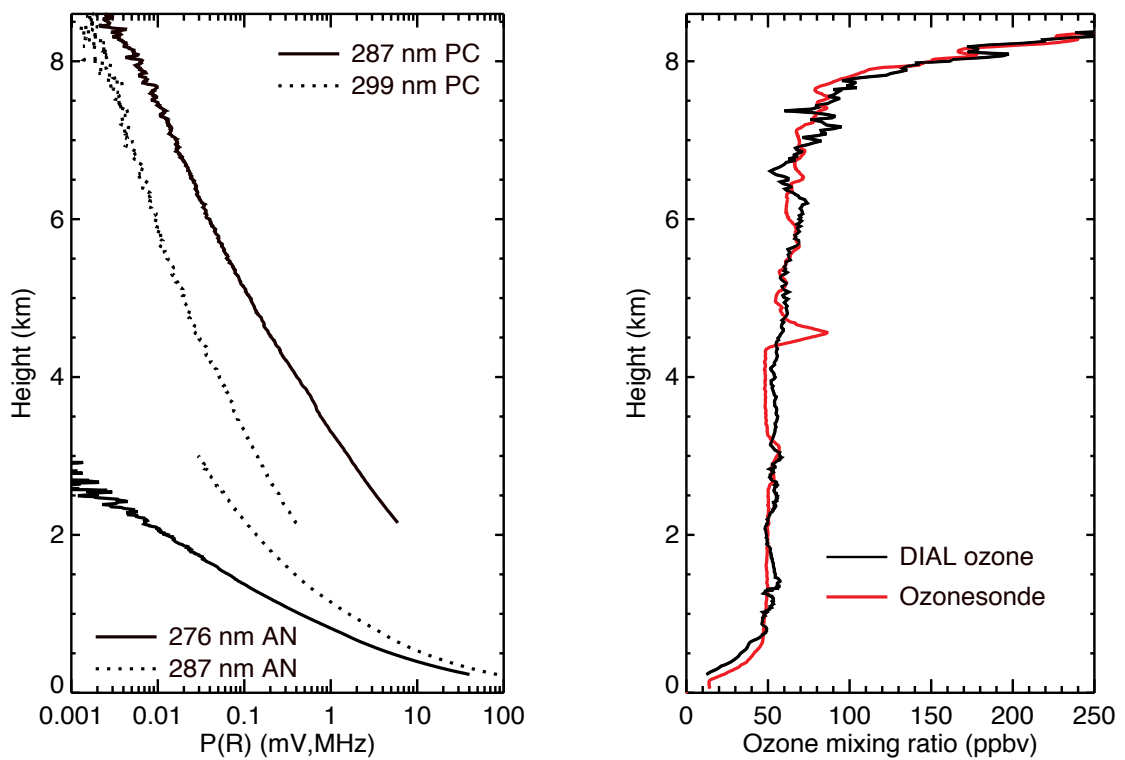
Figure 2.6: (Left) Lidar analog (AN) and photon counting (PC) backscatter signals obtained from Eureka Weather Station in April 2012. (Right) Ozone mixing ratio derived from the lidar signals using the analog wavelength pair 276/287 nm below range 1.8 km (height 332 m ASL) and the photon counting pair 287/299 nm above. In red is an ozone profile measured by an ozonesonde launched at Eureka during the lidar measurements.

wavelengths of the Stokes lines of CO_2 are calculated using the equation:

$$\lambda_i = \frac{1}{v_i} = \left(\frac{1}{\lambda_p} - iv_m \right)^{-1} \tag{2.4}$$

where i is the number of the Stokes component. Results for $\lambda_{1..3}$ yield the Stokes wavelengths 276.2 nm, 287.2 nm and 299.1 nm. These wavelengths, as well as the original 266 nm light, are within the solar blind region (below 300 nm) and are all situated on the Hartley ozone absorption band, making them useful for the daylight detection of ozone.

Because a single step can be used to obtain multiple closely spaced wavelengths of light, the Stimulated Raman Scattering (SRS) technique is commonly used in multiwavelength DIAL for the tropospheric and stratospheric measurement of atmospheric gasses of interest. This technique has the advantage of simplicity and compactness. Multiple useable wavelengths can be generated from a single laser source, significantly reducing complexity and cost. The disadvantages to this technique are that the generated wavelengths are not tunable as has proven useful in some DIAL systems (Fix et al. 2002, Nehrir et al. 2009), and that the generation of the higher order Stokes wavelengths is nonlinear and highly dependent on the efficiency of the lower order Stokes conversion. The consequence of the non-linear nature of this process is that relatively small reductions in energy output from the pump laser can significantly reduce the conversion efficiency of the higher order Stokes wavelengths.
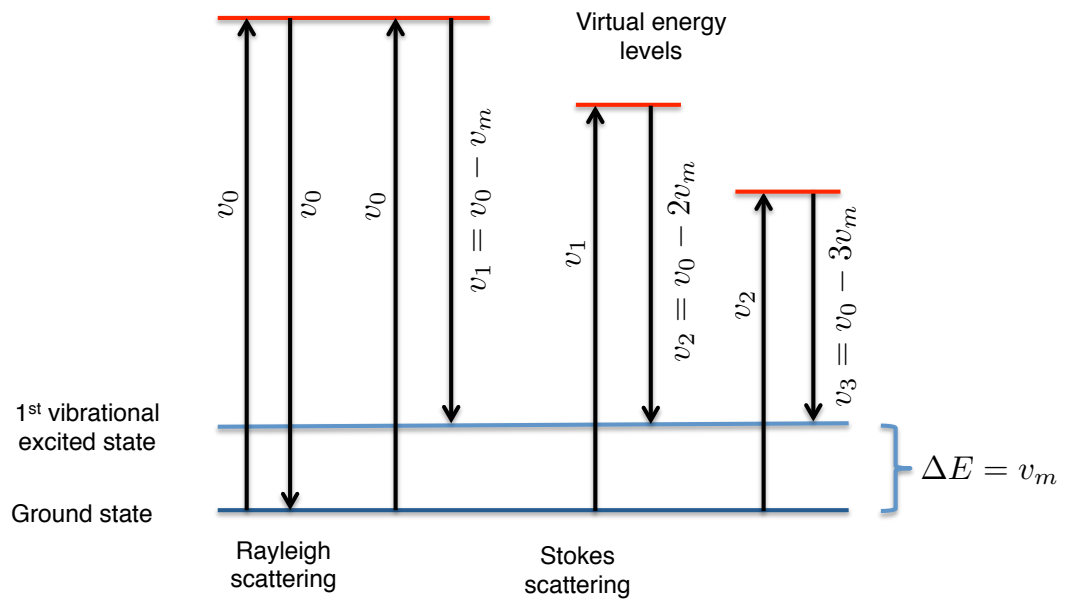
Figure 2.7: Raman scattering process for the first three Stokes wavelengths.

3 Measurements from the Amundsen ice breaker

3.1 Introduction

As part of the 2007-08 International Polar Year (IPY), the Canadian government funded an international, Arctic climate change study in which field work was performed on board the Canadian Coast Guard Ship (CCGS) Amundsen (Fig. 3.1a). The CCGS Amundsen is a Canadian research icebreaker that during March 2008 was stationed in the Amundsen Gulf as part of the Circumpolar Flaw Lead (CFL) measurement campaign (Barber et al. 2010). The Amundsen was located immediately south of Banks Island at an approximate location of $71°$ N and $121 - 124°$ W (Fig 3.1b). The vessel remained mostly stationary with respect to the sea ice, with occasional changes in position to accommodate sea ice studies. The location of the Amundsen at this time of year provided a unique opportunity to retrieve vertical profiles of ozone depletion events over the sea ice with high temporal and spatial resolution during the period of Arctic polar sunrise.

(a) Amundsen Icebreaker Ship. The laboratory container (circled) is located on the top deck between the bridge and smoke stack.

(b) GPS track (shown in red) of the Amundsen Icebreaker between March - April 2008

Figure 3.1: GPS track of the Amundsen during March 2008

3.2 DIAL Installation

The DIAL system was installed in a laboratory container (Fig. 3.2b) that housed experiments for the OASIS (Ocean Atmosphere Sea Ice Snowpack) project (Shepson et al. 2003). The laboratory was installed on the top deck of the Canadian research icebreaker CCGS Amundsen (Fig. 3.1a).

The lower height limit for the measurements was reduced to 52 m above the lidar ($\sim$72 m above sea level) using a removable mirror mounted to the exterior of the lab container (Fig. 3.2a). This allowed both the emitted light pulses and the telescope field of view to be directed at an angle of 10° above the horizontal.

3.3 Observations

The DIAL measurements alternated between zenith and slant viewing each day when conditions permitted. Full overlap between the emitted laser pulse and the telescope field of view occurred at a range of approximately 300 m and the signal received from within that range was not used in the ozone analysis.

A contour plot of the lidar ozone measurements over March and early April of 2008 from 60 m to 1000 m above the sea ice is shown in Figure 3.3. These data are a composite of both zenith and slant measurements. The contour is composed of individual profiles that were averaged temporally over a window of 60 minutes as well as over vertical bins.

(a) Installation of the external mirror to the top of the laboratory container. The external mirror was used to direct the lidar field of view to 10° above horizontal.

(b) Ozone DIAL operating in the laboratory container.

Figure 3.2: Ozone DIAL installed aboard the Amundsen Icebreaker ship.
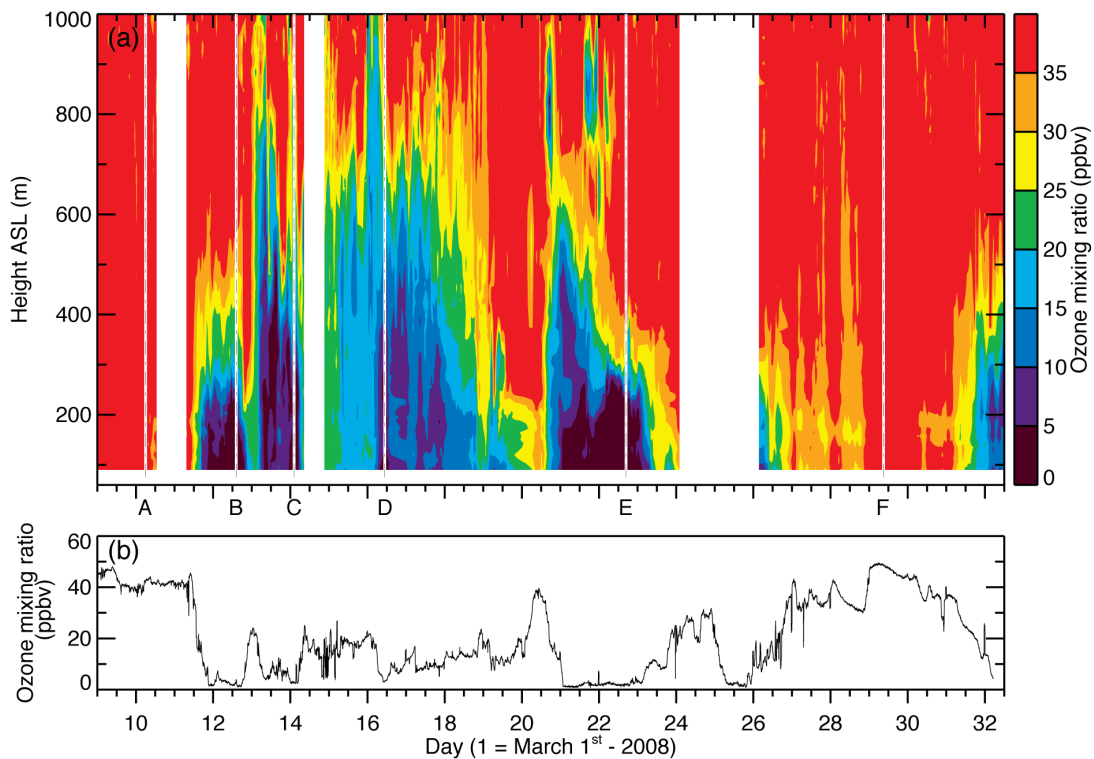
Figure 3.3: Ozone measurements aboard the Amundsen near the onset of polar sunrise (9 March to 2 April 2008). a) DIAL measurements as a function of time and height above sea level. Omitted data includes periods of repair time on the DIAL, as well as periods of low-level clouds or ice fog that interfered with the ozone retrieval. b) In situ ozone measurements recorded by a TECO 49C (Thermo Electron Inc., USA) with air sampling on the top deck of the ship, 25 m above sea level.

The range resolution of the analog signals used below height 332 m was 22.5 m while the photon counting signals were averaged to a range resolution of 75 m. A number of ozone depletion events (ODE's) were vertically resolved with the lidar and measured in situ aboard the ship (Figure 3.3).

The most complete ozone depletions, with mixing ratio less than 5 ppbv, occurred on March 12th, 13th–14th, 16th–18th, and 21st–23rd. These depletions, which lasted from one to two days, were quite shallow, with the most depleted pockets of air connected directly to the ground, and not extending past 250 m in height. Above this altitude the mixing ratio generally started increasing with altitude until background levels of 30 − 40 ppbv were observed. The greatest vertical extent was associated with the partial depletion in the period between March 14th and 19th, which reached a height of 1 km at times.

One of the aims of the measurement campaign was to determine if there was evidence for local ozone depletion in air not in contact with the ice surface. No such evidence was observed with the lidar. All observed ODEs were connected to the surface. There were instances where an isolated patch of air partially depleted in ozone (e.g., 15 ppbv) was vertically separated from the main ODE that extended from the surface (e.g., March 21/22). This only occurred in the region of mixing between the ODE and the overlying air with background ozone density. There were no cases of an isolated patch of ozone depleted air that was not directly above an ODE at the surface. Also, there was no measurable diurnal correlation between local sunlight and ozone mixing ratio at the surface,

or aloft. Diurnal variations of BrO concentrations over the sea ice were measured on board the Amundsen (Pöhler et al. 2010), indicating local generation of BrO, but the measured ozone concentrations did not exhibit similar diurnal variability (Barrie et al. 1989).

3.4 Analysis

Back trajectory calculations provided a basis for interpreting the origin and vertical structure of the observed ozone depletions. The calculations made use of the NOAA HYS-PLIT model (Draxler and Hess 1998), using GDAS (Global Data Assimilation System) meteorological data. The back trajectories were started at each hour for heights ranging from 100 m to 1000 m above sea level and were calculated for a 6-day period backwards starting from the location of the Amundsen at the time of measurement. The calculated back trajectories near the ground agree well with the wind direction, wind speed and atmospheric temperatures that were measured independently on board the vessel.

Throughout this work, one of the methods for characterizing the origins of the measured air was the Hybrid Single Particle Lagrangian Integrated Trajectory (HYSPLIT) Model. The accuracy and limitations of trajectory calculations has been the subject of a number of studies (Kahl 1996, Stohl 1998, Stunder 1996). Kahl et al. (1989) found that in the Arctic where in situ atmospheric measurements are sparce, 5-day horizontal errors of 500-800 km can expected. Stohl (1998) determined that while back trajectory calcula-

tions are often accurate, error of up to 20% of the travel distance can occur. The average distance travelled by the calculated 6-day back trajectories in this study is 5000 km, resulting in an estimated horizontal position error of up to 1000 km.

When considering the origin of the air mass the primary factor is if the air originated from northern latitudes over the sea ice, or from land to the south. The Arctic ocean has a surface area of roughly 15 million square km, making the estimated positional error of up to 1000 km unlikely to affect the conclusion that air originating from the north may have spent significant periods of time over sea ice. Despite the difficulty in quantifying the accuracy of the calculated back trajectories, the vertical and horizontal history of the air was found to be consistent with the local meteorological conditions, as well as with the measured ozone concentrations. Additionally, back trajectories calculated at different altitude levels were consistent indicating stability in the trajectory calculations. The calculated trajectories consistently show that lower temperature, ozone depleted air originated over the sea ice and spent most of the time within a few hundred meters of the sea ice surface, and that non-depleted air either originated from the south, or had little to no interaction with the sea ice surface.

Figure 3.4 shows the calculated back trajectories for six case studies that are indicated in Figure 3.3. In each case, whether or not an ODE was observed, the air had travelled from the north and over the sea ice before passing over the ship. An aspect of the back trajectories that had a more significant correspondence with the occurrence of ODEs was

33

Figure 3.4: Hysplit derived 144 h back trajectories at heights 100 (black/triangle), 300 (red/square), 600 (green/circle) and 1000 m (blue/diamond), for cases A-F indicated in Figure 3.3. The markers indicate a 12-h period of time has elapsed.

the amount of time that the air spent at heights below 500 m, where there would have been mixing with air that came in contact with the sea ice. For example, in case-A, when there was no ODE, the back trajectories that were started above the Amundsen at heights of 100 m, 300 m, 600 m, and 1000 m each spent the previous days well above height 500 m and descended only in the 12 hours prior to passing over the Amundsen (Fig 3.5a). In case-B the ozone mixing ratio was less than 5 ppbv up to a height of 220 m and then gradually increased to the background level of 30 ppbv at height 500 m. In this case the back trajectories starting from 100 m and 300 m above the ice surface had spent significant time below 500 m in the previous days, while the back trajectories starting at heights 600 m and 1000 m did not spend any time below 500 m in the previous six days. In case-C the air that was partially depleted in ozone, lying above the main surface ODE, extended up to a height of 1000 m (Figure 3.3a). Figure 3.5c shows that in this case all of the back trajectories that started below 1000 m had spent at least three of the past six days at heights within 500 m of the sea ice. Case-D is another example where the ozone depleted air extended to a height of 1000 m (Figure 3.3a), and the back trajectory analysis indicates that the measured air had ascended from below height 500 m up to 1000 m in the three days prior to passing over the Amundsen. In case-E the ODE extended only to a height of about 300 m. Figure 3.5e shows that the back trajectories starting at 100 m and 300 m had each spent the previous 4.5 days below height 500 m, but the trajectory starting at 1000 m remained well above height 500 m during the previous six days.
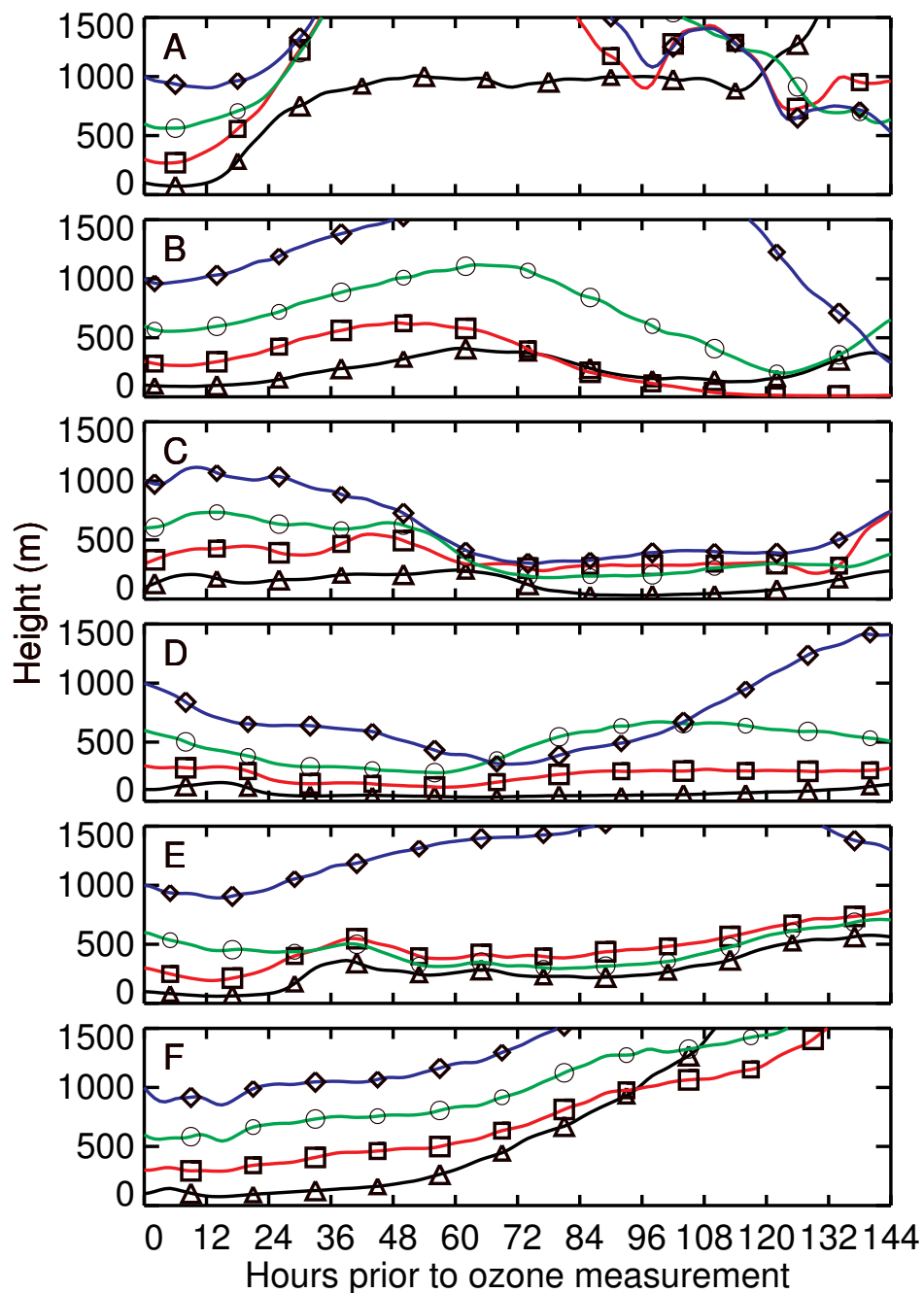
35

Figure 3.5: HYSPLIT back trajectories showing the six-day history of the altitude of the air measured at heights 100 m, 300 m, 600 m and 1000 m ASL for cases A-F indicated in Figure 3.3.

Despite that the uncertainty in back trajectory calculations is not exactly known, the case studies do show that there is a correspondence between the occurrence of ODEs and the altitude history of the air. By integrating the calculated altitude of the air masses over a 144 - hour period, it was found that lower average height was associated with lower ozone mixing ratios. An example of this for back trajectories calculated at 100 m is shown in Figure 3.6a. Depletion events were associated with air masses closely connected to the ground. During periods of strong depletions with ozone mixing ratios of 10 ppbv or less, the associated air mass was found to have a 6 - day average altitude of 500 m and lower, close to the previously estimated height of 400 m for the boundary layer over Arctic sea ice (Bottenheim et al. 2002). For the period of time between March 9th and 25th, a positive linear correlation of 0.65 was found (Figure 3.6b) between the lidar measured mixing ratios and the calculated 6-day historical mean altitude of the corresponding air masses.

There are exceptions to the pattern in terms of the altitude history of the air. For example, the back trajectory that started at height 600 m in case-E did spend time at heights between 500 m and 300 m, but the ODE did not extend above 300 m. In case-F there was no ODE at any height and the back trajectories had all descended from greater heights over the past six days. The air passing over the Amundsen at heights 100 m and 300 m had been below 500 m for the previous two days and yet there was no ODE near the surface. This is another exception that implies there are factors other than height

37
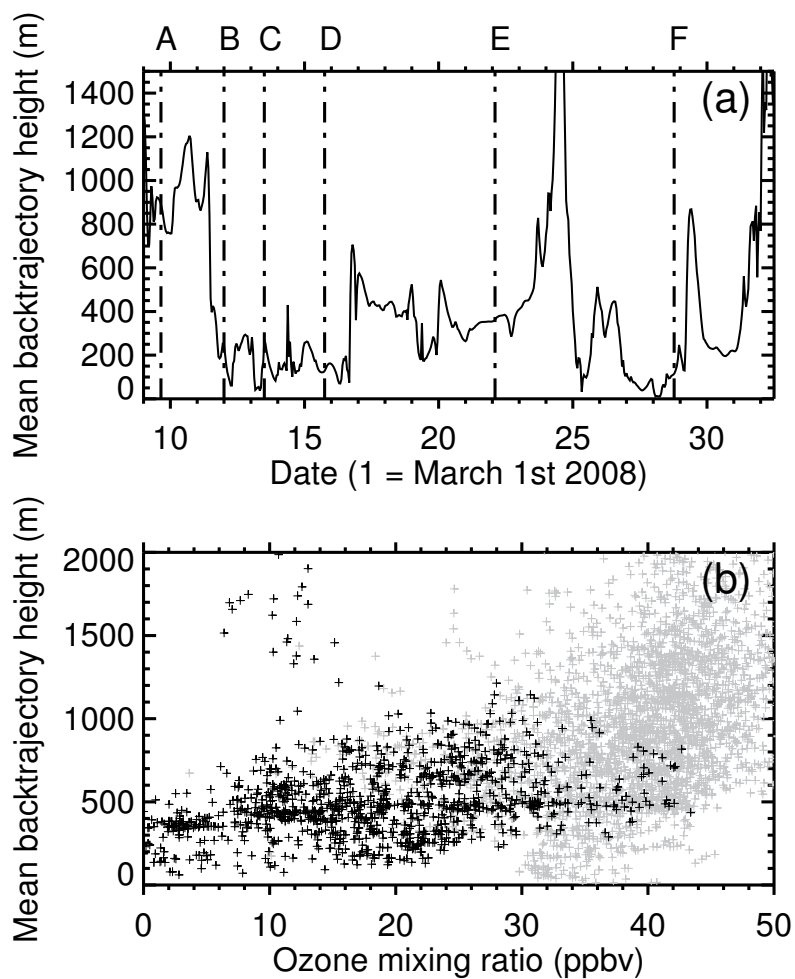
Figure 3.6: The average HYSPLIT 144 hour back trajectory altitudes calculated for air masses originating 100 m ASL over the Amundsen in one-hour resolution for 9 March to 2 April. b) A comparison between the DIAL ozone mixing ratios for the data in Figure 3.3, and the mean back trajectory altitudes calculated every 100 m for 100 m to 1000 m. Potential temperatures greater than -25 °C are in grey, and less than -25 °C black. The correlation constant between mixing ratio and mean back trajectory altitude is 0.65.

above the surface that affect ozone. It was found that temperature was another important factor.

Temperature profiles were acquired with a zenith-oriented microwave radiometer (TP/WVP-3000) capable of measuring with a vertical resolution of 50 m for heights below 1 km. (Güldner and Spänkuch 2001, Liljegren et al. 2001). Profiles were recorded once per hour and a continuous record exists for all but two days in March 2008.

A contour plot of the potential temperature measurements from 80 to 1000 m is shown in Figure 3.7a. Comparison between Figures 3.3 and 3.7 indicates that air with low ozone mixing ratio also has low potential temperature. (The correlation of ozone mixing ratio with absolute temperature was not as strong as with potential temperature.) This suggests it is the temperature that air aloft would have had while previously near the surface that is important. In cases B and E the potential temperature near the ground was less than -30 °C and increased with altitude. In both cases, the strong depletion of ozone near the ground ended with a sharp increase in mixing ratio corresponding to a potential temperature of -27 °C at altitudes of 200 – 250 m.

For case-C and case-D the near surface temperature was colder than in the previous two cases, and the potential temperature inversion was less pronounced. In both cases partial depletions extended above 700 m in height. In each case an ozone mixing ratio greater than 25 ppbv corresponded to potential temperatures greater than -25 °C and mixing ratios below that decreased linearly with potential temperature. This trend was also
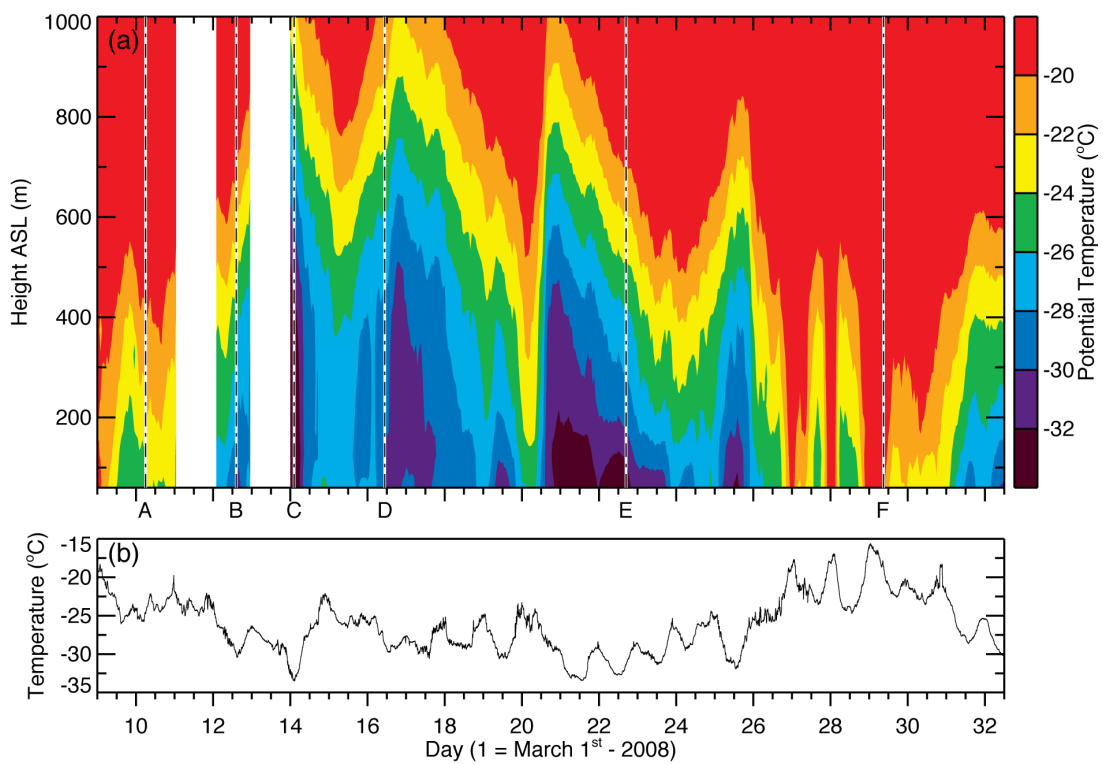
Figure 3.7: Temperature measurements aboard the Amundsen near the onset of polar sunrise (9 March to 2 April 2008). (a) Potential temperature from 60 to 1000 m calculated from temperatures recorded by a microwave radiometer. (b) Local temperatures in degrees Celsius recorded aboard the ship 14 m above the sea ice. All dates and times are in GMT, local time was GMT -6h.

apparent in case-A in which an ODE was not observed and temperatures were relatively high (greater than -25 °C) at the ground and aloft.

The scatter plot (Figure 3.8) of ozone mixing ratio and potential temperature shows a strong statistical correlation with a positive linear correlation constant of 0.85. The strongest depletions at the ground occurred at temperatures below -25 °C.

As previously noted, the case on 29 March 2008 (case-F) did not follow the pattern established with respect to altitude history in the back trajectory. As in case-A, there was no sign of ozone depletion, and this period of time is marked by a high ozone mixing ratio slightly above normal background levels. Unlike case-A, the calculated back trajectories indicated that the air measured at the surface had been below a height of 200 m for approximately 60 hours, a condition associated with ODEs in the previous cases. This period of time was characterized by warm temperatures (greater than -20 °C) over the sea ice, and is thus consistent with the previous cases in which the ODEs occurred only in air with potential temperature below -25 °C.

The altitude history of the air measured in case-F (Fig. 3.5) suggests that the typical un-depleted values of ozone ($\approx$ 40 ppbv) measured at the surface was the result of downward transport of ozone rich air. This is consistent with Strong et al. (2002) who found that during an extended 9-day depletion event in Alert, NU, the primary source for replenishing boundary layer ozone was the downward vertical transport of ozone rich air from aloft.
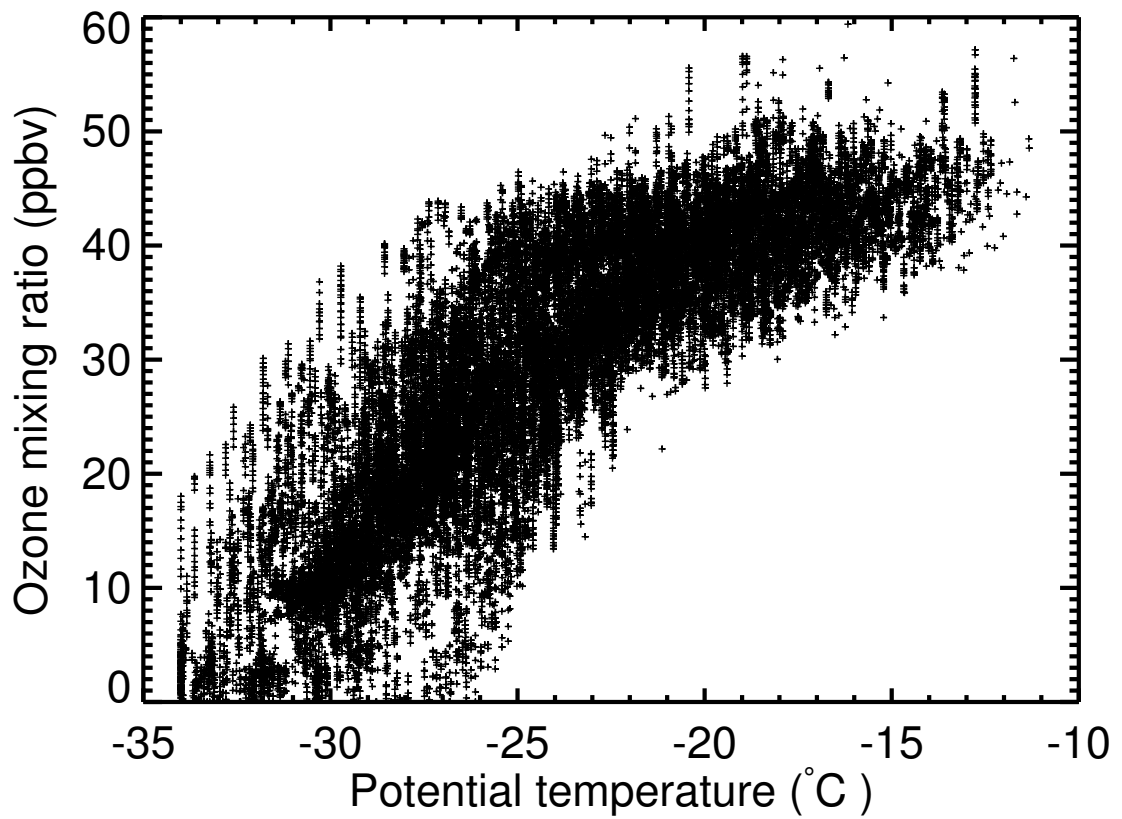
Figure 3.8: Scatterplot of the DIAL derived ozone-mixing ratios from 60 m–700 m to the potential temperatures over the same altitude ranges from 9 March to 2 April 2008. The correlation constant of 0.85.

While the uncertainties in the back trajectory analysis are not quantified, comparison with the profiles of measured potential temperature gives confidence in the back trajectory analysis. The cases where air had risen from the surface (case-C and case-D) also have relatively low potential temperature up to greater heights. The cases where the back trajectory indicates that air had descended toward the surface (case-A and case-F) have relatively warmer potential temperature, again as expected. This also suggests that the correspondence of ODEs with low potential temperature is not separable from the correspondence with proximity to the sea ice surface. The air that was cooled substantially by prolonged turbulent heat exchange with the sea ice surface would also have low potential temperature. This then explains two remaining apparent exceptions to the overall pattern. In case-E the air arriving at height 600 m had spent time below 500 m in the calculated back trajectory, but the measured potential temperature was relatively warm at -22 °C (compared to the surface temperature of -32 °C), which indicates that there was not substantial contact with the surface in the previous days. In early April there was a depletion despite that the average heights in the back trajectory analysis were well above 500 m. However, the measured potential temperature was relatively cold and well below -25 °C, which suggests the air had spent time near the surface. It was found that the ozone depleted air did actually spend time near the surface when the back trajectory was extended beyond six days in duration.

3.5 Summary

The Amundsen CFL/OASIS campaign during the 2007-2008 International Polar Year provided a unique opportunity to investigate Arctic boundary layer ozone depletion events directly over sea ice. The differential absorption lidar provided a continuous record of the vertical distribution of ozone above the ship. A number of full and partial ozone depletion events were observed during March 2008 and all were in contact with the sea ice. No depletions were observed in isolated layers separated from the surface. Backward trajectory analysis indicated that most of the ozone-depleted air had spent extended periods within 500 m of the sea ice. A strong positive correlation was also found between ozone mixing ratio and potential temperature. No ODEs were found to occur at any altitude when the potential temperature was higher than -25 °C. Periods of normal, or higher than normal ozone concentrations were recorded when sampling warm ($<$ -20 °C) air masses originating from the free troposphere that had no recent connection to the ground.

The observed ODEs correspond to two factors, prolonged periods within 500 m of the sea ice, and low potential temperature. We interpret that the source for the measured ozone depletions was long-range transport of cold air masses that had extended periods of contact with sea ice by turbulent mixing within the atmospheric boundary layer. The observed ozone depletion events were primarily the result of previously depleted air masses being transported over the ship, rather than local chemistry. These results are

consistent with previous studies that have found a correlation between Arctic ozone depletion events and the length of time an air mass is connected to the sea ice (Bottenheim et al. 2009, Frieß et al. 2004), and low temperatures (Ramacher et al. 1999, Strong et al. 2002).

4 Airborne lidar measurements of surface ozone depletion over Arctic sea ice

4.1 Introduction

A downward viewing differential absorption lidar (DIAL) was operated aboard the Polar 5 research aircraft (Fig. 4.1) as part of the PAMARCMIP 2011 (Polar Airborne Measurements and Arctic Regional Climate Model Simulation Project) measurement campaign (Herber et al. 2012). The lidar measurements occurred during flights over the sea ice north of Barrow, Alaska, on 31 March 2011 and 3 April 2011. During these flights boundary layer depletions of ozone were measured over a range of 300 km from Barrow. All the observed ozone-depleted air throughout the flights occurred within 300 m - 500 m of the sea ice surface. A back trajectory analysis of the measured air indicated that the ozone-depleted air originated from over the ice, while non-depleted air at the surface originated from over land. An investigation into the altitude history of the ozone-depleted air suggests a strong inverse correlation between measured ozone concentration

and the amount of time the air directly interacted with the sea ice.

4.2   DIAL Installation

The DIAL was installed within a single aircraft rack with dimensions of $56 \times 64 \times 130$ cm, which is a self-contained unit (Figs. 4.2-4.3) (apart from the laser power supply) with internal thermal control and vibration isolation. The laser and telescope view out through a window on the rack, which consists of two optical quality, UV anti-reflection coated glass plates, with argon gas filling the gap in order to avoid frosting. The rack is mounted to the seat rails with the window aligned above a port that is open to the atmosphere below the aircraft.

The optical layout of the DIAL system is nearly identical to that used in Chapters 2 and 3 (See Chapter 2 - Fig. 2.3 for the schematic). For this campaign a PMT and 266 nm interference filter were added in order to record a 266 nm channel. Backscattered light was collected with a 15 cm diameter off-axis parabolic mirror and a 1.5 mm diameter optical fiber bundle positioned in the focal plane, 500 mm from the mirror, to form a receiver field of view of 3 mrad. The four wavelengths were separated in the receiver by the transmittance and reflectance from a series of tilted interference filters with bandwidths of 1 nm. Photomultipliers were used to detect the optical signals and the data acquisition employed both analog to digital conversion and photon counting in order to achieve linearity over a high dynamic range. The raw data were recorded with a range gate of

Figure 4.1: The Polar 5 research aircraft. Basler BT-67: rebuilt and modernized DC-3

7.5 m and an integration period of 200 laser shots (10 s). The collected lidar profiles were averaged spatially and temporally in order to reduce the measurement uncertainty. The 266/287 nm analog signals were used to generate ozone profiles to a range of 2 km. At greater ranges, photon-counting signals were used to determine ozone levels near the surface.

4.3   Observations

The DIAL system was operated during three flights over the sea ice north of Barrow Alaska between the dates of 30 March and 3 April 2011. Presented here are measurements from two flights on 2 April 2011, at 22:00 UTC and 30 March 2011 01:00 UTC. For both flights the lidar return signals were averaged temporally over a window of 200 s, which corresponds to an average distance of approximately 12 km at the aircraft mean ground speed of 220 km/hr. Spatial averaging was also applied to the recorded signals such that the vertical resolution was 22.5 m for the analog and 75 m for the photon counting. At a flight altitude of 2200 m, the typical backscatter return signal from the surface was a photon counting rate of 30 MHz. This moderate signal strength did not cause any detector signal induced noise.

For the measurements in this study, there was not a significant contribution to the signal by aerosol and cloud particles, and the differential absorption and scattering due to aerosol had a negligible effect on the derived ozone concentration. Measurements where

Figure 4.2: The DIAL installed aboard the Polar 5. The lidar is contained in the aircraft rack bolted to the seat tracks.

Figure 4.3: The DIAL installed aboard the Polar 5. Hinged panels allow access to the Licel electronics and data logging PC.

clouds or blowing snow over the sea ice were a significant factor were omitted from the analysis. The molecular scattering and extinction coefficients were calculated from atmospheric densities determined using data from meteorological radiosondes launched from Barrow, AK, MET station (71.30° N, 156.78° W).

4.3.1   Flight on 2 April 2011

On 2 April 2011, at 22:00 UTC the Polar 5 aircraft departed Barrow for a flight track over the sea ice for a distance of 325 km to the north east. Similar measurements were obtained during the other two flights. The outbound half of the flight, shown in red in Figure 4.4, was a low level flight at a height range 100 – 200 m above the sea ice. The DIAL measurements were carried out only during the return flight leg (black line in Fig. 4.4) while the aircraft was at a height of 2.2 km. A contour plot of the DIAL ozone measurements along this flight track is shown in Fig. 4.5.

A persistent ozone depletion was observed close to the surface throughout most of the flight. At the beginning of the measurement (indicated as case A in Fig. 4.5), approximately 300 km northeast of the nearest land mass, ozone mixing ratios of 10 ppbv were observed at the surface, extending up to a height of 250 m above the sea ice. Above this altitude the mixing ratio started increasing with altitude until at an altitude of 400 m the background levels of approximately 40 ppbv were observed. The general trend throughout this flight is that ozone concentration increased toward land while the vertical depth
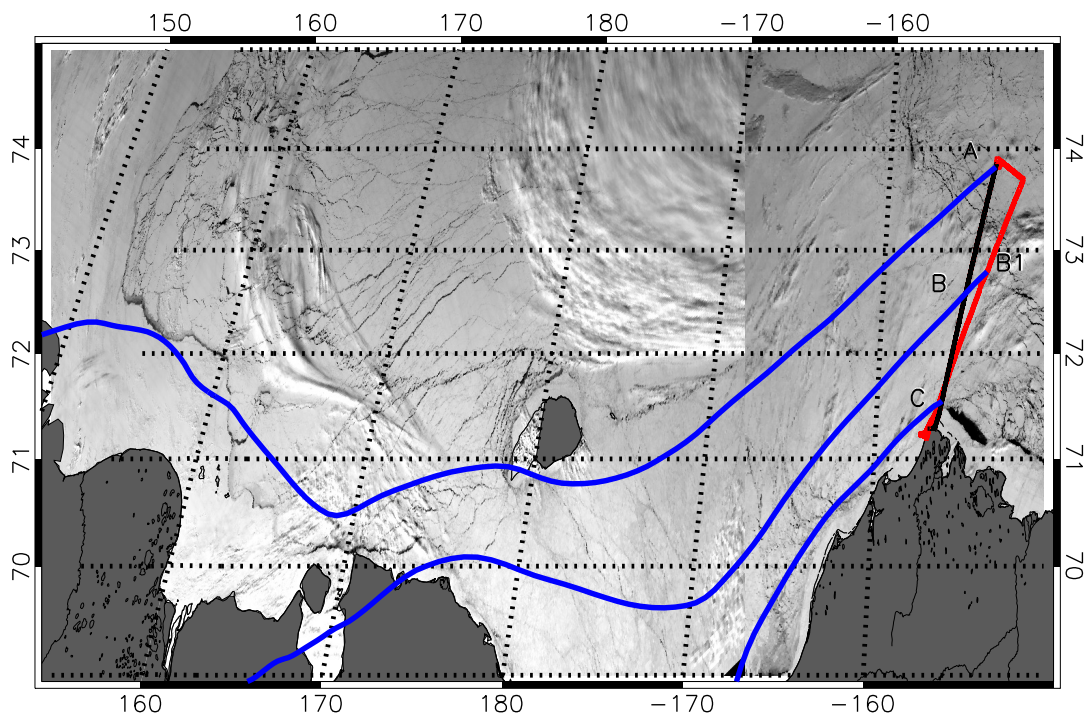
Figure 4.4: Flight track of the Polar 5, out of Barrow Alaska overlaid on corresponding images from the MODIS instrument on the Terra satellite (Band 2, 841–876 nm). The black line indicates the portion of the inbound flight when the ozone DIAL was operational (3 April 00:45–02:15 UTC), red the outbound flight (2 April 21:50–3 April 00:45). The positions used for the case studies in the analysis (A, B, C, B1) are indicated along the flight path. Calculated air back trajectories at height 100 m (blue) are shown for the points A, B and C and B1.
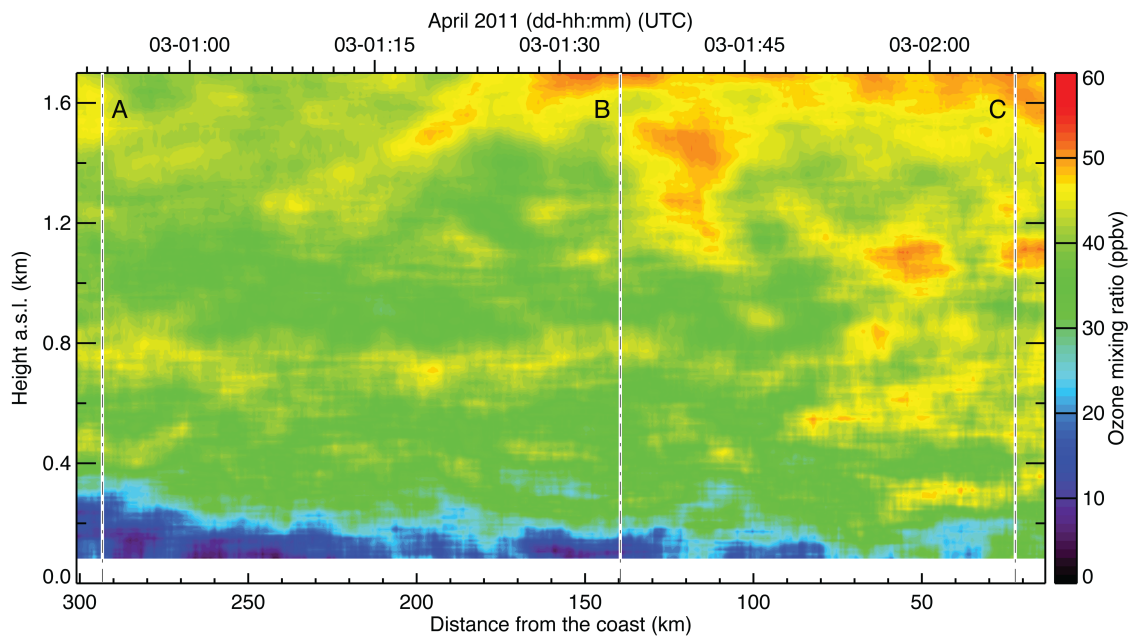
Figure 4.5: DIAL measurements of ozone mixing ratio along the track of the aircraft shown in Fig. 4.4. Lines labeled (A), (B) and (C) correspond to the positions of the aircraft labeled in Fig. 4.4, where the corresponding air back trajectories have been calculated.

of the depletion also decreased. Within 20 km of the coast the surface ozone depletion is almost non-existent.

In situ ozone measurements were taken using a TE49C (Thermo Electron Inc., USA) with an air-sampling inlet located at the top of the aircraft. This provided a validation for the DIAL ozone measurements near the ice surface. The aircraft height on the outbound flight path was mostly within 100 m of the surface for sea ice thickness measurements, but at five locations there were ascents to heights ranging from $150 - 200$ m for instrument calibrations followed by immediate descent (Fig. 4.6). These ascents provided vertical profiles of in situ ozone measurements that can be compared with the DIAL measurements on the return flight leg. Figure 4.7 shows the ozone vertical profiles measured with the DIAL at three locations that will be used for case studies in the analysis. The location for the vertical profile of ozone measured by the DIAL in case B (Fig. 4.7-b) corresponds to the position of an in situ vertical profile taken during the outbound portion of the flight (the position is labeled as case B1 in Fig. 4.6-b) as determined by a backwards trajectory calculation. The DIAL and in situ vertical profile measurements are seen to be in agreement within the TECO accuracy of ± 1 ppb, and the DIAL measurement uncertainty of ± 3.5 ppb at 150 m above the surface of the ice.
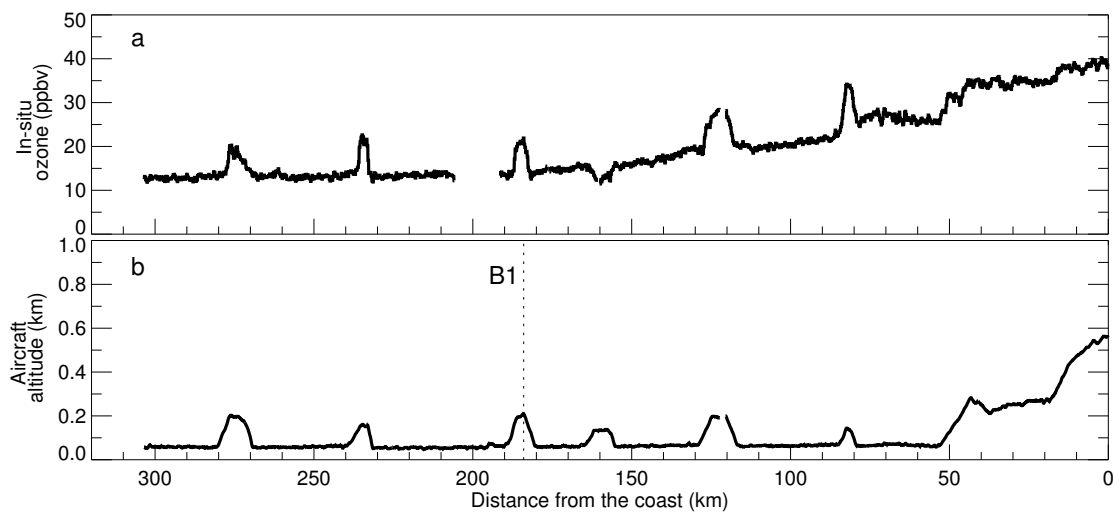
Figure 4.6: a) In situ ozone measurements along the outbound flight track (black trace in Fig. 4.4) with the distance from the coast of Alaska. b) Aircraft altitude along the outbound flight track. B1 indicates the position of the aircraft during the outbound flight as labeled in Fig. 4.4.
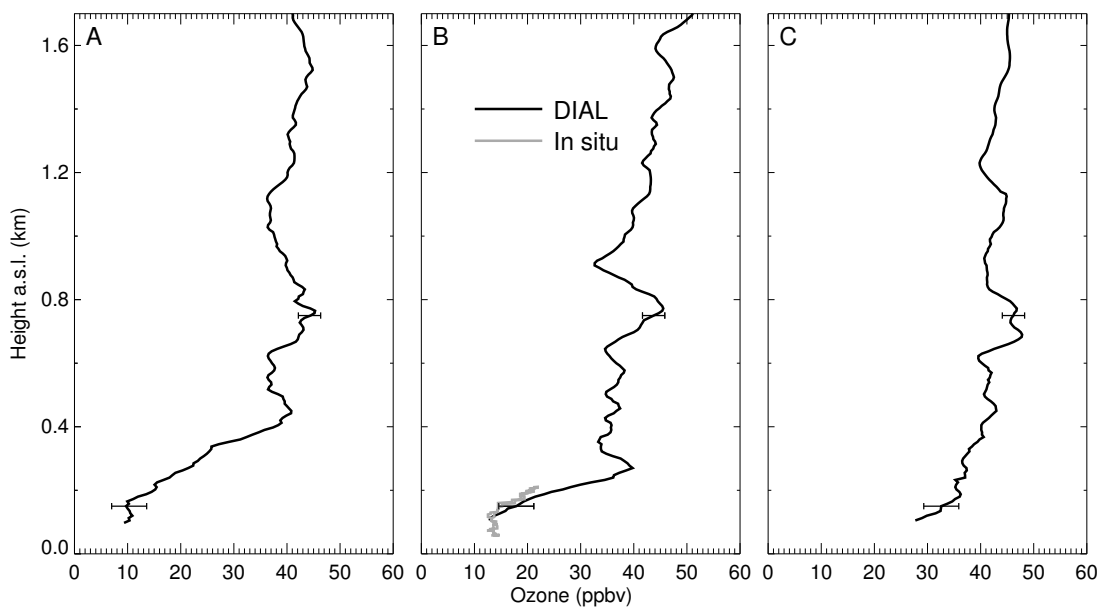
Figure 4.7: Measured vertical profiles of ozone mixing ratio with the DIAL along the inbound flight track, and in situ measurements (grey line) along the outbound flight track (position B1 in Figs. 4.4 and 4.6b). Cases (A), (B), and (C) correspond to the positions indicated in Figs. 4.4 and 4.5. The indicated uncertainty in the DIAL measurement is one standard deviation in the photon counts, propagated through the ozone derivation.

4.3.2   Flight on 31 March 2011

On 31 March 2011, at 01:00 UTC, the Polar 5 departed Barrow for a flight to the east ranging 170 km over the sea ice. The outbound flight legs, shown in black in Figure 4.8, were a combination of a low level flight 100-200 m above the sea ice, and an ascent to an altitude of 6600 m. The DIAL measurements were carried out only during the return flight leg (red in Fig. 4.8) while the aircraft was at a height of 2.2 km. A contour plot of the DIAL ozone measurements along this flight track are shown in Fig. 4.9.

During this leg of the flight, surface winds resulted in blowing snow over the ice surface, making accurate ozone retrieval by the DIAL below height 375 m impossible. The presence of blowing snow at the surface can be seen in the backscatter ratio of the returned lidar signals. Figure 4.10 shows the effect on the recorded signal at a wavelength of 299 nm throughout the flight.

Above the interference caused by the blowing snow, the top of an ozone depleted layer was observed throughout the flight leg. Near the beginning of the measurement period (indicated as case A in Fig. 4.9), approximately 150 km west of the nearest land mass, accurate retrieval of ozone was possible to height 375 m. Between 600 - 1500 m the ozone concentrations stayed consistent at approximately 40 ppbv. Below 600 m ozone mixing ratios began to drop at a rate of 10 ppbv per 100 m.

The vertical structure of ozone stayed relatively consistent through out the flight.
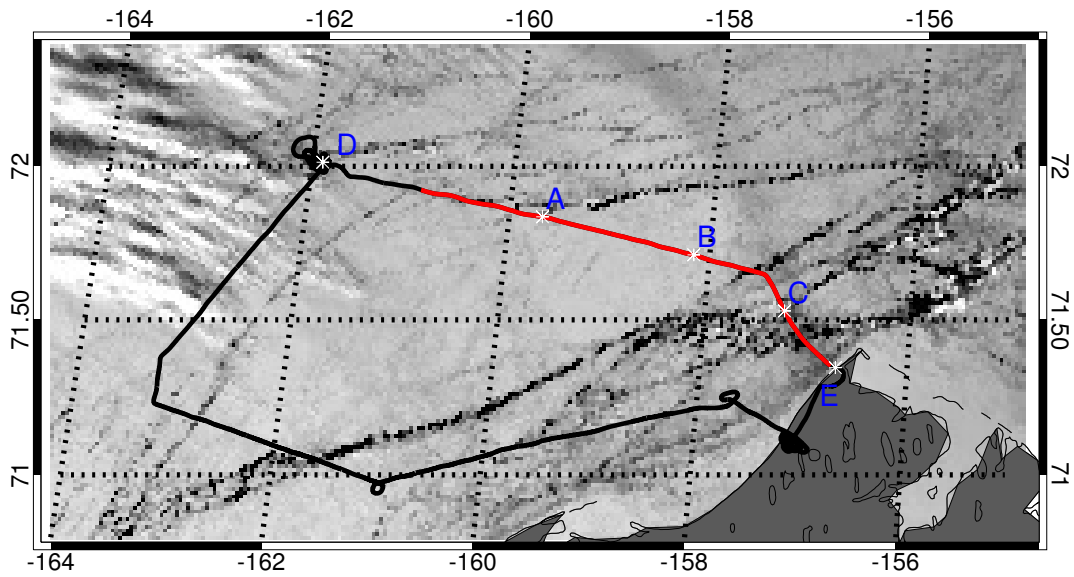
Figure 4.8: Flight track of the Polar 5, for Flight 1 on 31 March 2011 out of Barrow Alaska overlaid on corresponding images from the MODIS instrument on the Terra satellite (Band 2, 841–876 nm). Red indicates portion of the inbound flight track when the DIAL was active, and black the outbound track. A-E labels indicate the positions used for the case studies in the analysis.
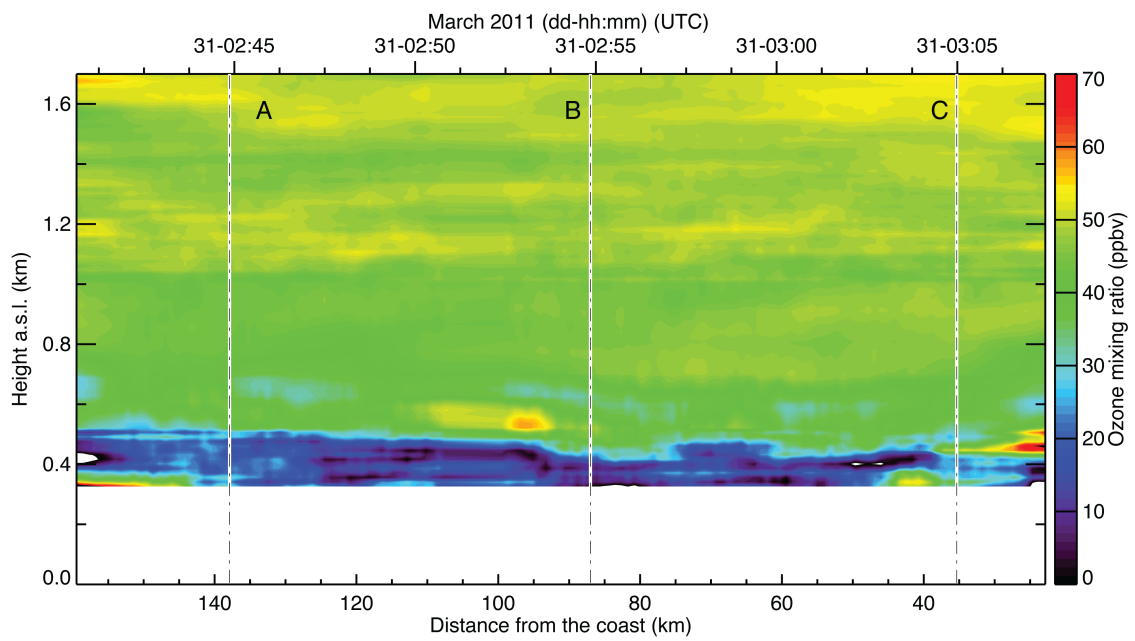
Figure 4.9: Polar 5 ozone contour plot for Flight 1 on 31 March 2011.
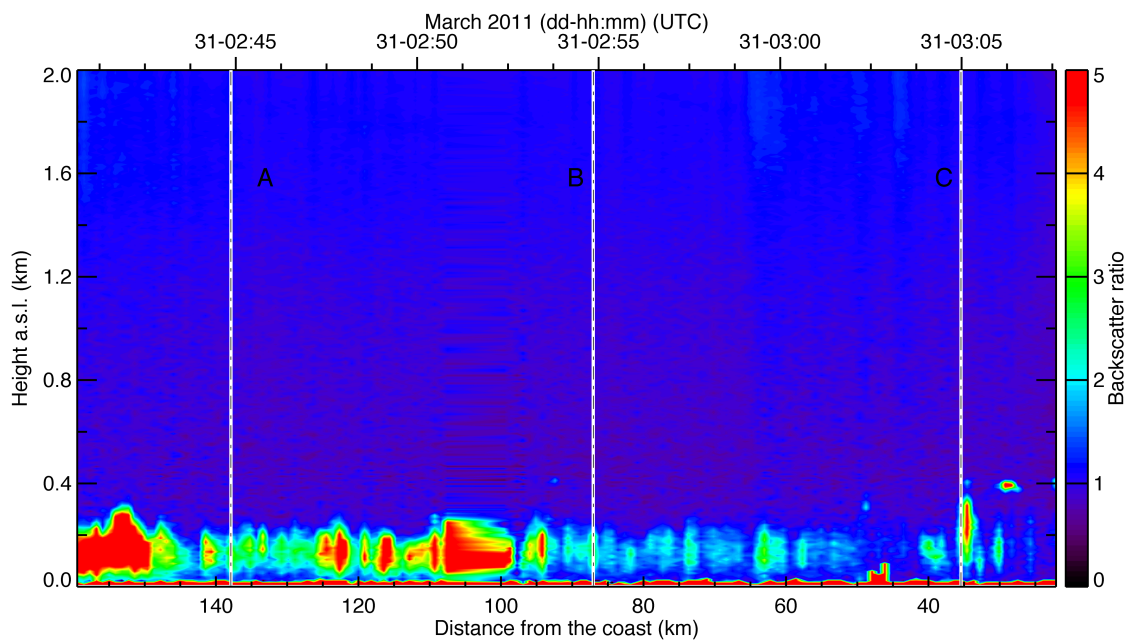
Figure 4.10: Backscatter ratio at 287 nm as a function of range from the aircraft. A ratio higher than 1 indicates the presence of aerosols, blowing snow or ice crystals.

In case B (Fig. 4.11-B) a decrease in ozone mixing ratio begins at height 600 m, and continues until the lower limit of the DIAL measurement altitude of 370 m. Closer to land (case-C Fig. 4.11) the depth of the ozone depletion has decreased by approximately 150 m. Ozone was measured by the DIAL at 40 ppbv down to an altitude of 450 m before the sharp decrease in ozone mixing ratio begins to occur.

The DIAL measurements were accompanied by in situ vertical profiles of ozone recorded by the TE49C before and after the DIAL measurement period. Prior to the DIAL measurements (labeled D in Fig. 4.8) the aircraft ascended from an altitude of 60 m to 6600 m. The ozone profile recorded during this ascent is shown in Figure 4.11-D. Near the sea ice surface, an ozone mixing ratio of 18 ppbv was measured between height 60-400 m. Above this height, the mixing ratio began to increase with altitude until at height 600 m no depleted air remained and ozone concentrations of 40 ppbv were observed. The rate of increase of ozone with altitude between 400-600 m is nearly identical to that recorded by the DIAL after the ascent of the aircraft (case A). After the DIAL measurement period, a vertical profile of ozone was recorded close to land by the TE49C during the descent of the aircraft while landing (case-E in Fig. 4.8). In this case, the vertical depth of the ozone depletion has decreased by approximately 150 m, similar to the decrease in ozone depletion depth noted by the DIAL in case-C (Fig. 4.8-C).

In situ measurements onboard the aircraft during the low level flights on the outbound leg captured vertical ozone profiles during periods of ascent and descent. The locations

of these profiles are labeled D and E in Fig. 4.8. The vertical ozone profiles are shown in Fig. 4.11. At the furthest points from land, the depletion is approximately 200 m greater in height than near land. This can clearly be seen in profiles A and D (the furthest DIAL and in situ ozone profiles, respectively) compared to profiles C and E (the closest DIAL and in situ ozone profiles, respectively).

4.4 Analysis

Back trajectory analysis of the air measured by the DIAL during the flight was performed with the NOAA HYSPLIT model (Draxler and Hess 1998), using GDAS (Global Data Assimilation System) meteorological data. The historical back trajectories were calculated every two minutes for the period of time in which the DIAL was active for heights ranging from 100 m to 2000 m above sea level and were calculated for a 6-day period backward starting from the GPS location of the aircraft at each time interval.

During the 2 April 2011 flight, the strongest depletion was observed at the Northern most extent of the flight track, approximately 300 km from the northern tip of Alaska (indicated as case A in Fig. 4.5). The ozone-mixing ratio was less than 10 ppbv up to a height of 250 m and then increased to the background level of $30 - 40$ ppbv at height 400 m. In this case the back trajectories shown in Fig. 4.12a indicate that the air up to a height of 1000 m originated from the West over the Arctic sea ice. An analysis of the altitude history for case A (Fig. 4.13a) indicates that the air at 100 m and 300 m above the
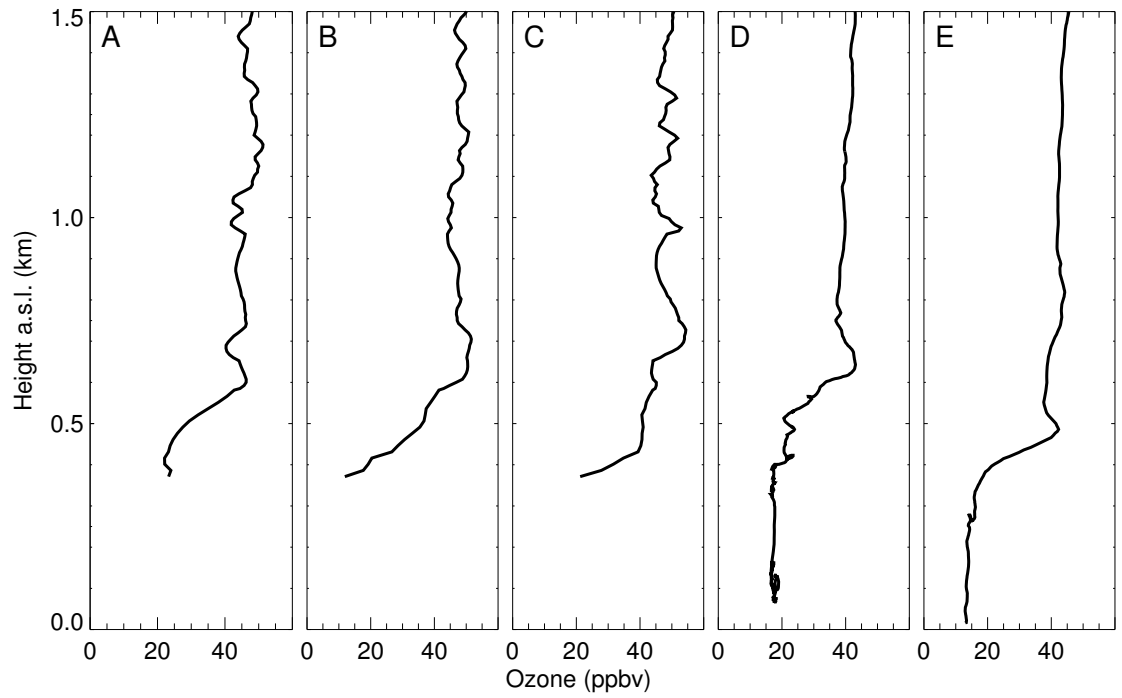
Figure 4.11: DIAL profiles, labeled A-C and in situ ozone profiles D-E for cases A-E labeled in Fig. 4.8.

ice surface had spent significant time below 350 m in the previous days, while the back trajectories starting at heights 500 m and 1000 m did not spend any time below 350 m in the previous six days.

In case B, approximately 140 km from land, the ozone depletion was observed to extend from the surface to a height of about 200 m (Figs. 4.5 and 4.7b). The depleted ozone concentration was not as low as observed in case A (Figs. 4.5 and 4.7a). Back trajectory analysis (Fig. 4.12b) indicates that the origin of the measured air at an altitude of 100 m had shifted slightly to the south, such that the air closest to the surface spent more time over land than over the sea ice in comparison to case A. The altitude history (Fig. 4.13b) shows that air measured at height 300 m spent much less time below an altitude of 350 m in comparison to case A.

Near the end of the flight (case C), as the aircraft approached the coastline, the DIAL measured normal background levels of ozone (Figs. 4.5 and 4.7c). There was no ozone depletion event at the coastline. back trajectory analysis indicates that the air at 100 m above sea level (ASL), while spending the previous 60 hours within the boundary layer, originated from the south and was not in contact with sea ice over the Arctic Ocean (Fig. 4.12c). The air measured at 300 m ASL spent very little time within 300 m of the sea ice prior to being measured, and the air above 300 m spent no time within 300 m of the sea ice during the six days prior to being measured near Barrow, AK (Fig. 4.13c).

Open leads and first year ice have been considered to be an important source of

65
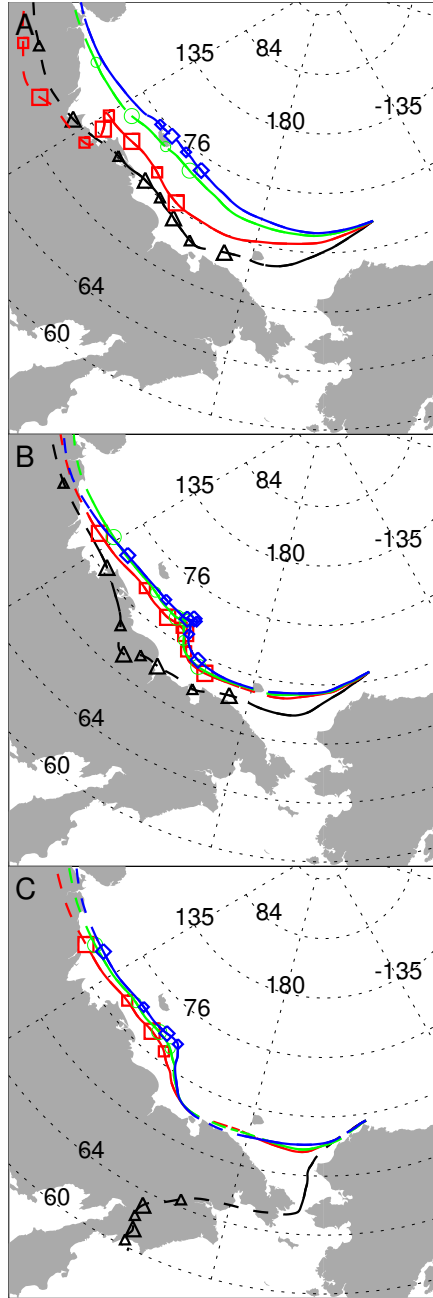
Figure 4.12: Calculated back trajectories of air in which ozone was measured during the flight of 2 April 2011. The endpoint of the trajectories in A, B, and C correspond to the locations of the aircraft labeled in Figs. 4.4 and 4.5, and the cases in Fig. 4.7. Symbols indicate a period of 12 hours has elapsed for the corresponding back trajectory. The trajectories are shown for air measured by the DIAL at heights 100 m (black-triangle), 300 m (red-square), 500 m (green-circle) and 1000 m (blue-diamond).
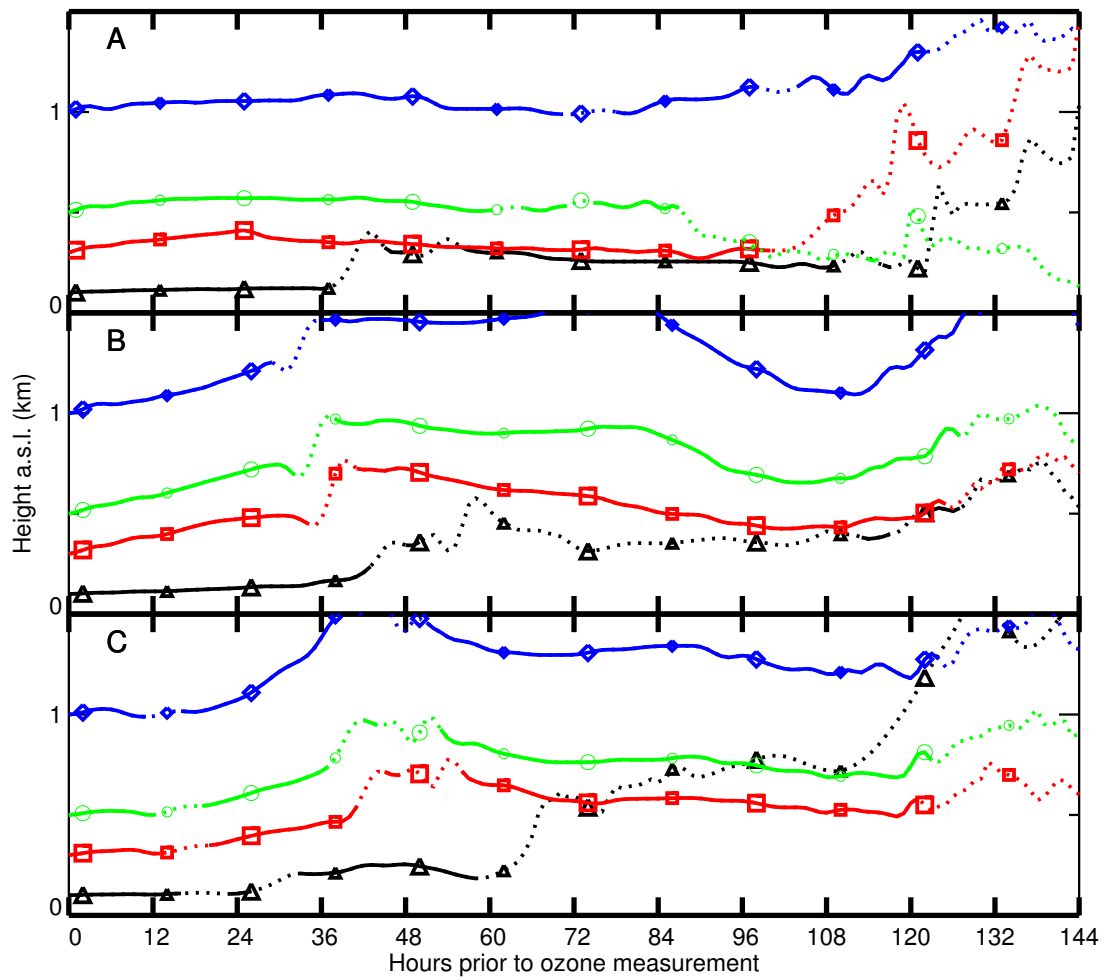
Figure 4.13: Altitude history of the calculated back trajectories at heights 100 m (black-triangle), 300 m (red-square), 500 m (green-circle) and 1000 m (blue-diamond). The end-point of the trajectories in A, B, and C correspond to the location of the aircraft indicated in Figs. 4.4 and 4.5 and the cases in Fig. 4.7. Solid lines indicate that the air is over ice, dotted lines indicate land. Coloured symbols on each trajectory correspond to those in Fig. 4.12.
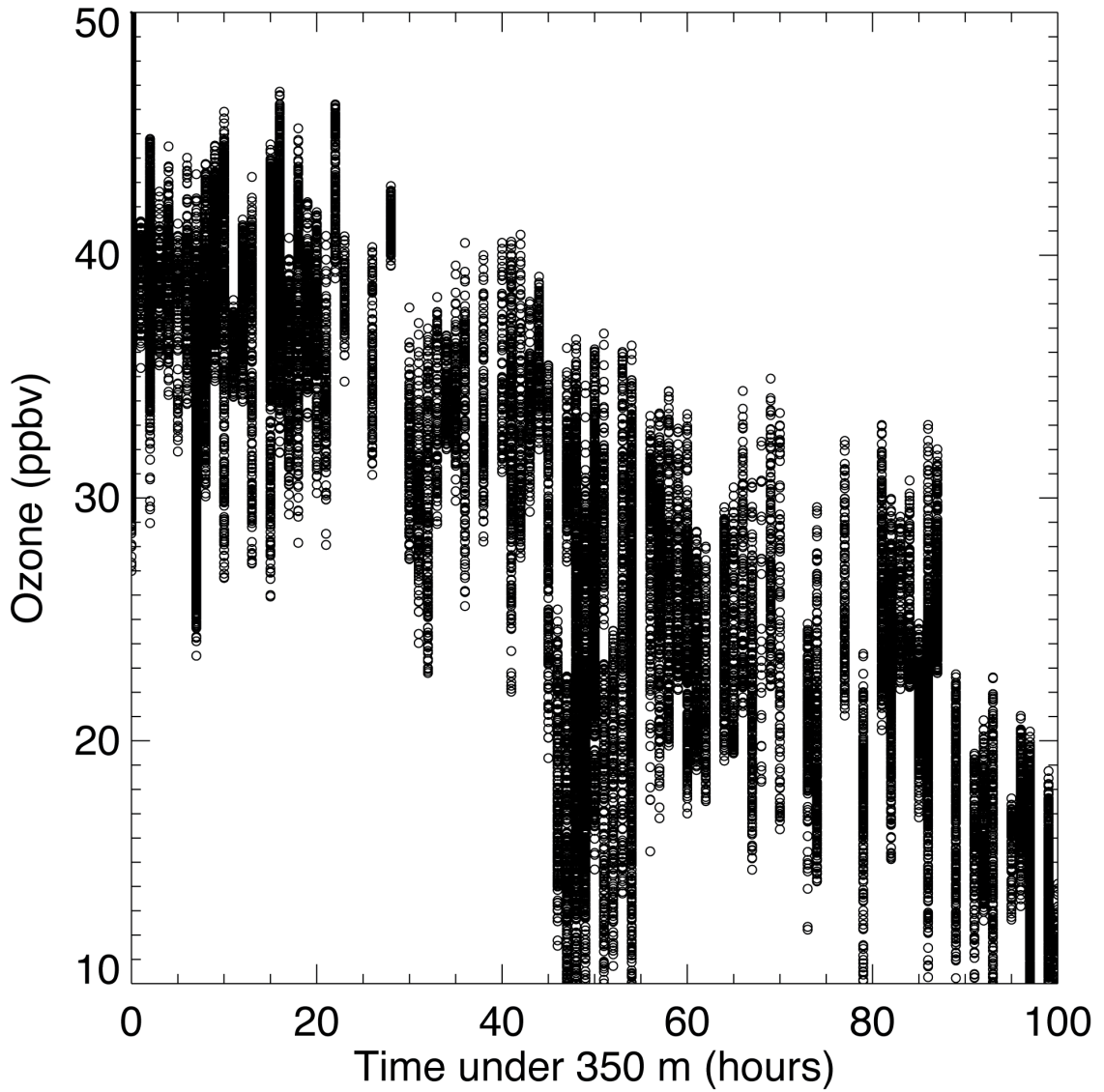
Figure 4.14: Measured ozone concentrations vs. time the measured air spent at heights below 350 m over the sea ice during the six days prior to being measured.

the bromine that causes surface level ozone depletion (Piot and von Glasow 2008). A comparison of calculated back trajectories to images from the MODIS instrument on the Terra satellite (Fig. 4.4) indicated that for case A, the air measured at an altitude 100 m travelled over an area with a significant amount of open water or recently frozen over leads. The leads are seen in the East Siberian Sea as dark jagged features in the MODIS image (latitude $150° E$ - $180° E$). MODIS imagery taken a few hours before the flight (2 April, 21:25 UTC) shows a number of open or recently frozen over leads near the northern segment of the flight path. Measurements of sea ice thickness by a tethered EM induction instrument (e.g., Haas et al. 2010) during the outbound segment of the flight (red flight path in Fig. 4.4) indicated approximately 20% open or newly frozen water (Haas 2012).

These case studies indicate that there was a correspondence between the ozone concentrations over the sea ice, and the history of the air. By calculating the amount of time a back trajectory spent within 350 m of the sea ice over the previous few days, and comparing that with the measured ozone value, it was found that lower ozone mixing ratios were associated with air that had spent a longer amount of time in close proximity with the sea ice (Fig. 4.14). The general trend during this flight was that longer periods of time near the sea ice were associated with lower measured ozone mixing ratios.

During the flight of 31 March 2011, a layer of ozone depleted air extending up to a height of 500 m was measured by the DIAL. Back trajectory analysis of the measured

69

Figure 4.15: History of the calculated back trajectories for Flight 1. A - C correspond to the times indicated in Figure 4.9. Solid lines indicate that the air is over ice, dotted lines indicate land.

air (locations indicated by A, B and C in Figure 4.15) show that it originated from over the Beaufort Sea and circulated in the general vicinity near the sea ice for a number of days before being measured by the DIAL. The trajectory analysis of the air for cases A-C (Fig. 4.16 A-C) show that the air measured throughout the flight originated from similar locations and altitudes for all three cases. The air depleted in ozone had a history of contact with the sea ice surface for a number of days prior to being measured. The altitude history of the air indicates that ozone depleted air spent several days within 250 m of the sea ice surface prior to being measured. This is consistent with the vertical structure of the depletion in which the vertical extent of the depletion was near 500 m throughout the flight. In situ vertical profiles of ozone were recorded during ascents and descents of the aircraft are consistent with the DIAL measurements and confirm that the layer of ozone depleted air extended down to the sea ice surface.

It has been previously demonstrated (Jones et al. 2009) that ODE's can develop under conditions of high wind that lead to blowing snow. Modelling studies (Yang et al. 2008, 2010) have also indicated that blowing snow events may be a significant source of sea salt aerosols as a precursor for bromine, which would lead to a depletion event. These models have shown that blowing snow events can lead to a bromine explosions, reducing ozone near the surface to concentrations ranging between 0-10 ppbv. Weather observations at Barrow AK at the time of the flight recorded mean wind speeds at the surface of 9 m/s gusting up to 13 m/s, conditions favourable to the presence of blowing snow.

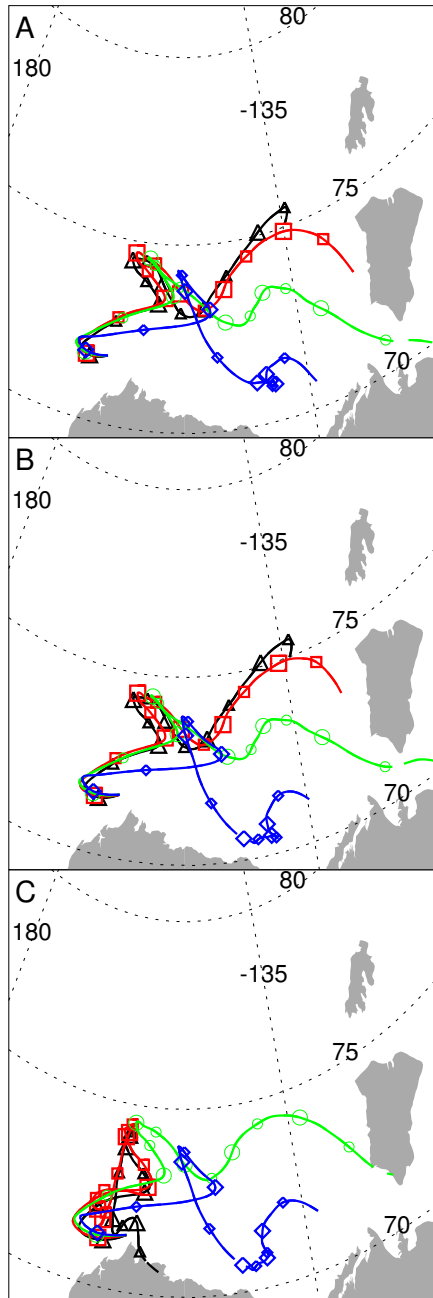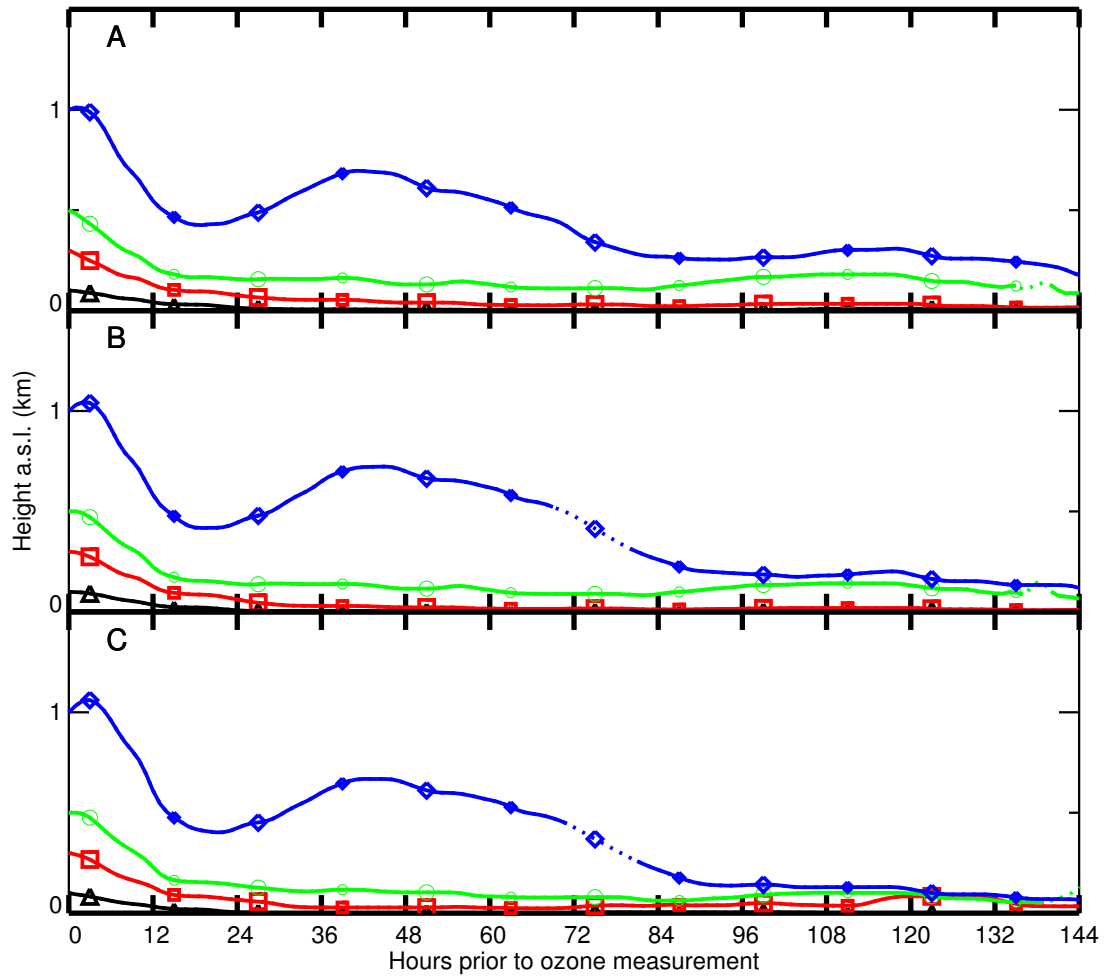Figure 4.16: Altitude history of the calculated back trajectories for Flight 1. A - C correspond to the times indicated in Figure 4.9. Solid lines indicate that the air is over ice, dotted lines indicate land.

4.5 Summary

The airborne DIAL measurements from the flights beginning on 30 March and 2 April 2011, provided a continuous record of the vertical structure of a surface ozone depletion event over a horizontal range of 170 km and 300 km respectively. During the first flight the DIAL was unable to accurately measure ozone concentrations directly above the surface due to ice crystal clouds. In situ measurements during ascent and descent of the air craft were able to record vertical profiles of ozone at altitudes below 400 m. The in situ profiles above height 400 m are consistent with the ozone measured by the ozone DIAL, and show a persistent depletion of ozone throughout the ice crystal layer to altitudes ranging between 400 and 500 m. Back trajectory analysis of the measured air showed that the air within 1 km of the surface spent the previous 6-days over the sea ice to the north of Barrow, and that the air depleted in ozone up to a height of 500 m was at an altitude below 250 m for a number of days prior to being measured.

During flight 2 the DIAL started measuring ozone concentrations at a distance of 300 km from the Alaska coastline. At this point the layer of air adjacent to the sea ice was depleted in ozone up to a height of 300–400 m above the surface. Analysis of the prior trajectory of the measured air indicated that the ozone-depleted air had spent extended periods of time within 350 m of sea ice. Close to the coastline the air was not depleted in ozone, and the corresponding back trajectory analysis indicated that this air had spent

73

significant time over land, or did not have a history of being within the surface layer over the sea ice. The observed layer of ozone depleted air was limited in vertical extent to the boundary layer and was always in contact with the surface of the Arctic Ocean. There was no evidence of isolated layers of ozone depleted air above the boundary layer.

The measurements thus indicate that the primary mechanism for the ozone depletion occurred within the boundary layer where turbulent mixing would result in contact with the frozen ocean surface. Images from the MODIS instrument on the Terra satellite over the area upwind from the April 2nd flight path show the presence of leads in the ice with open or recently frozen water, and these are a possible source of the bromine required for the photochemical depletion of ozone.

One of the aims of the experiment was to determine whether or not there was evidence for ozone depletion in air that was not adjacent to the sea ice surface, as suggested by McElroy et al. (1999) and measured in the Antarctic by Jones et al. (2010). No such evidence was found during the flights reported here. The results indicate that the ozone depletions occurred only in air that had been in contact with the ice surface. All of the air that was measured to be depleted in ozone was found to have a recent history of being confined to within 300 m of the surface. There were no observations of ozone-depleted air that was not connected to the surface. This is consistent with the findings of a previous study discussed in Chapter 3 in which the same DIAL instrument provided measurements of ozone from the surface on board the Amundsen Coast Guard Icebreaker

ship during the entire month of March 2008 (Seabrook et al. 2011). This is also consistent with previous studies using back trajectory analysis (Bottenheim et al. 2009, Frieß et al. 2004) that have found a correlation between Arctic ozone depletion events and the length of time prior to being sampled that an air mass was within the surface layer over the sea ice.

5 Ground based lidar measurements at Eureka weather station

5.1 Introduction

In September 2007 a differential absorption lidar was constructed and tested in the laboratory at York University. After testing at York the lidar was disassembled and transported to the Eureka weather station (Fig. 5.1 and 5.2) (79°59' N, 85°57' W, 10 m ASL) on Ellesmere Island, Nunavut Canada, for the purpose of measuring vertical profiles of tropospheric ozone between altitudes of 300 m and 8 km. A number of further visits to Eureka occurred over subsequent years for the purpose of maintenance, or for full time operation of the DIAL during a measurement campaign. When York University personnel were not on site, the lidar was operated by CANDAC staff. The lidar was in operation between September 2007 and April 2012.

Observations made at Eureka weather station included several surface level ozone depletion events (ODE's) within the lower troposphere. The vertical depth of the deple-

Figure 5.1: Location of the Eureka Weather Station on Ellesmere Island, Nunavut, Canada (79°59' N, 85°57' W).
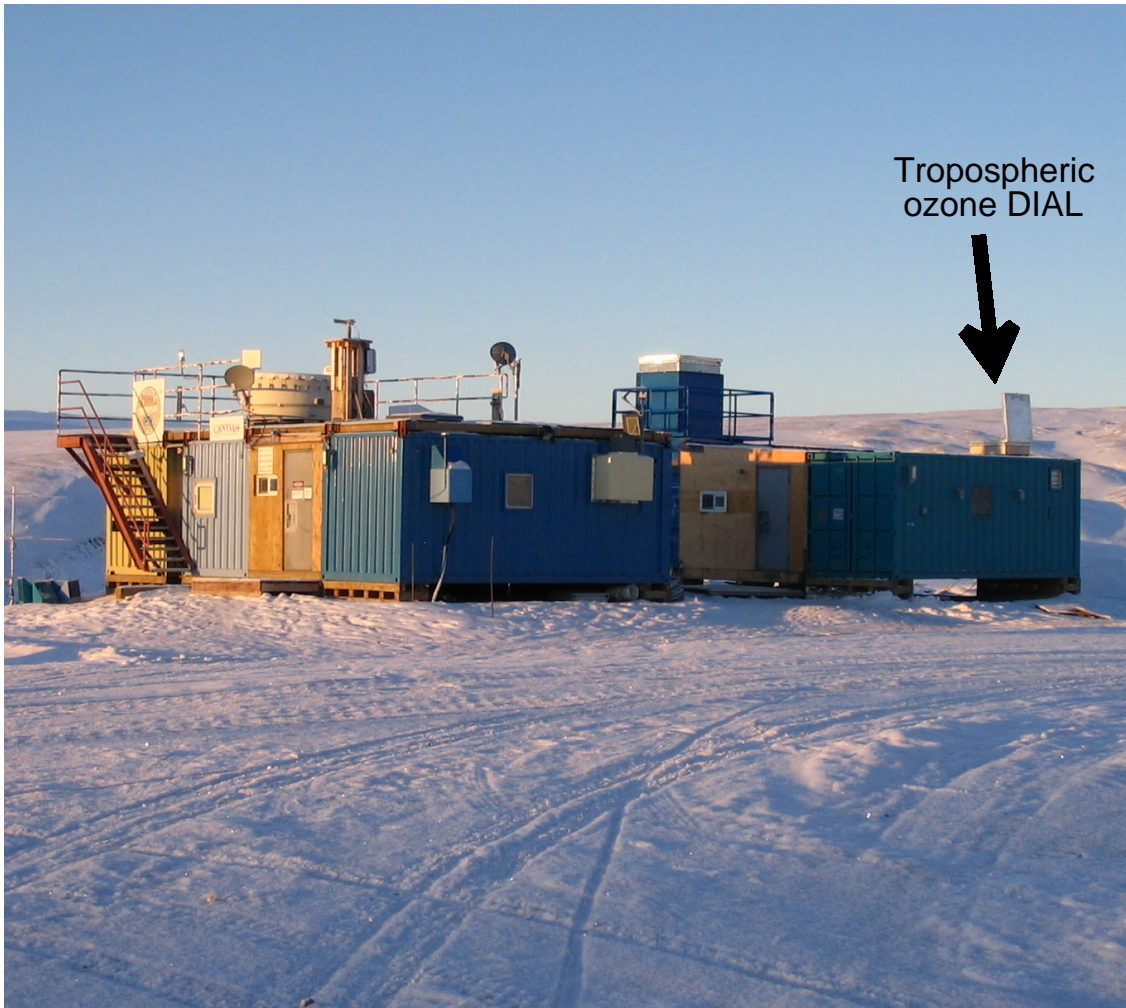
Figure 5.2: The Zero Altitude Pearl Auxiliary Lab (0PAL) housing the tropospheric ozone DIAL at Eureka NU. The open hatch for the tropospheric ozone DIAL can be seen on the top of the right-most structure.

tions ($O_3 < 20$ ppbv) ranged in altitude from $400 - 1500$ m, and all observed depletions were connected to the surface. Back trajectory calculations of the air measured over Eureka show that depleted air masses originated from over the arctic sea ice and had direct contact with the ocean surface for long periods of time through turbulent mixing in the atmospheric boundary layer. Periods in which no ozone depletions were measured occurred when the air measured over Eureka originated from over land, or from the free troposphere. In both cases, no extended periods of direct contact with the ocean surface occurred. The origin of the measured air masses was also found to have direct implications on the temperature of the measured air. Air that was in contact with the sea ice was found to have lower potential temperature than air that originated from above the atmospheric boundary layer, leading to a direct correlation between the vertical structure of the ozone depletions and the vertical potential temperature profiles measured over Eureka.

The vertical structure of the ozone depletions over Eureka was found to differ from depletions measured by the DIAL directly over the sea ice (Seabrook et al. 2011, 2013). Unlike the previous chapters in which vertical ozone profiles were measured directly over the sea ice (Chapters 3 and 4), Eureka is an inland weather station surrounded by mountainous terrain. It will be shown that the topography of Ellesmere Island has a direct impact on the vertical structure of the ozone measured over Eureka. The vertical depth of the depletions over Eureka exceeds the typical height of the ABL in the Arctic

due to the influence of surrounding mountain ranges. The terrain was also responsible for increases in ozone measured over Eureka, as mountain blocking effects prevented the ozone depleted air in the ABL from reaching inland. This effect was assessed using a Froude number analysis to estimate the flow blocking potential of the surrounding terrain. A link will be established between periods of non-depletions over Eureka, and the flow blocking of boundary layer air from over the sea ice.

5.2   DIAL installation

The Eureka DIAL system was constructed and tested at York in the summer of 2007, and then assembled at Eureka in September of the same year. The DIAL was installed inside a modified shipping container that was wired for electricity and heating, and connected to a central causeway with a collection of containers housing other scientific equipment (Fig. 5.2).

The lidar viewed the atmosphere through an anti-reflective (AR) coated quartz window mounted at the bottom of an insulated chimney that extends down into the DIAL lab (Fig. 5.3a). When the lidar was not in operation the window was protected from the elements by a metal hatch installed on the roof of the container (Fig. 5.2) that was opened and closed manually.

Due to the possibility of a large thermal gradient across the window interface, frost formation on the window was a concern. In order to alleviate this issue, the window was

mounted at the bottom of a chimney that extended into the shipping container so that it was easily accessible to the operator for inspection and cleaning. This also allowed heated air to be passed over the window in order to ensure frost free operation, but this extra step was typically not needed.

A schematic diagram of the DIAL system is shown in Figure 5.5 and photographs are shown in Figures 5.3 and 5.4. The fourth harmonic of a Q-switched Nd:YAG laser (266 nm, 70 mJ per pulse, 20 Hz repetition rate) was focused into a gas cell filled with 140 PSI of CO_2 to generate pulsed light at wavelengths 276 nm, 287 nm and 299 nm by stimulated Raman scattering (Nakazato et al. 2007) and then directed along the zenith into the atmosphere. Full overlap between the emitted laser pulse and the telescope field of view occurred at a range of approximately 250 m and the signal received from below that range was not used in the ozone analysis.

Backscattered light was collected with a 20 cm off axis parabolic mirror and a 1.5 mm diameter optical fiber positioned in the focal plane, 1000 mm from the mirror, to form a receiver field of view of 1.5 mrad. Initially the three wavelengths were separated by splitting the collected light with a pair of partially reflective 50/50 mirrors, and directing a portion of the separated light through the appropriate interference filter as seen in Figure 5.5. In 2009 the receiver was upgraded to a tilted filter model (identical to the receiver shown in Figure 2.3) in which the three wavelengths were separated by the transmittance and reflectance from interference filters tilted at angles of 5 degrees and
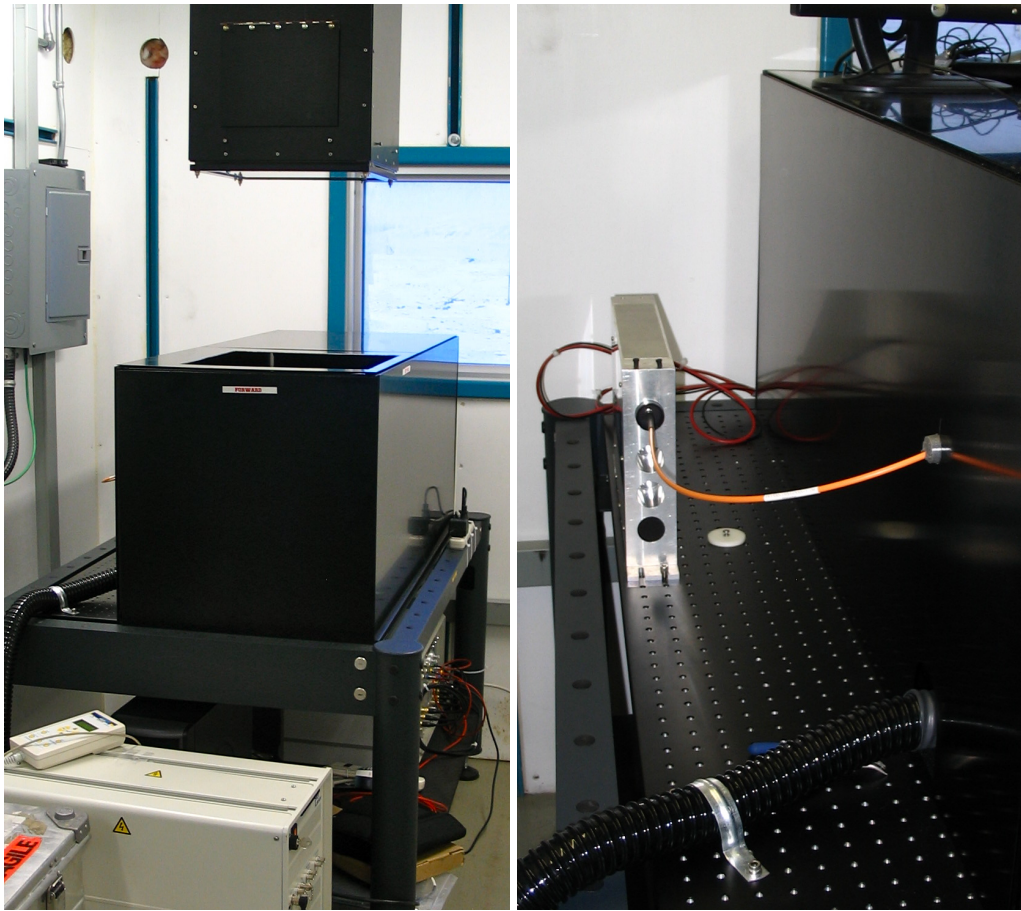
(a) Ozone DIAL installation at Eureka.　　(b) Optical fiber to spectral filter box.

Figure 5.3: Ozone DIAL installed at Eureka.
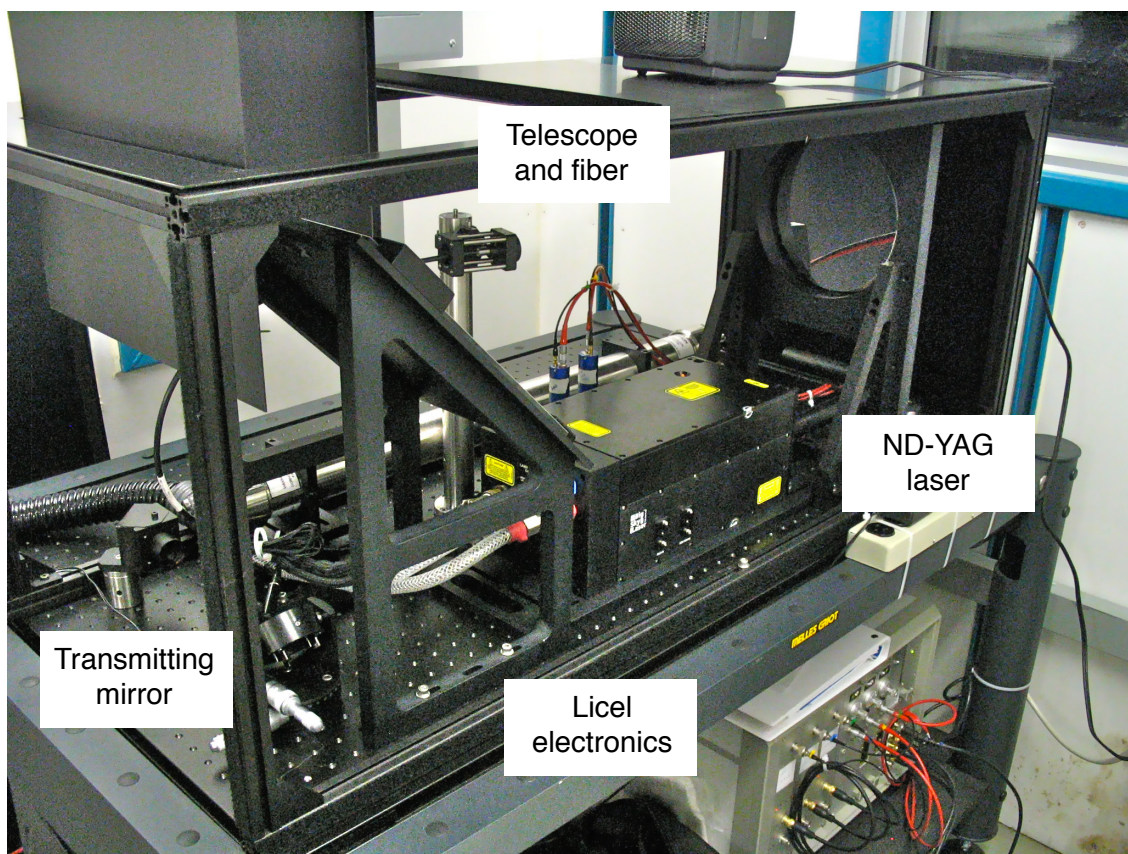
Figure 5.4: Ozone DIAL installed at Eureka.

having bandwidths of 1 nm.

In both cases, photomultiplier detectors generated electrical signals that were recorded using photon counting for the weak signals from distances greater than 1.8 km and using analog to digital conversion for the strong signals in the near range. The raw data was recorded with a range gate of 7.5 m and an integration period of 1200 laser shots (1 min). During data processing the collected lidar profiles were averaged both spatially and temporally in order to reduce the measurement uncertainty. The amount of averaging applied is dependent on the desired measurement range. The 276/287 nm analog signals were used below a height of 1.8 km and the 287/299 nm photon counting signals were used at greater heights.

Data was recorded by a Windows PC installed in the lab and connected to the LICEL data acquisition electronics. Collected data sets were automatically uploaded to a FTP server and made available for analysis, typically the next day.

5.3   Topography of Ellesmere Island

The Arctic Cordillera mountain system covers much of Ellesmere Island, with some features exceeding heights of 2500 m. Running along the North of Ellesmere island are a series of mountain ranges running approximately 400 km from the southeast to the northwest, it is a major topographic feature interacting with air originating from over the sea ice to the North of Ellesmere Island.
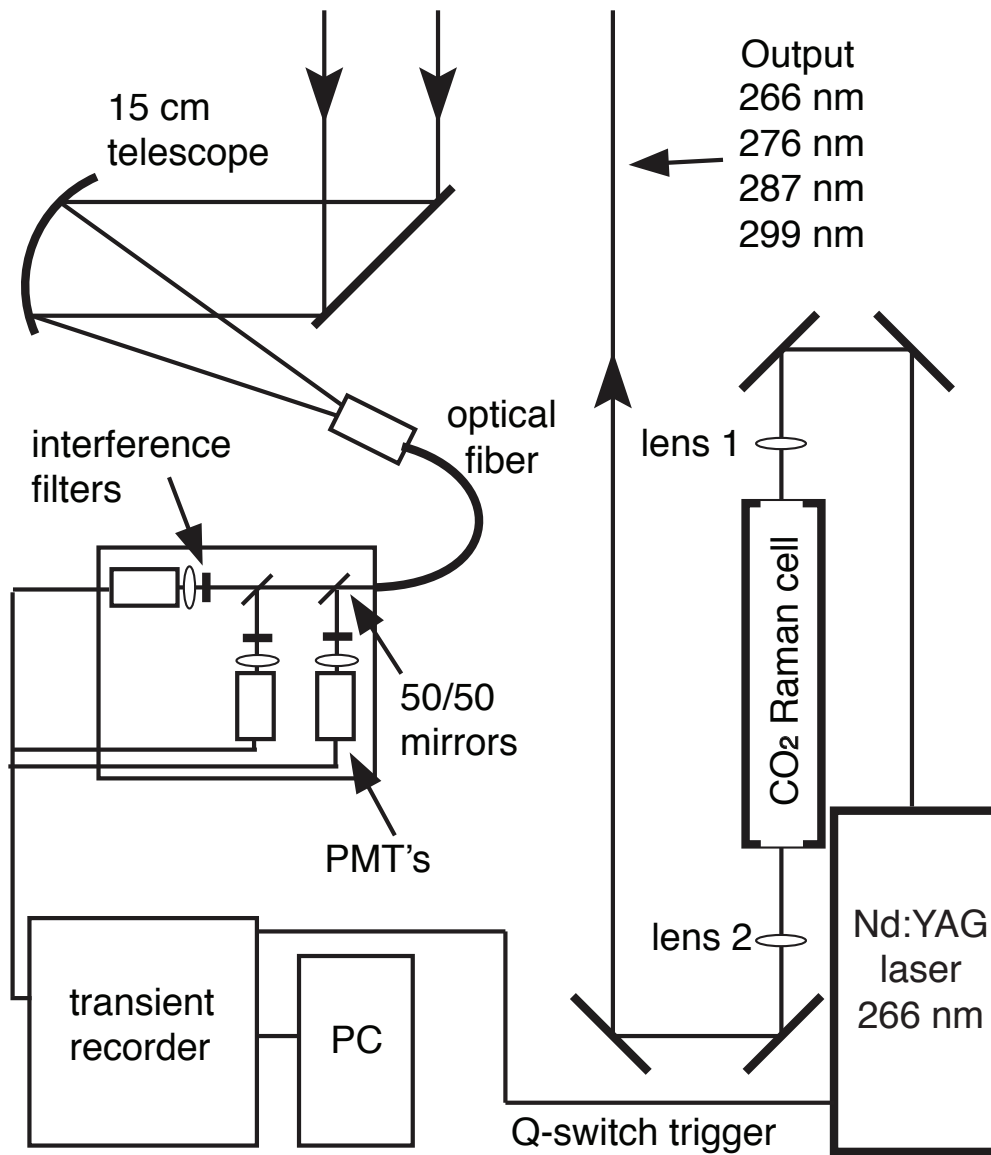
Figure 5.5: Schematic of the Eureka ozone DIAL (DIAL-A).

Fig. 5.6 shows the topography of Ellesmere island, with Eureka indicated on the map at 85° W, 80° N. Air from over the sea ice typically originates from the North or the East and this air interacts with the British Empire mountain range that runs for approximately 400 km across the northern edge of Ellesmere island, and a mountain range with features up to 2000 m in altitude that runs parallel to the British Empire range for approximately 200 km to the East of Eureka.

It was observed that the traversal of these mountain ranges by air originating from over the sea ice had a significant affect on the vertical structure of ozone measured over Eureka. No surface ozone depletions were observed during periods in which air near the sea ice surface was blocked by topography. Ozone depletion events were observed when the air nearest to the ice surface reached Eureka. This air arrived at Eureka due to having no interaction with the mountain ranges, or by flowing over the topography.

5.4   Froude number

While a comprehensive treatment of mesoscale dynamics is beyond the scope of this work, a basic overview will prove insightful into the dynamics of the air measured over Eureka, and the effect of Ellesmere Islands' topography on the ozone concentrations measured in the troposphere over Eureka. The effects on air flow due to topography can be generally be described in terms of the Froude number (Smith 1980, Wang and Chen 2003). In this case the Froude number expresses a non-dimensional ratio of the wind
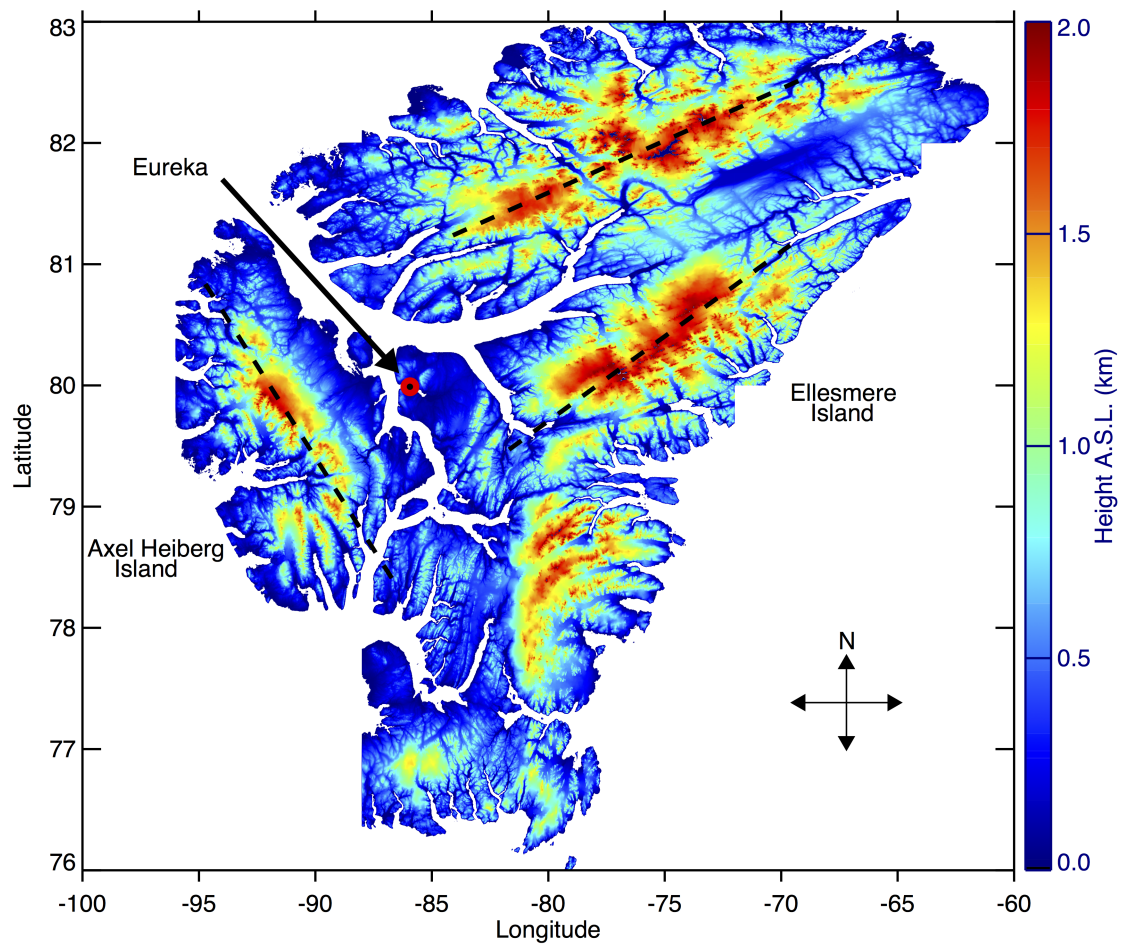
Figure 5.6: Topography of Ellesmere Island and Axel Heiberg Island.

orthogonal to the mountain range versus local atmospheric stability (determined by the potential temperature profile between the surface and mountain top) and is given by

$$F_r = \frac{U}{h_0 N_A} \tag{5.1}$$

where h_0 is the height of the feature relative to the surrounding topography, U is the wind component orthogonal to the geographical feature and N_A is the average Brunt-Väisälä Frequency (the oscillation frequency of a vertically displaced air parcel within a statically stable environment). Using the method of Reinecke and Durran (2008) in which the Froude number can be calculated under conditions in which the Brunt-Väisälä frequency is nonuniform with height, the average Brunt-Väisälä frequency between the surface and the height of the mountain h_0 is given by

$$N_A = \frac{1}{h_0} \int_0^{h_0} N_z \, dz \tag{5.2}$$

where

$$N_z = \left(\frac{g}{\theta_0} \frac{\partial \theta_z}{\partial z} \right)^{\frac{1}{2}} \tag{5.3}$$

where θ_z is vertical profile of the potential temperature, g is the local acceleration of gravity, and z is the geometric height of the air mass.

Calculation of the Froude number will give a general indication of whether air will

flow over a topographic feature, or be blocked due to a lack of kinetic energy required to flow over the top of the feature. There are three general Froude regimes which are considered here. When $F_r < 1$, then the kinetic energy of the air mass is insufficient to carry the air over the topography. When this occurs the air is diverted and flows around the obstacle, or in the case of large mountain ranges, is blocked. This horizontal divergence is compensated for by the descent of warm air from aloft (Smith 1980, Wang and Chen 2003). When $F_r > 1$, then the airflow proceeds over the terrain and down the lee side with no significant oscillations. In the case of $F_r \approx 1$, then there is the likelihood of mountain wave activity.

5.5 Observations

The raw backscatter data were collected with one minute averaging (1200 laser pulses at 20 Hz). Vertical ozone profiles were derived from lidar return profiles that have been processed with a boxcar smoothing filter of width 60 minutes. The derived ozone profile from each day were processed independently and merged together to form the contour plot in Fig. 5.7. The boxcar smoothed analog signals used below height 1000 m were typically fit to a 1st order polynomial with a range of 22.5 m (3 bins). The polynomial fit for the photon counting signals was typically fit over 75 m up to range 1500 m (10 bins).

Atmospheric data used to correct for differential molecular scattering, and to determine the number density of the atmosphere were acquired from twice daily (midnight and noon UTC) radiosonde launches. Weekly ozonesonde launches were used to validate the DIAL ozone retrieval during periods in which an ozonesonde launch, and DIAL measurements coincided (see Fig. 2.6).

A contour plot of the measured ozone profiles taken during a measurement campaign during the spring of 2008 is shown in Figure 5.7. Two depletion events (labeled 1-2 in Fig. 5.7) ranging in maximum vertical depth from 800 m – 1500 m were recorded during this period and will be referred to as case 1 and case 2 respectively. The depletion event in case 2 ended with the descent of ozone rich air from the free troposphere. A period of enhanced ozone was observed over Eureka (Fig. 5.7-3) starting around 17 May. This

period of ozone enhancement will be referred to as case 3.

5.5.1 Case 1: 21 – 25 March 2008

A contour plot of the vertical profiles of measured ozone between 250 m and 1.5 km for the period of 21 – 25 March 2008 is shown in Figure 5.8. On 22 March, the ozone depleted air was accompanied by blowing snow near the surface. This interfered with the ability to retrieve ozone profiles from the lidar data, and was removed from data set. The missing data appears as a white gap in the contour plot.

The ozone depleted air was connected directly to the surface, with the lowest values of measured ozone found nearest to the ground. Above height 500 m the ozone mixing ratio generally started increasing with altitude until background levels of 30 – 40 ppbv were observed. The maximum vertical depth of ozone depleted air was measured to be 1300 m (Fig. 5.8-C) and occurred mid day on 23 March 2008.
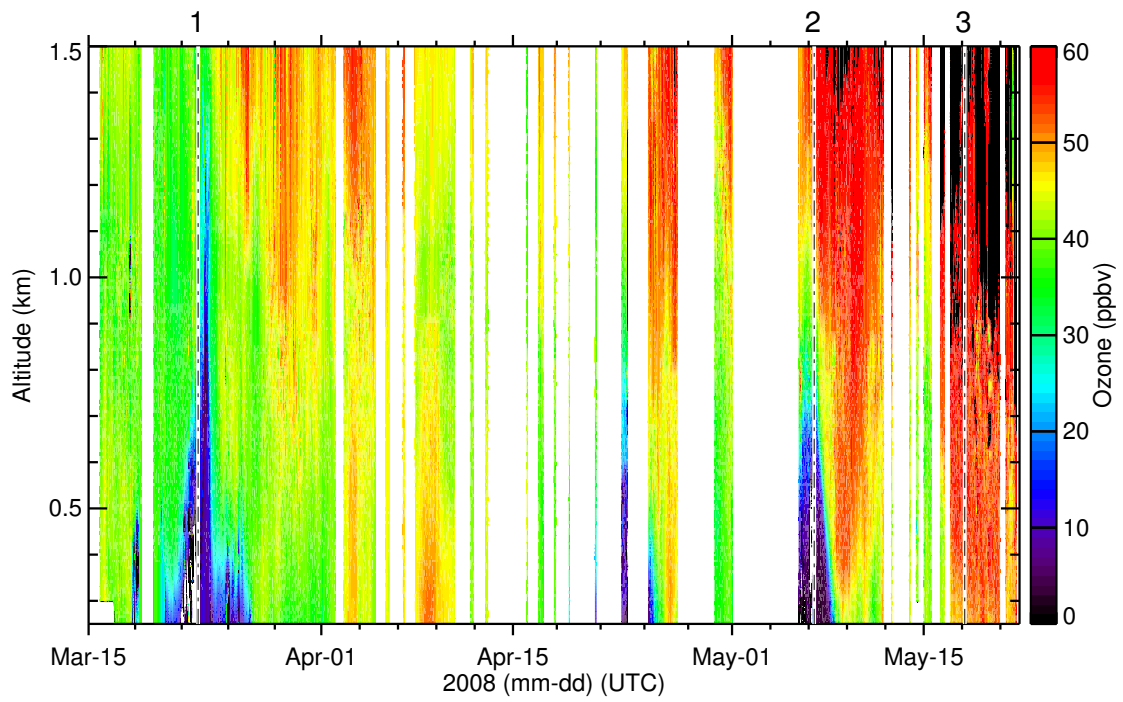
Figure 5.7: DIAL measurements of ozone during the spring months after polar sunrise at height above sea level from March – May 2008 at Eureka. Periods of interest are labeled as cases 1-3 at the top of the figure.
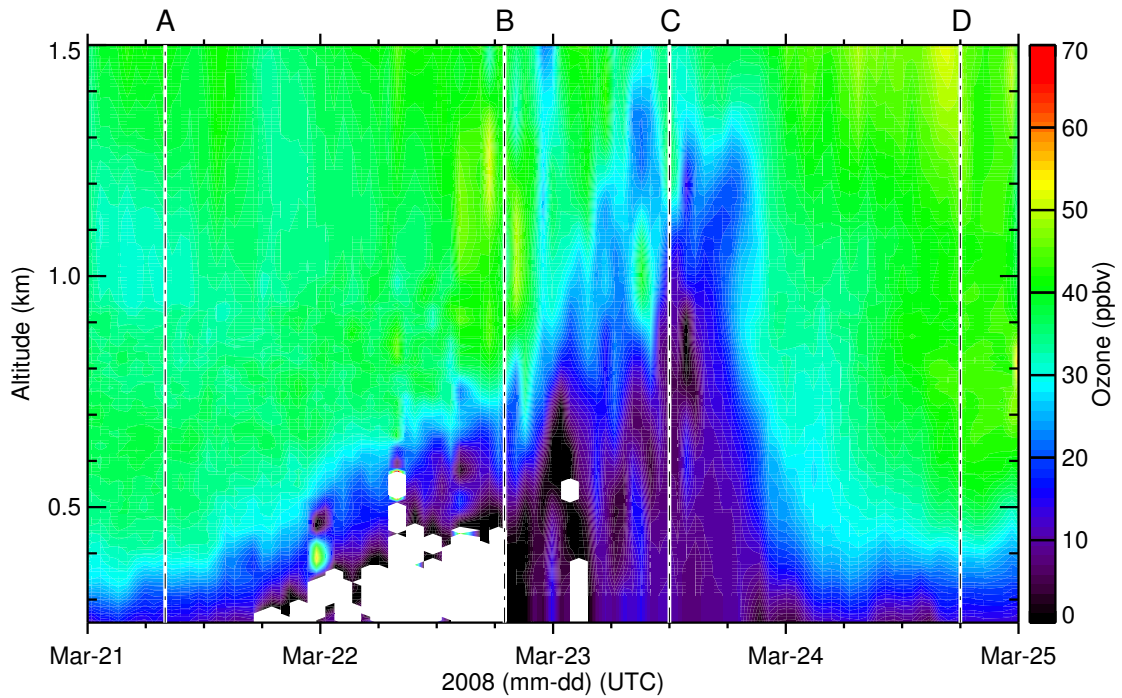
Figure 5.8: Case 1: DIAL measurements of ozone concentrations from 300 – 1500 m at Eureka from 21 – 25 March 2008. White gaps in the data indicate where ozone retrieval was not possible. Periods of interest are labelled A-D.
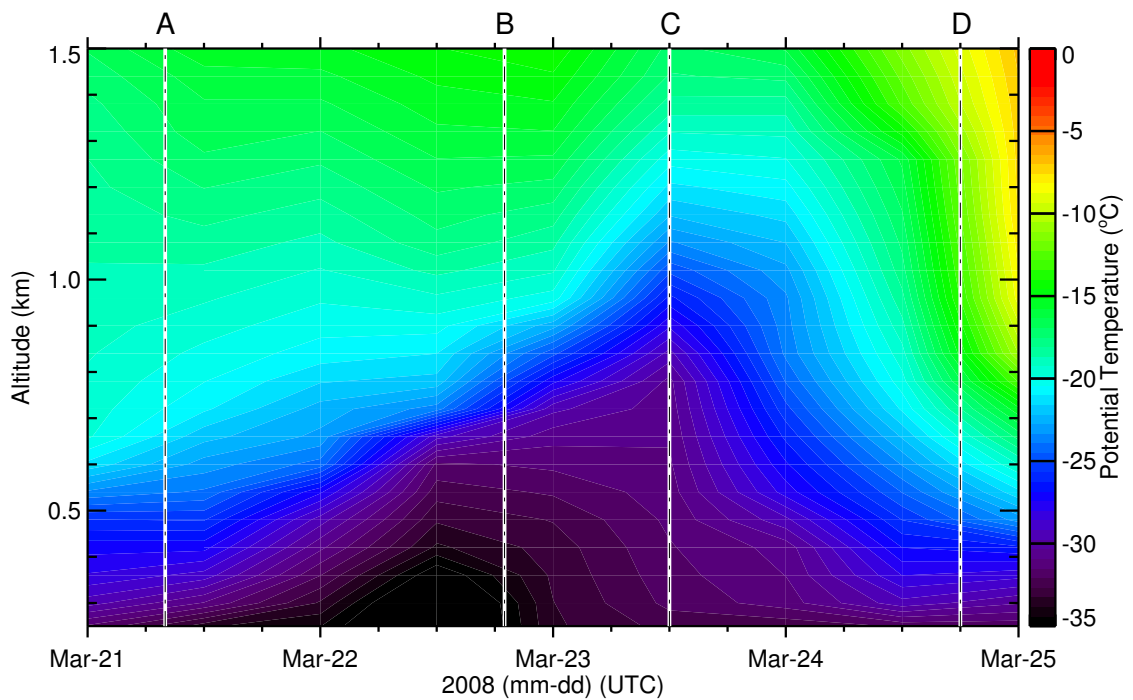
Figure 5.9: Radiosonde measurements of potential temperature from height 250 – 1500 m over Eureka from 21 – 25 March 2008.

5.5.2   Case 2: 6 – 8 May 2008

In early May 2008, nearing the end of the Arctic spring, an ODE extending to an altitude of 700 m occurred (Fig. 5.7-2). The onset of the depletion was not captured by the DIAL due to precipitation.

Figure 5.10 shows the ozone concentrations derived from DIAL measurements at Eureka from 6 – 11 May 2008. An ODE extending up to an altitude of 700 m was recorded between 6 – 8 May 2008 (Fig. 5.10 cases A-B). The period immediately following the depletion was notable due an ozone enhancement event in which higher than normal levels of ozone were recorded in the lower troposphere. During the depletion event the elevated concentrations of ozone were measured above an altitude of 1100 m, and began extending towards the ground as the ODE dissipated. (Fig. 5.10 cases C-D). As with case 1, interference from blowing snow near the surface resulted in periods of time in which ozone retrieval from the recorded data was not possible.

A correlation between low temperatures and ozone depletions has been previously noted by a number of studies (Nghiem et al. 2012, Pöhler et al. 2010, Zeng et al. 2003), as well as a link between ozone depletions and downward trending potential temperature (Koo et al. 2012, Zeng et al. 2003). Radiosonde measurements (Fig. 5.11) show the presence of lower temperatures over Eureka starting on 3 May 2008, marking this date as the likely beginning of the ozone depletion.

Figure 5.10: Case 2: DIAL measurements of ozone after polar sunrise at Eureka from 6 – 12 May 2008. Periods of interest are labelled A-D.

Figure 5.11: Potential temperature over Eureka calculated from radiosonde measurements of temperature 6 – 12 May 2008.

5.5.3   Case 3: 16 – 21 May 2008

Between 16 – 21 May 2008 (Fig. 5.7-3), the ozone DIAL was in near continuous operation and measured enhanced levels of ozone over Eureka down to an altitude of 250 m. The derived ozone from the period between 14 – 21 May at altitudes between 250 – 1500 m is shown in Figure 5.12. No ozone depletions were recorded during this period, but higher than normal concentrations of ozone were observed descending over Eureka between 15-17 of May, with concentrations of 55 ppbv measured near the surface, and reaching up to 70 ppbv at an altitude of 1 km. On 15 and 16 of May, it was observed that downward transport of ozone rich air from the free troposphere occurred at a rate of approximately $1.4\,\mathrm{cm\,s^{-1}}$. This ozone enhancement near the surface was observed by the DIAL for a period of four days.
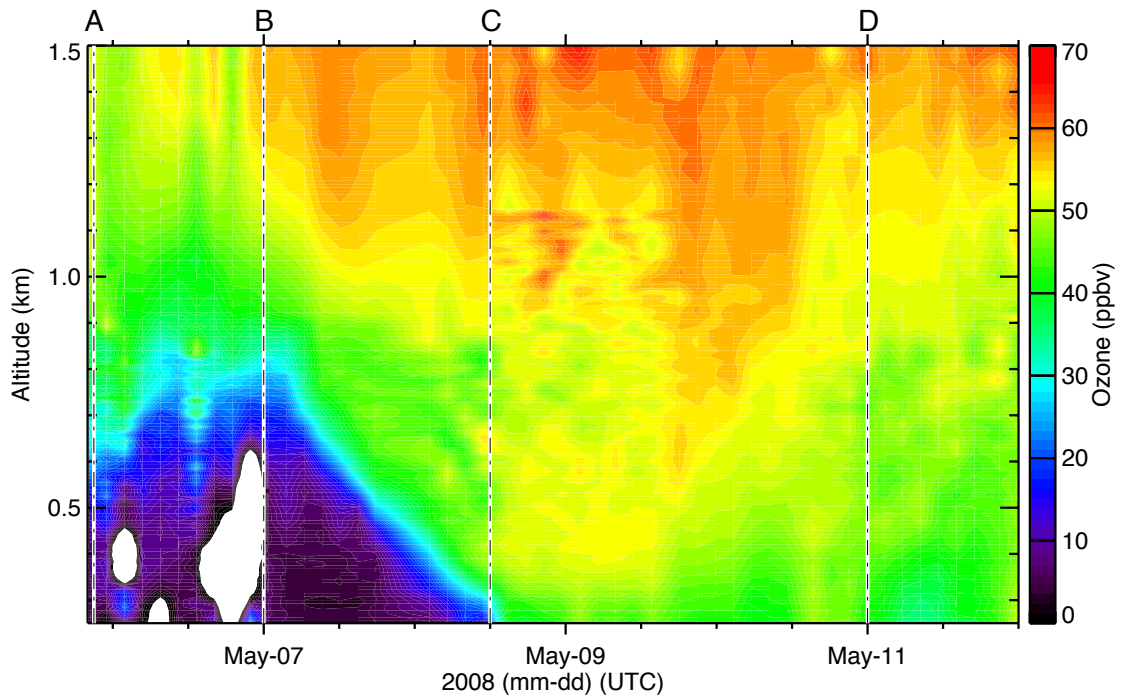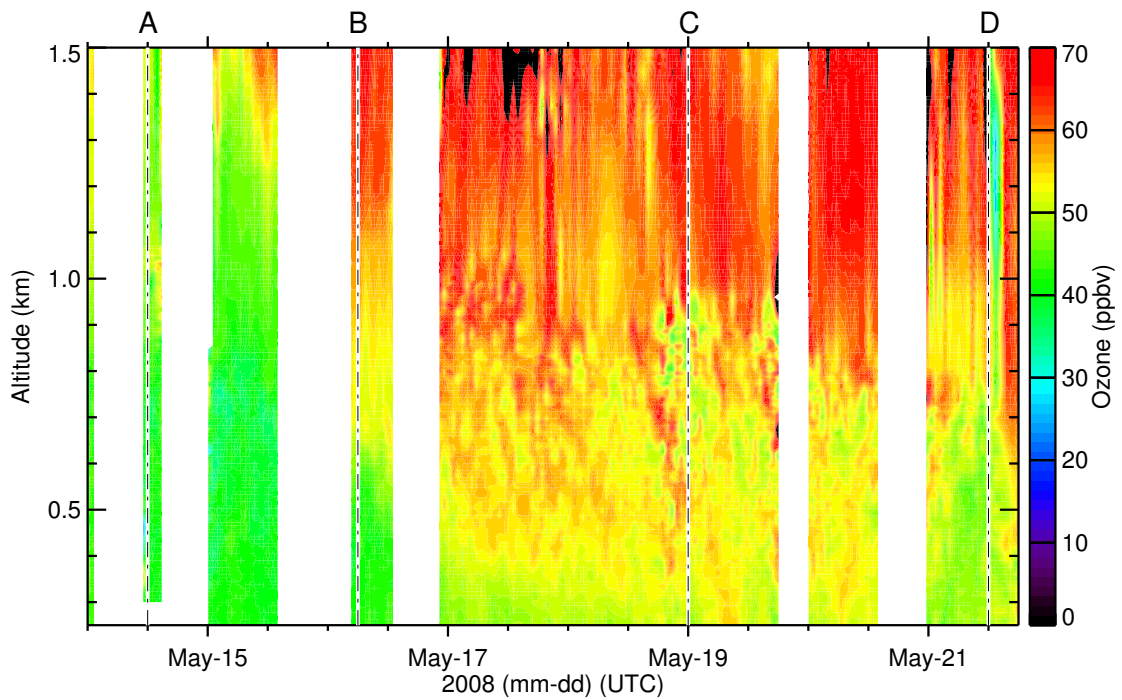
Figure 5.12: Case 3: DIAL measurements of ozone after polar sunrise at Eureka from 14 – 21 May 2008. Periods of interest are labelled A-D.
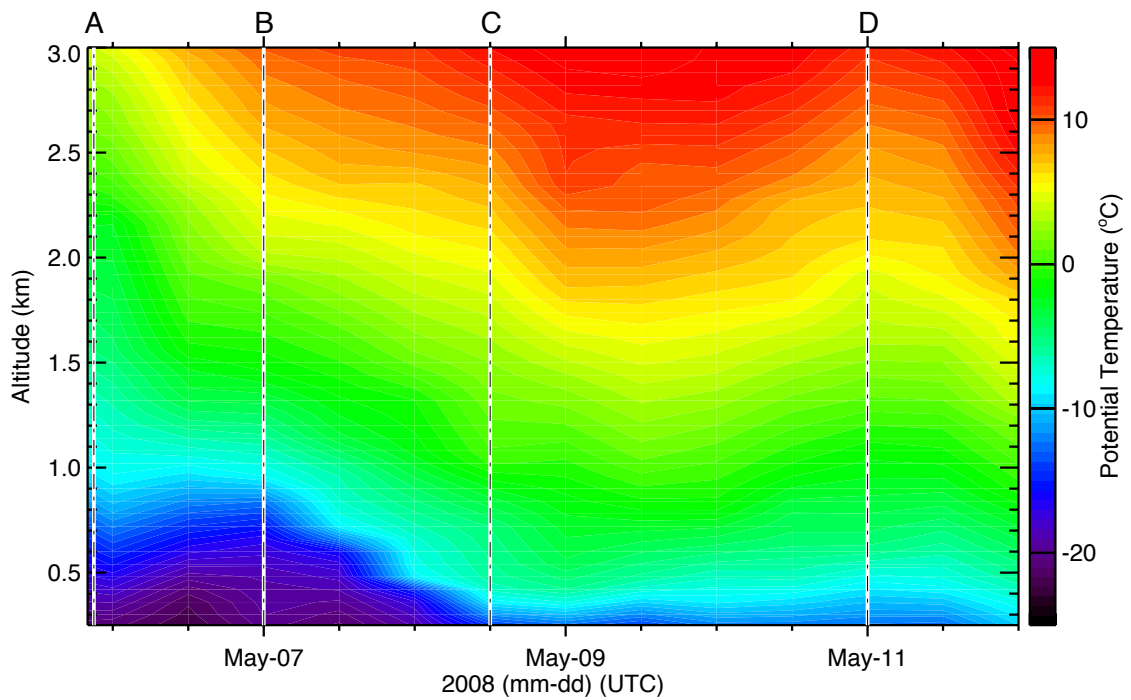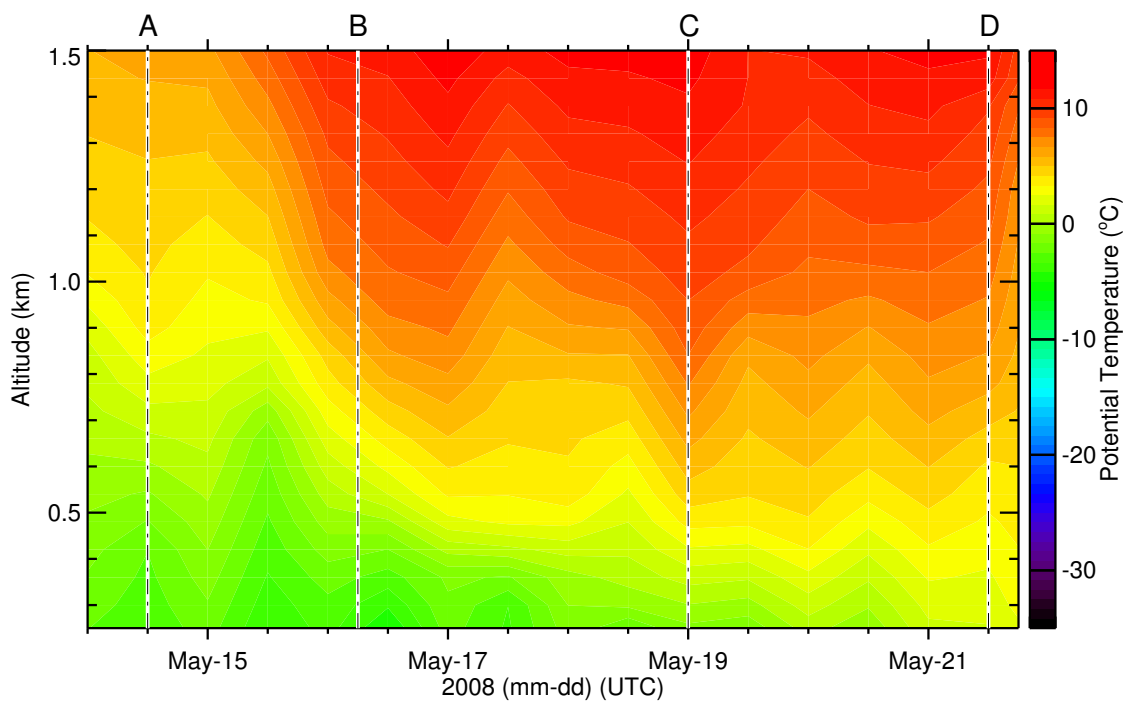

Figure 5.13: Potential temperature over Eureka calculated from radiosonde measurements of temperature 14 – 21 May 2008.

97

5.6 Analysis

Back trajectory calculations of the air measured over Eureka were performed. For each case discussed in the previous chapter, back trajectories were started at various points in time (labeled A-D in Figures 5.8, 5.10 and 5.12 for cases 1-3 respectively) for heights ranging from $100\,m - 1000\,m$ ASL and were calculated for a 6 day ($144\,h$) period backwards starting from the location of the Eureka lidar installation at $79.99° N$, $85.94° W$. The HYSPLIT model using the GDAS data set was used to determine the atmospheric back trajectories.

For instances in which a back trajectory indicated an earlier interaction between air measured over Eureka, and mountainous features over height $300\,m$ at the sea-land boundary of Ellesmere island, a Froude analysis (Section 5.4) was performed on the air mass as it interacted with the topography, in order to evaluate the potential for flow blocking as the air passed over the terrain. In order to calculate flow blocking potential, back trajectories were followed back to the time and location in which the air interacted with mountainous terrain. Vertical profiles of pressure, temperature, wind speed and wind direction at the selected time and location were extracted from the GDAS1 model and terrain height was taken from the terrain profiles calculated from the back trajectories. An example calculation of the Froude number is given below.

Figure 5.14 shows the potential temperature and orthogonal wind speeds calculated

from the GDAS data set for air located at 83° N, 75° W. Air from this location was measured over Eureka on 11 May 2008 during a period of time in which higher than normal levels of ozone were recorded.

For each Froude number determination, the back trajectories of air measured over Eureka were followed back until a period of time when the air was over the sea ice, just prior to any interaction with the terrain of Ellesmere Island. The GDAS1 data set is gridded with a resolution of 1° in latitude and longitude, the grid point nearest to the location determined by the air back trajectory was selected and the relevant atmospheric parameters (vertical profiles of the U and V velocity components of the wind, temperature and pressure) were extracted from the GDAS1 data set. The topography of Ellesmere Island was determined along the track determined by the back trajectories, and the highest geographic feature along that path was used to determine the value of the terrain height to be used in determining the Froude number. The relative orientation of three relevant mountain ranges (Shown as dashed lines in Fig. 5.6) was determined in general for each mountain range. The vertical profiles of potential temperature, as well as the wind component orthogonal to the mountain range direction were calculated (Fig. 5.14) for each back trajectory being investigated.

The average Brunt-Väisälä frequency is calculated from vertical profiles of potential temperature and wind velocity (Fig. 5.14) using equations 5.3 and 5.2. The Froude number is then calculated using equation 5.1. In this example case, the Froude number

was calculated to be 0.10, which falls into the $F_r < 1$ regime, indicating that air near the surface had insufficient kinetic energy to carry the air over the topography and was blocked by the terrain. The altitude history of the calculated back trajectory indicates that this horizontal divergence of blocked air was compensated for by the descent of air from an altitude of 2 km to an altitude of 500 m (Smith 1980, Wang and Chen 2003). This ozone rich, free tropospheric air was then measured over Eureka. The data used for this example corresponds to the back trajectory shown in Figure 5.18-D for the air measured over Eureka at an altitude of 500 m.

5.6.1 Case 1: 21 – 25 March 2008: Ozone depletion

The DIAL measured ozone profiles for the period of 21 – 25 March 2008 (case 1) are shown in Figure 5.8. Periods of interest are labeled A – D. For each of these periods A – D, the position and altitude history of the air measured at a number of different altitudes, have been calculated for a 144 hour period prior to the ozone measurement. These back trajectories are shown in Figures 5.15 and 5.16 respectively. The colour scheme of the plotted trajectories is consistent between the two figures with the colours red, green, yellow blue and black corresponding to air over Eureka at altitudes of 100 m, 300 m 500 m, 700 m and 1000 m above sea level. The air trajectories are shown as solid lines, and the vertical profile land features traversed by the air are shown as dashed lines of the same colour in Fig. 5.16.
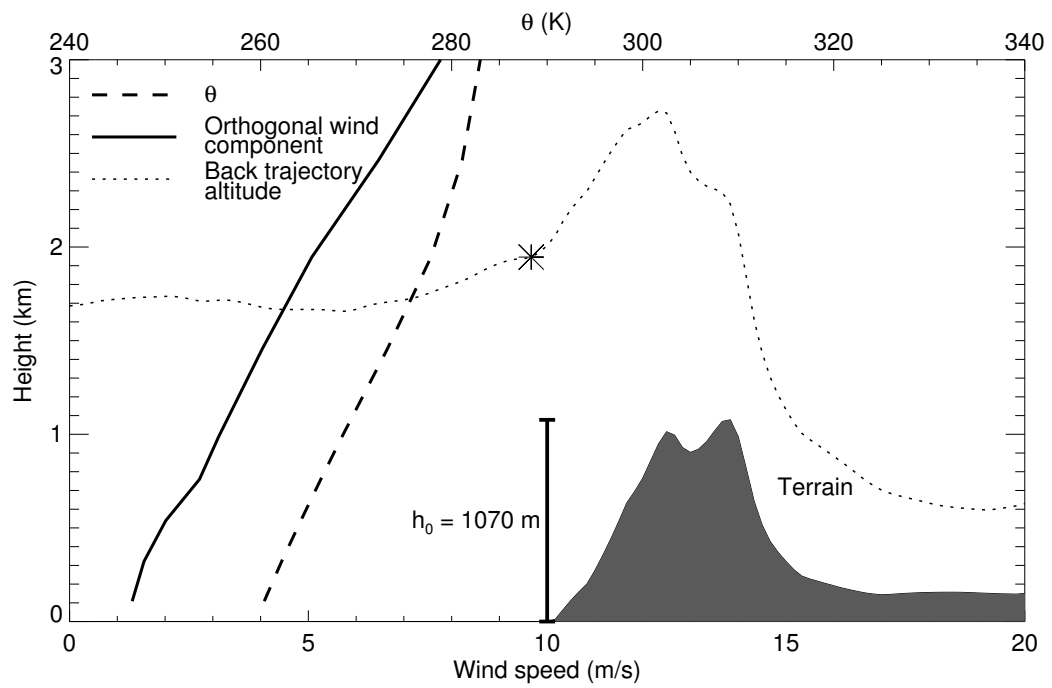
Figure 5.14: GDAS model sounding data used to calculate Froude number. Wind direction if from left to right.

Prior to 22 March 2008, the air originated from the south over the North American land mass (Fig. 5.15-A), travelling in a counterclockwise trajectory bearing North. On 22 March the origin of the airmass over Eureka shifted to the north (Fig. 5.15-B) with the air originating from over the arctic sea ice near the pole. The altitude history of the air (Fig. 5.16-B) during this period indicates that the air measured at 100 m and 300 m spent at a number of days within 500 m of the sea ice surface. During this period an ozone depletion from the ground up to a height of 500 m (Fig. 5.8-B) was observed over Eureka. This period was characterized by ice crystals in the lower atmosphere and moderately high winds ($5.5 - 8.5\,\mathrm{m\,s^{-1}}$) resulting in blowing snow near the surface. Due to the interference from the snow and ice crystals up to an altitude of 400 m, accurate retrieval of ozone concentrations below 400 m are not possible during this period.

The maximum vertical depth of the depletion occurred on 23 March 2008 (Fig. 5.8-C), the origin of the air over Eureka was from the west over the frozen Arctic Ocean (Fig. 5.15-C). The altitude history of the air during this time (Fig. 5.16-C) indicates that the air measured between 100 m and 1000 m ASL was in contact with the sea ice for much of the previous 6-day period, consistent with the previous observations showing that ozone depleted air typically has had an extended period of contact with the sea ice surface. Passage over the terrain near Eureka is responsible for the vertical depth of the depletion with ozone poor air measured up to 1200 m from the surface. During this period the wind speed of the air over Eureka increased to a value of $15\,\mathrm{m\,s^{-1}}$ between

200 – 800 m. Higher wind speeds appear to have allowed the boundary layer ozone depleted air to pass over the mountainous terrain and over Eureka, and returning to a greater height on the lee side of the mountains. This is most evident during this period of time when looking at the altitude history for the air measured at 700 m and 1000 m in (the orange and blue traces respectively in Fig. 5.16-C). Back trajectory calculations show that this air spent a long period of time adjacent to the sea ice before interaction with the mountainous terrain on Ellesmere Island.

Froude number calculations for the air at the land sea interface (Table 5.1) are consistent with the observed vertical structure of ozone concentrations, and the atmospheric conditions measured at Eureka. The low Froude numbers calculated for cases 1-A and 1-D indicate the likelihood of significant topographic blocking effects as the air passed over the vertical features of Ellesmere Island. This is apparent in the back trajectory altitude histories, (Fig. 5.16 A and D) where approximately 24 hours before ozone measurements were taken, air from higher altitudes descended to replace air that was blocked by vertical features reaching heights of nearly 1500 m. This topographic blocking corresponds to during periods when the ozone levels near the surface are high. This is particularly significant in case 1-D, where unlike case 1-A, the geographic origin of the measured air was over the sea ice. Had topographic blocking of the air adjacent to the sea ice not occurred, a strong depletion near the surface would have been observed.

In contrast, during the onset of the depletion event (case B) the height of the terrain

traversed by the air was less by approximately 600 m, and the calculated Froude number for the air originating at an altitude of 100 m over Eureka was 0.75, indicating that very little blocking of the air by the terrain occurred. For the back trajectories at higher altitudes the Froude number drops to below 0.3, indicating that that air at lower altitudes was blocked or diverted by the terrain, limiting the vertical depth of the depletion.

In case C, the effect of higher wind speeds combined with slightly lower terrain are reflected in the high Froude numbers calculated for this period of time as the air passed over the features seen in Figure 5.16-C approximately 20 hours before passing over Eureka. Air with a history of interaction with the sea ice surface flowed over the terrain with negligible topographic blocking and was measured at slightly higher altitude on the lee side of the terrain. The increase in Froude number is consistent with the wind speed increase measured between 22 and 23 of March, and with the increased depth of ozone depletion.

Vertical profiles of temperature from radiosonde launches during the period between March 21-25 (Fig. 5.11) show a marked decrease in potential temperature associated with ozone depleted air, supporting the back trajectory evidence that the ozone depletions originated during air/sea ice interaction leading to lower air temperatures, and that non-depleted air is warmer as a result of originating from lower latitudes, or from the free troposphere.
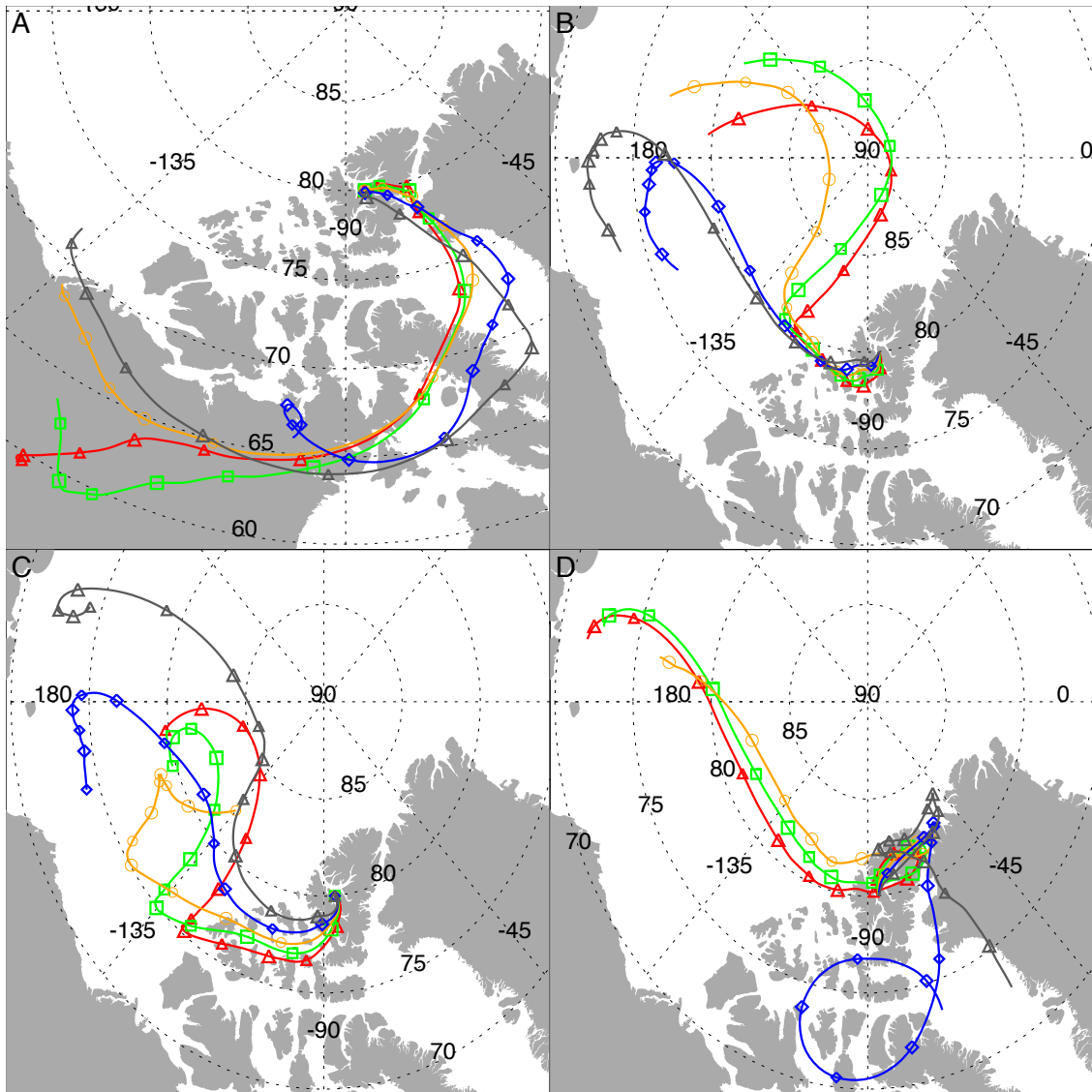
Figure 5.15: 6-day back trajectories of air measured over Eureka from 21 – 25 March 2008. Cases A – D correspond to the A – D labels in Fig. 5.8.
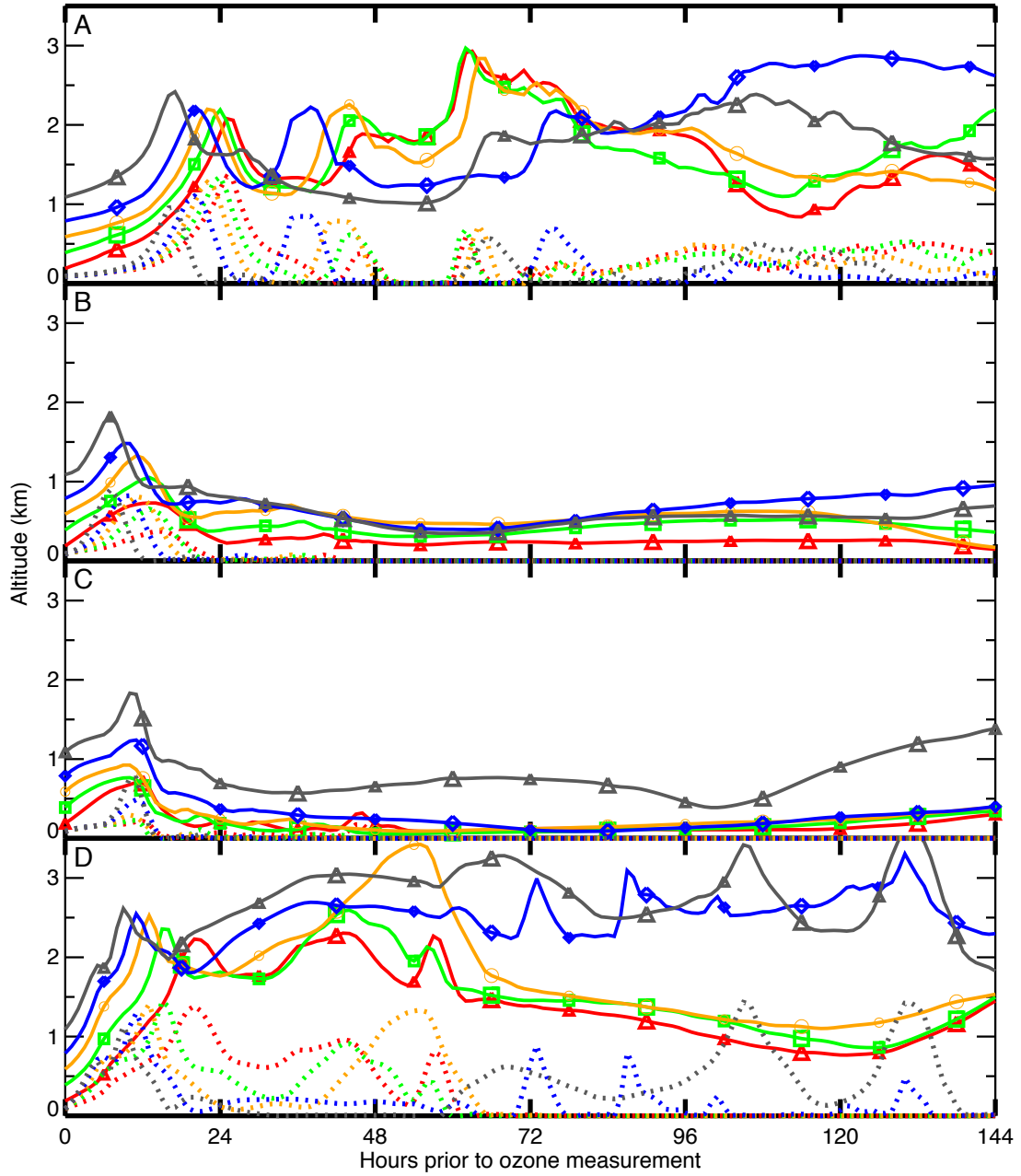
Figure 5.16: 6 day altitude history of air measured from 21 to 25 March, 2008. Cases A – D correspond to the A – D labels in Fig. 5.8. Red, green, orange, blue and grey correspond to air measured by the DIAL at altitudes of 100, 300, 500, 700 and 1000 m. Land below the back trajectories is shown as a dashed line in the corresponding colour.

Case	100 m	300 m	500 m	700 m	1000 m
1A	0.29	0.16	0.12	0.08	0.03
1B	0.74	0.23	0.30	0.29	0.27
1C	3.50	5.80	2.90	0.99	0.51
1D	0.07	0	0	0.13	0

Table 5.1: Froude number for air measured from 21 – 25 March, 2008. A – D correspond to the A – D labels in Fig. 5.8 for Case 1.

5.6.2 Case 2: 6 – 12 May 2008: Ozone depletion

Between May 6 – 8 2008, an ozone depletion event extending to an altitude of 700 m was recorded by the DIAL. The vertical ozone profiles are shown in Figure 5.10. Back trajectories of the air measured by the DIAL during the depletion event indicate that the ozone depleted air spent a period of time north of Eureka over the Arctic sea ice (Fig. 5.17 cases A-B) before passing over Ellesmere Island. The altitude history of the calculated back trajectories for cases A and B (Fig. 5.18 cases A-B) show that at the air measured at height 100 – 500 m over Eureka, (red, green and yellow plots respectively) was within 500 m of the ice surface for a number of days prior to measurement. In both of these cases, the ozone depletion was associated with the arrival of colder air. The potential temperature contour in Figure 5.11, indicates that during this period cooler air ($<$ -15 °C) has extended up to 700 m and closely mirrored the duration and vertical depth

of the ozone depletion.

Back trajectories (Fig 5.18) indicate that the air measured at Eureka passed over mountainous terrain when crossing the land/sea interface. Froude number calculations (Table 5.2 A - B) show that for the air measured nearest the surface, little to no blocking of air by the surrounding terrain occurred, allowing ozone depleted air to reach Eureka. This interpretation is supported by the radiosonde records from the same period of time (Fig. 5.11), showing colder air over Eureka up to an altitude of 1000 m at the time of the ODE. The source of this cold air mass is boundary layer air with a long history of close interaction with the sea ice surface.

Immediately following the ODE, the ozone DIAL recorded enhanced concentrations of ozone above Eureka that descended to 300 m over the surface (Fig. 5.10-C). The calculated trajectories show that the air measured over Eureka originated from over the surface of the sea ice (Fig. 5.18-C) and above the ABL from the free troposphere (Fig. 5.18-C), remaining at a height above 1000 m while over the sea ice.

The calculated trajectories indicate that the air measured over Eureka originated from above the a.b.l. until interaction with the mountainous topography of Ellesmere Island, which resulted in warm, ozone rich air from the free troposphere descending on the lee side of the mountain range before passing over Eureka. Atmospheric conditions at the time suggest that the cause for this was interaction with the mountain ranges on the northern portion of Ellesmere island that led to a low Froude number blocking situa-

tion in which the slow moving air below 1000 m was blocked by the terrain and the air at 1000 m and above was able to flow over the mountain ranges and replace the air at lower altitudes. Froude number calculations (Table 5.2) for cases C and D indicate that significant topographic blocking by the Ellesmere Island mountain ranges was likely, the altitude history (Fig. 5.18 C - D) of the air and the calculated low Froude number support the interpretation that interaction with the terrain resulted in topographic blocking, causing air from higher altitudes to descend, replacing the air displaced by the terrain. An increase in potential temperature during this period (Fig. 5.11-C), is consistent with the interpretation that warm ($\theta >$ -10 °C) ozone rich air from the free troposphere extended down to 300 m replacing the colder ozone depleted air from the previous day.

Case	100 m	300 m	500 m	700 m	1000 m
2A	2.5	1.1	0.46	.39	0.26
2B	1.3	0.89	0.69	0.45	0.17
2C	0.11	0.13	0.22	0.15	0.09
2D	0.14	0.11	0.21	0.22	0.24

Table 5.2: Froude number for air measured from 6 – 12 May, 2008. A – D correspond to the A – D labels in Fig. 5.10 for case 2.
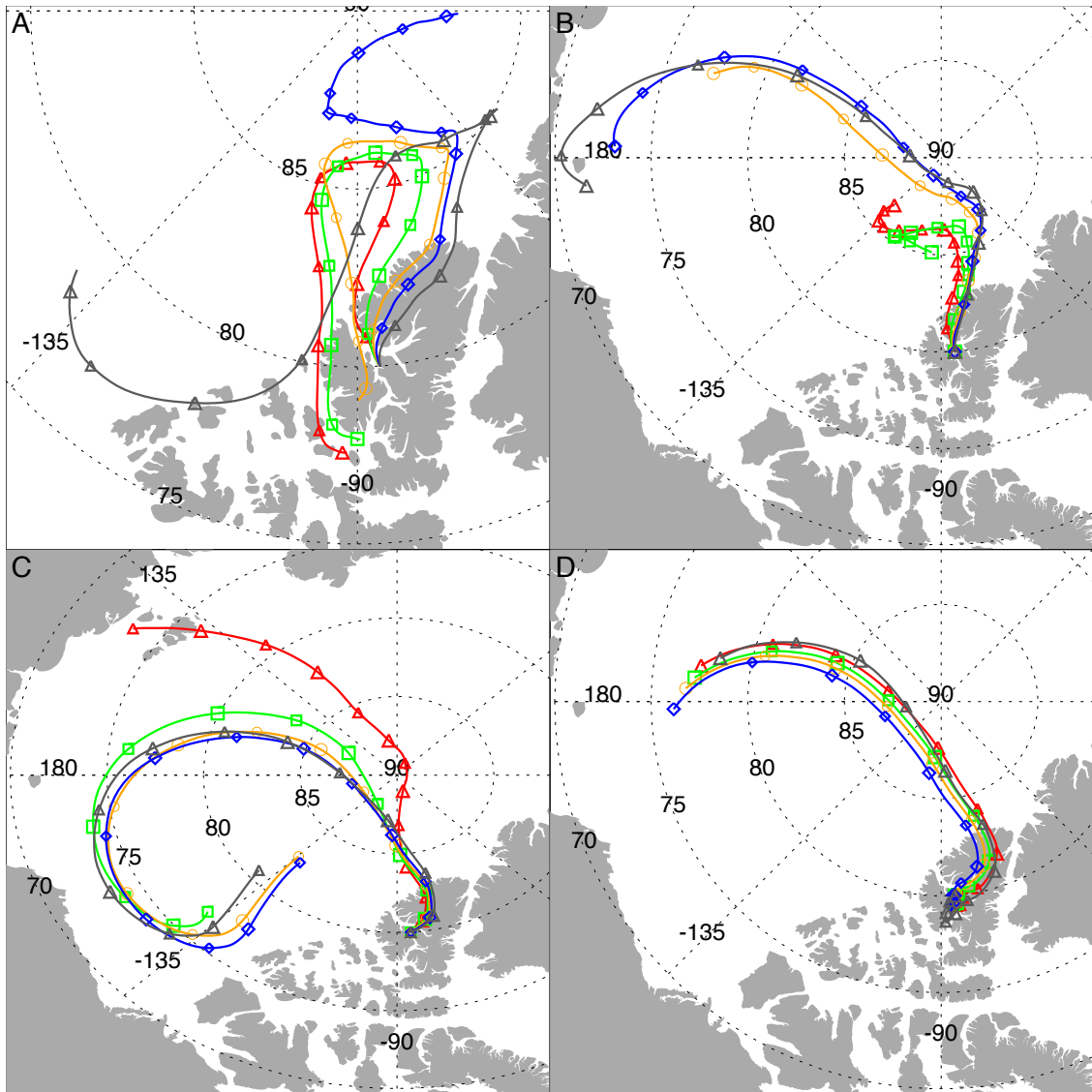
Figure 5.17: 6 day back trajectories of air measured over Eureka from 6-12 May, 2008. Cases A-F correspond to the A-F labels in Fig. 5.10.
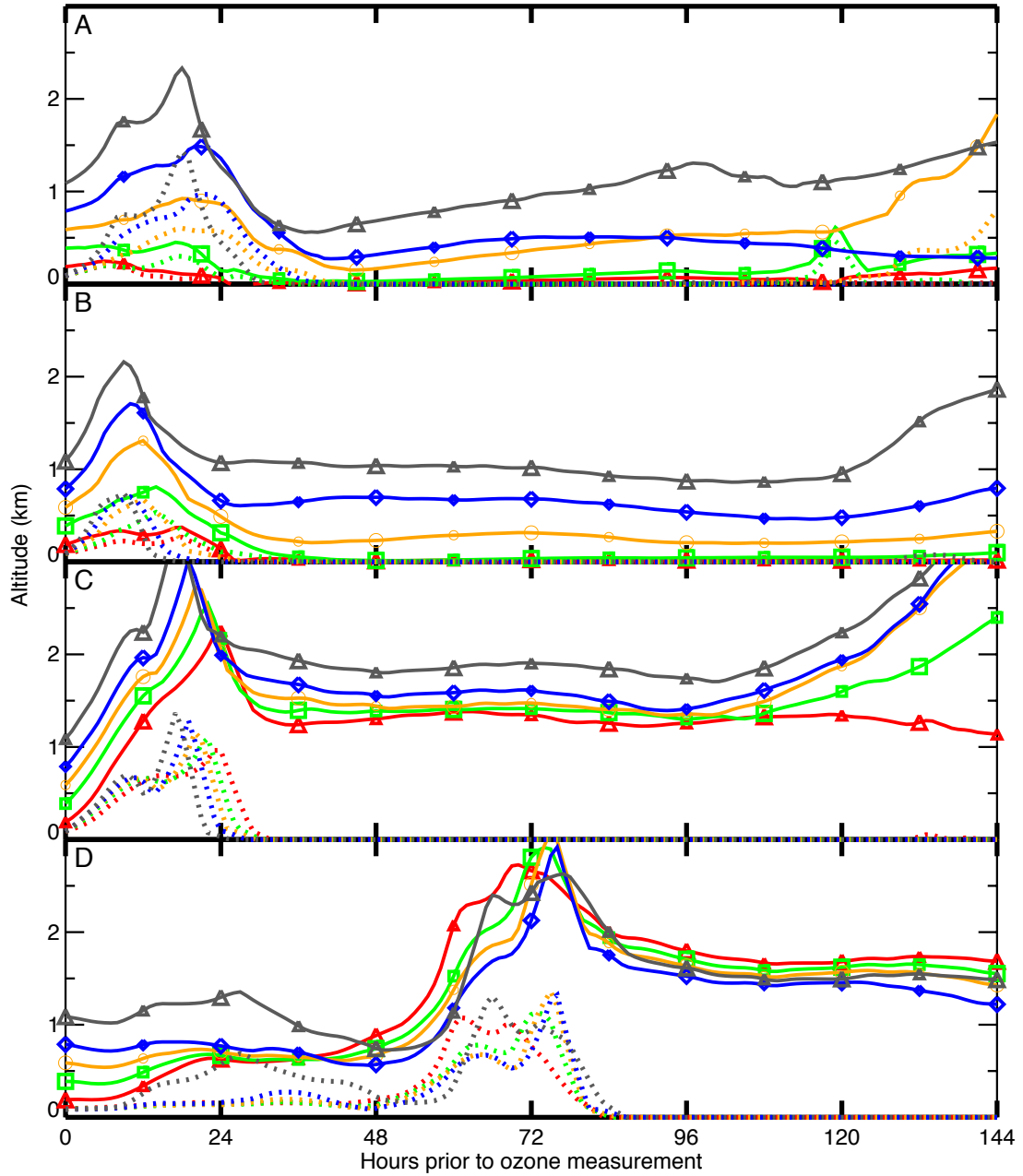
Figure 5.18: 6 day altitude history of air measured from 6 to 12 May, 2008. Cases A-F correspond to the A-F labels in Fig. 5.10. Red, green, orange, blue and grey correspond to air measured by the DIAL at altitudes of 100 m, 300 m, 500 m, 700 m and 1000 m. Land below the back trajectories is shown as a dashed line in the corresponding colour.
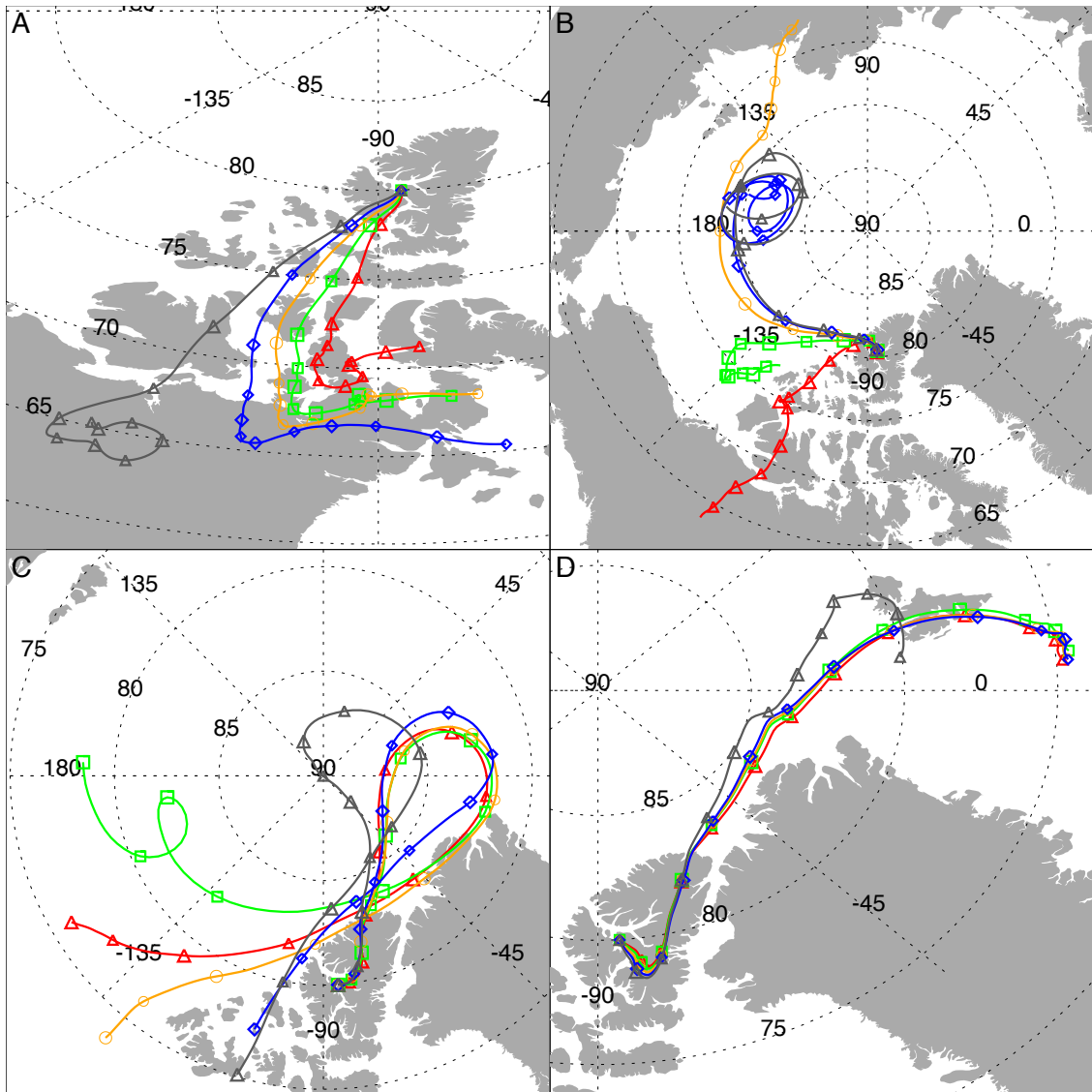
Figure 5.19: 6 day back trajectories of air measured over Eureka from 14 – 21 May 2008. A – D correspond to the labels in Fig. 5.12.
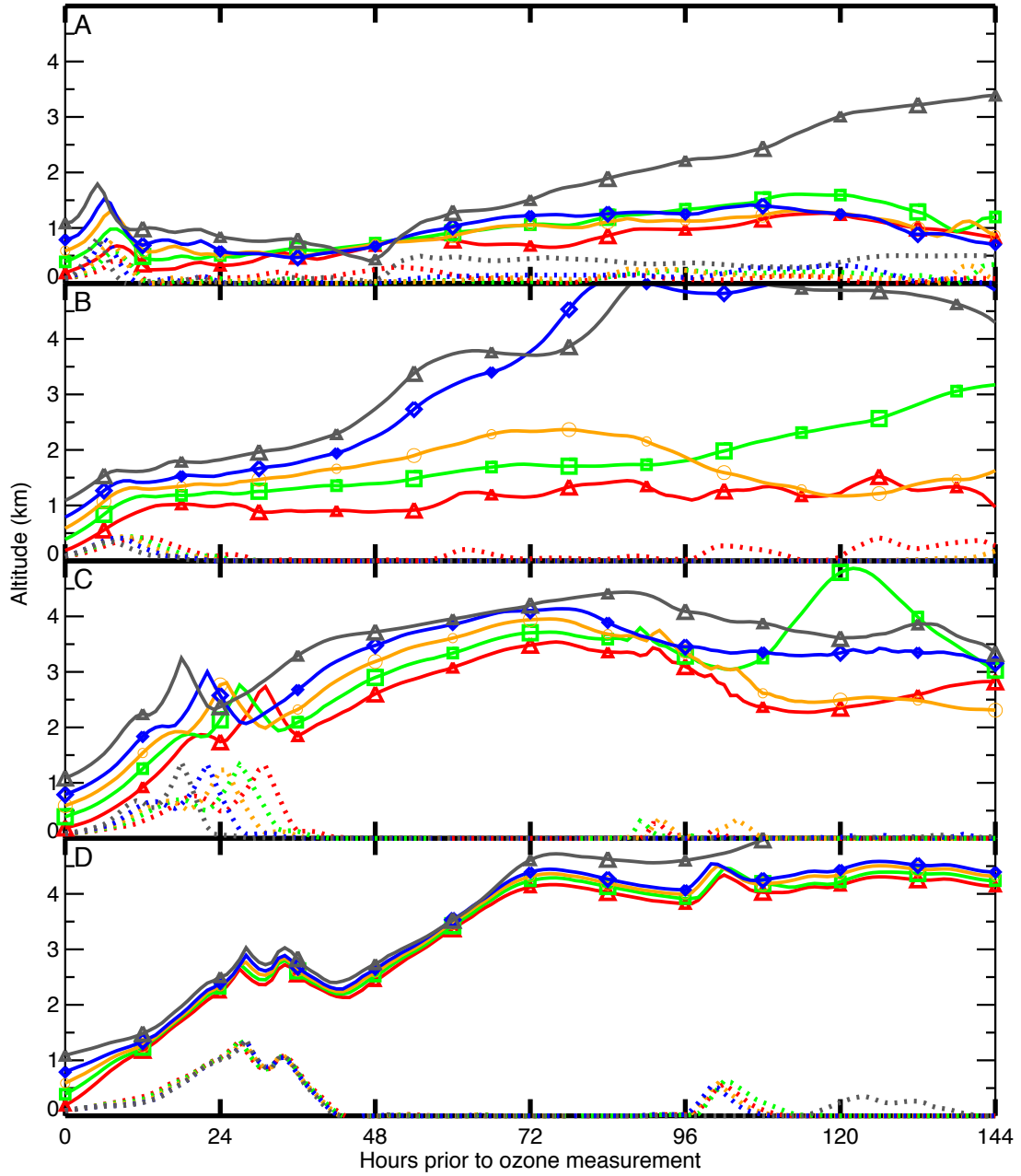
Figure 5.20: 6 day altitude history of air measured from 14 – 21 May, 2008. Cases A – F correspond to the A-F labels in Fig. 5.12. Red, green, orange, blue and grey correspond to air measured by the DIAL at altitudes of 100 m, 300 m, 500 m, 700 m and 1000 m. Land below the back trajectories is shown as a dashed line in the corresponding colour.

5.6.3 Case 3: 14 – 21 May 2008: Ozone enhancement

Between 16 – 21 May 2008 (Fig. 5.7-3), the ozone DIAL was in near continuous operation and measured enhanced levels of ozone over Eureka down to an altitude of 250 m over the sea ice. The derived ozone from the period between 14 – 21 May at altitudes between 250 – 1500 m is shown in Figure 5.12.

Case	100 m	300 m	500 m	700 m	1000 m
3C	0.02	0.07	0.21	0.22	0.14
3D	0.05	0.04	0.20	0.20	0.24

Table 5.3: Froude number for air measured from 14 – 21 May, 2008. A – D correspond to the A – D labels in Fig. 5.12 for Case 3.

Just prior to the ozone enhancement event, normal levels (≈ 40 ppbv near the surface) of ozone were recorded by the DIAL. An example of this is the ozone recorded on 14 May at noon shown in figure 5.12-A. During this period, back trajectories indicate that the air originated from the south from over the mainland and the southern islands of the Canadian Arctic Archipelago (Fig. 5.19-A). The air spent an extended period of time over land and at altitudes between 1000 – 2000 m ASL (Fig. 5.20-A). This air spent little time over sea ice (except for gaps between islands) and little time within the ABL. In this case no ozone depletion would be expected, and the dial measurements bear this out.

On 16 May, the DIAL measured increasing levels of ozone at an altitude of 1000 m up

114

to 60 ppbv at 1100 m (Fig. 5.12-B). Ozone levels near the surface remained consistent with the levels measured 18 hours previously (Case-A) but the contour clearly shows enhanced levels of ozone beginning to descend towards the surface over Eureka. Back trajectories show the air measured nearest the surface originated from the south from over the North American mainland and Canadian Arctic Archipelago, and the ozone measured nearest the surface is consistent with this. The same back trajectories also indicate that the air measured at higher altitudes had shifted in origin and originated from the east from over the arctic sea ice with origins north of Russia at $80°$ N air originated from the south from over the mainland and the southern islands of the Canadian Arctic Archipelago (Fig. 5.19-A).

The potential temperature profile (Fig. 5.13) shows that the temperature above Eureka above 500 m increased by $5°C$ over the same time period that the higher levels of ozone were recorded. The increase in potential temperature at these altitudes also matches with the back trajectories indicating a shift in the origin of the air measured by the DIAL above 300 m

Later in the week, from 17-21 May, the enhanced ozone episode continues, with high levels of ozone ($O_3 > 50$ ppbv) extending down to 250 m and reaching 60 ppbv at 800 m for a number of days (Fig. 5.12-C-D). During this period of time, back trajectories indicate that the air measured over Eureka between $100 - 1000$ m originated from the over the arctic sea ice to the north of Eureka (Fig. 5.19-C-D), from heights ranging

115

between $3000 - 6000\,\text{m}$ (Fig. 5.20-C-D), before passing over the northern mountain ranges on Ellesmere Island where it appears that blocking effects from the topography blocked the air below an altitude of $2000\,\text{m}$ from reaching Eureka.

Froude number calculations for cases C and D during the ozone enhancement yielded near zero values, indicating significant topographic blocking by terrain reaching heights between $1 - 1.5\,\text{km}$. This is consistent with the interpretation that ozone depleted air is not measured over Eureka when topographic features block the near surface ozone depleted air. Radiosonde records show an increase in potential temperature over Eureka during this time period, as well as the descent of warmer air from higher altitude that occurred at the same time as the ozone rich air, independently indicating that the source of the ozone rich air mass was the descent of warm air from the free troposphere.

5.7 Summary

The DIAL instrument at Eureka provided measurements of the vertical structure of tropospheric ozone between altitudes of $300 - 8000\,\text{m}$. A number of full and partial ozone depletion events were observed during polar sunrise seasons. Back trajectory analysis indicated that the air depleted in ozone spent extended periods of time within the atmospheric boundary layer over the sea ice. As with the results from the Amundsen, a strong positive correlation was found between ozone mixing ratio and the potential temperature measured by radiosonde launches at Eureka. Early in the spring no ODEs were found to

116

occur at any altitude when the potential temperature was higher than -25 °C. Later in the year as average temperatures in the Arctic increased a similar correlation was found. In this case the cutoff temperature was -13 °C, higher than that observed earlier in the year. This indicates that the temperature correlation is not the result of temperature dependent chemistry, but rather an indication that the ozone depleted air had a recent history of interacting with the colder surface of the sea ice. Periods of normal, or higher than normal ozone concentrations were recorded when sampling warmer air masses originating from the free troposphere that had no recent connection to the ground.

The observed ODE's correspond to two factors: prolonged periods over the Arctic sea ice within the atmospheric boundary layer, and low potential temperature. The implication is that the source for the measured ozone depletions was the long-range transport of ozone depleted air that was the result of extended contact with the frozen ice surface due to turbulent mixing within the atmospheric boundary layer.

The vertical depth of the depletions were found to be strongly influenced by the surrounding topography of Ellesmere Island. The interaction of ozone depleted air near the sea ice surface with the mountainous terrain, resulted in the vertical extension of ozone depleted air up to an altitude of 1500 m ASL

Additionally, topographic blocking of ABL air from over the sea ice was observed to be responsible for the erosion of depletion events, as well as the source of periods of ozone enhancement near the surface.

Froude number calculations during interaction between the air trajectories and the elevated topography of Ellesmere island indicate that the effect of the terrain has a significant effect on the vertical structure and depth of ozone measured at Eureka. Topographic blocking during periods in which wind speed is low leads to periods of time in which no depletions are recorded at Eureka, while depletion events occurred when measured air passed over terrain at most 1 km in height, with wind speeds high enough to carry the air over the feature. Periods in which determination of the Froude number indicate that flow blocking occurred showed no evidence of ozone depletion over Eureka, implying that flow blocking along the coast prevented boundary layer ozone depleted air from reaching Eureka.

In addition to preventing ozone depleted air from reaching inland, topographic blocking may be responsible for episodes of ozone enhancement over Eureka. Back trajectory calculations show that warm ozone rich air descending from the free troposphere was responsible for the higher concentrations of ozone recorded in May 2008. In these cases the air measured at Eureka traversed topographic features between $1 - 1.5$ km in height. The calculated Froude numbers indicate the likelihood of near total blocking of the air by these mountain ranges, resulting in the descent of higher altitude air masses on the lee side of the terrain.

Temperatures over Eureka measured every twelve hours by radiosonde show a strong correlation between ozone concentration and relative potential temperature. It was found

118

that low ozone concentrations were coincident with lower temperatures, and higher ozone concentrations with high potential temperature. This supports the interpretation that ozone depleted air spent long periods of time near the cold surface over the sea ice, while warm ozone rich air measured over Eureka had either recently descended from the free troposphere, likely due to mesoscale interactions with the topography, or originated from warmer climates to the south.

These results are consistent with previous studies that have found a correlation between Arctic ozone depletion events and the length of time an air mass is connected to the sea ice (Bottenheim et al. 2009, Frieß et al. 2004, Seabrook et al. 2011, 2013), and low temperatures (Ramacher et al. 1999, Seabrook et al. 2011, Strong et al. 2002).

6   Conclusions

Three variations of an ozone DIAL were built and tested at York University, and deployed for a number of field projects in order to measure vertical profiles of tropospheric ozone in the Arctic. The field campaigns included measurements from the research icebreaker Amundsen, from the Polar-5 aircraft, and at the Eureka weather station on Ellesmere Island. These DIAL measurements provided a rare look at the vertical structure of ozone in the lower troposphere and demonstrated that depletion events are connected to the sea ice surface through convective mixing.

During the Amundsen CFL/OASIS campaign, the differential absorption lidar provided a continuous record of the vertical distribution of ozone above the ship throughout March 2008. A number of full and partial ozone depletion events were observed during this period. No depletions were observed in isolated layers separated from the surface, and all were found to be in contact with the sea ice. The lack of detection of elevated layers of ozone depleted air does not support the speculation regarding free tropospheric Bromine chemistry as a significant ozone sink. It was expected that if significant chemi-

cal destruction of ozone was taking place above the boundary layer then some evidence of elevated depletions would have been found during the course of this nearly month long measurement campaign.

Backward trajectory analysis indicated that most of the ozone-depleted air had spent extended periods within 500 m of the sea ice. A strong positive correlation was also found between ozone mixing ratio and potential temperature. No ODEs were found to occur at any altitude when the potential temperature was higher than -25 °C. Periods of normal, or higher than normal ozone concentrations were recorded when sampling warm ($<$ -20 °C) air masses originating from the free troposphere that had no recent connection to the ground.

The airborne DIAL measurements recorded during two flights aboard the Polar 5 allowed for the measurement of tropospheric ozone over a large area of sea ice in a relatively short period of time. As with the Amundsen measurements, there was no evidence of isolated layers of ozone depleted air above the boundary layer. The measurements thus indicate that the primary mechanism for the ozone depletion occurred within the boundary layer where turbulent mixing would result in contact with the frozen ocean surface. Images from the MODIS instrument on the Terra satellite over the area upwind from the flight path show the presence of leads in the ice with open or recently frozen water, and these are a possible source of the bromine required for the photochemical depletion of ozone.

At Eureka, the only measurement campaign to include measurement of ozone over land, a number of full and partial ozone depletion events were observed during polar sunrise seasons. back trajectory analysis indicated that the air depleted in ozone required extended periods of time within the atmospheric boundary layer over the sea ice. As with the results from the Amundsen, a strong positive correlation was found between ozone mixing ratio and the potential temperature measured by radiosonde launches at Eureka. Early in the spring no ODEs were found to occur at any altitude when the potential temperature was higher than -25 °C. Later in the year as average temperatures in the Arctic increased a similar correlation was found, but the cutoff temperature was higher at -13 °C indicating that this correlation is not the result of temperature dependent chemistry, but rather an indication that the ozone depleted air had a recent history of interacting with the colder surface of the sea ice. Periods of normal, or higher than normal ozone concentrations were recorded when sampling warmer air masses originating from the free troposphere that had no recent connection to the ground.

The vertical extent of the measured depletions were found to be strongly influenced by the surrounding topography of Ellesmere Island. Ozone depleted air up to a height of 1.5 km above sea level was observed due to vertical mixing cased by interaction with the surrounding topography. Additionally, topographic blocking of ABL air from over the sea ice was observed to be responsible for the prevention of depletion events, as well as the cause of periods of ozone enhancement near the surface. Froude number calculations

during interaction between the measured and and the elevated topography of Ellesmere island indicate that the terrain has a significant effect on the structure and extent of ozone measured at Eureka. Topographic blocking during periods in which wind speed is low, or the air interacts with mountainous terrain leads to periods of time in which no depletions are recorded at Eureka, while depletion events occurred when measured air passed over terrain at most 1 km in height, with wind speeds high enough to carry the air over the feature.

The observed ODEs in all three measurement campaigns correspond to two factors, prolonged periods within 500 m of the sea ice, and decreased potential temperature of the depleted air mass. This supports the interpretation that the source for the measured ozone depletions was long-range transport of cold air masses that had extended periods of contact with sea ice by turbulent mixing within the atmospheric boundary layer. The observed ozone depletion events were primarily the result of transport of already depleted air masses, rather than local chemistry. These results are consistent with previous studies that have found a correlation between Arctic ozone depletion events and the length of time an air mass is connected to the sea ice (Bottenheim et al. 2009, Frieß et al. 2004), and low temperatures (Ramacher et al. 1999, Strong et al. 2002).

7 Appendices

7.1 Choice of DIAL on/off wavelengths

The key considerations when choosing wavelength pairs for a specific species of interest is in choosing a pair of wavelengths that maximizes the difference in absorption by the species of interest, while minimizing the wavelength separation such that the molecular and particulate scattering properties of the pair is not significantly different.

The Hartley band (Fig. 7.1) is a strong UV absorption band centred at 255 nm which corresponds to electronic transitions of ozone (Liou 2002). This absorption band consists of some weak structure overlaid on a strong absorption continuum. The on/off wavelengths for the DIAL were chosen to lie on this absorption band. A number of considerations must be taken into account when choosing the wavelength pairs used for ozone retrieval. Because the Harley ozone absorption band is stronger deeper into the UV, the use of shorter wavelengths increase sensitivity, but decrease the effective range as atmospheric scattering and strong ozone absorption increase the atmospheric extinction coefficient. The use of longer wavelengths increase range, but also solar background.
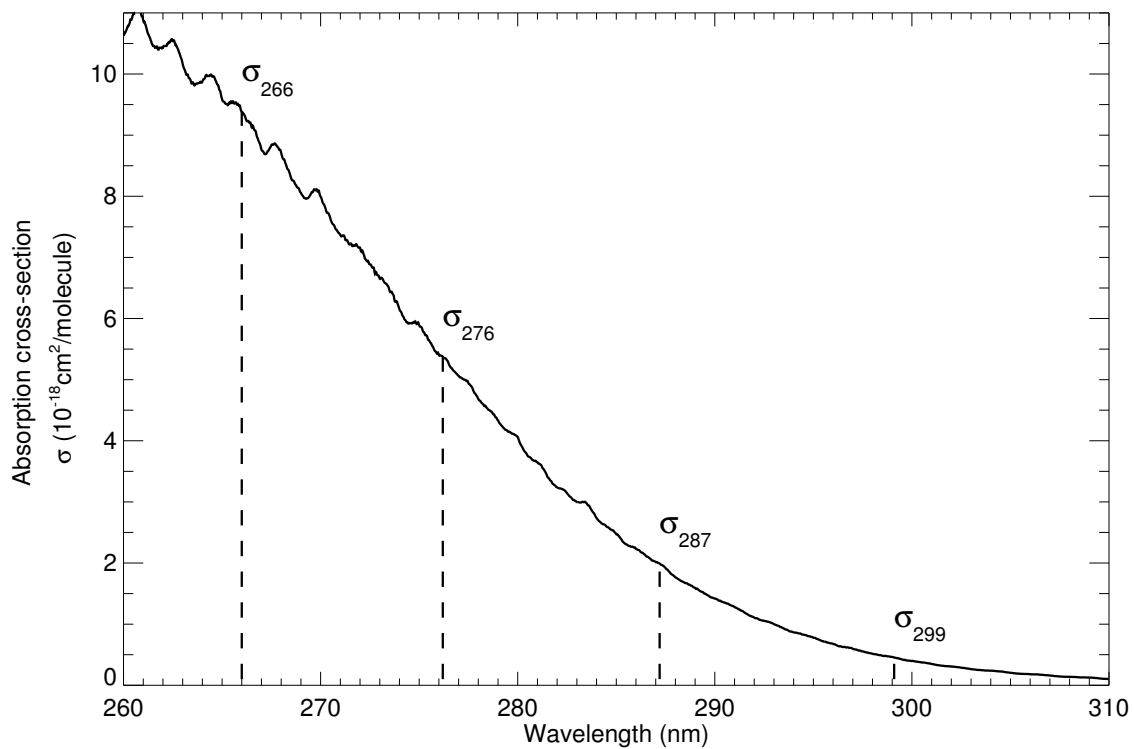
124

Figure 7.1: The Harley Band - Ozone absorption band in the UV

Wider spacing between the on/off wavelengths increases the sensitivity to ozone, but also aerosol interference as the differential scattering and extinction of aerosols becomes a significant factor that can not be ignored.

From Chapter 2, it was shown that the number density of the species of interest from a pair of DIAL wavelengths can be represented by

$$n(r) = n'(r) + \Delta n_b(r) + \Delta n_e(r) \tag{7.1a}$$

$$n'(r) = \frac{-1}{2\Delta\sigma} \left\{ \frac{\mathrm{d}}{\mathrm{d}r} \left[\ln \frac{P_{\mathrm{on}}(r)}{P_{\mathrm{off}}(r)} \right] \right\} \tag{7.1b}$$

$$\Delta n_b(r) = \frac{1}{2\Delta\sigma} \left\{ \frac{\mathrm{d}}{\mathrm{d}r} \left[\ln \frac{\beta_{\pi,\mathrm{on}}(r)}{\beta_{\pi,\mathrm{off}}(r)} \right] \right\} \tag{7.1c}$$

$$\Delta n_e(r) = \frac{-1}{\Delta\sigma} \Delta\alpha \tag{7.1d}$$

For the purpose of estimating the effect the choice of DIAL wavelength pairs has on the differential scattering correction terms (equations 7.1c and 7.1d) it can be assumed that the wavelength dependence of molecular and aerosol optical scattering has a power law dependence with a constant Angstrom coefficient of 4 in the case of molecular scatter, and an undetermined Angstrom coefficient, u in the case of aerosols.

$$\alpha_p = \frac{\text{constant}}{\lambda^u} \tag{7.2}$$

In most practical cases, the wavelength difference $\Delta\lambda$ between the "on" and "off" DIAL pairs is deliberately chosen to be small. In this case an approximate scattering

126

relationship between the "on" and "off" wavelengths can then be written as

$$\alpha_{p,\text{on}}(r) = \alpha_{p,\text{off}}(r) \left[1 + u\frac{\Delta\lambda}{\lambda_{\text{off}}}\right] \tag{7.3}$$

Using this relationship the differential extinction correction factor from equation 2.3d can be reformulated as

$$\Delta n_e(r) = \frac{1}{\Delta\sigma}\left[\alpha_{\text{on}}(r) - \alpha_{\text{off}}(r)\right] \approx -B_\lambda\left[u\alpha_{\text{p,off}}(r) + 4\alpha_{\text{m,off}}(r)\right] \tag{7.4}$$

where B_λ is known as the spectrum factor where

$$B_\lambda = \frac{1}{\lambda_{\text{off}}\left[\dfrac{\Delta\sigma}{\Delta\lambda}\right]} \tag{7.5}$$

and is directly proportional to the ozone retrieval error caused by the atmospheric differential extinction between the "on" and "off" wavelengths $\Delta n_e(r)$. From this it can be seen that error in the ozone retrieval from the DIAL method can be greatly reduced by selecting an on/off wavelength pair that minimizes the wavelength difference $\Delta\lambda$ while maximizing the differential absorption coefficient $\Delta\sigma$ of the species of interest. It can be seen in Figure 7.2, where a lower spectrum factor indicates less relative error due to aerosol and molecular scattering, that for the purpose of reducing sensitivity to atmospheric differential scatting, the choice of closely spaced wavelengths such as 287 nm and 299 nm does not provide a benefit with regards to sensitivity over further spaced apart wavelength pairs that have a much larger differential ozone absorption coefficient.
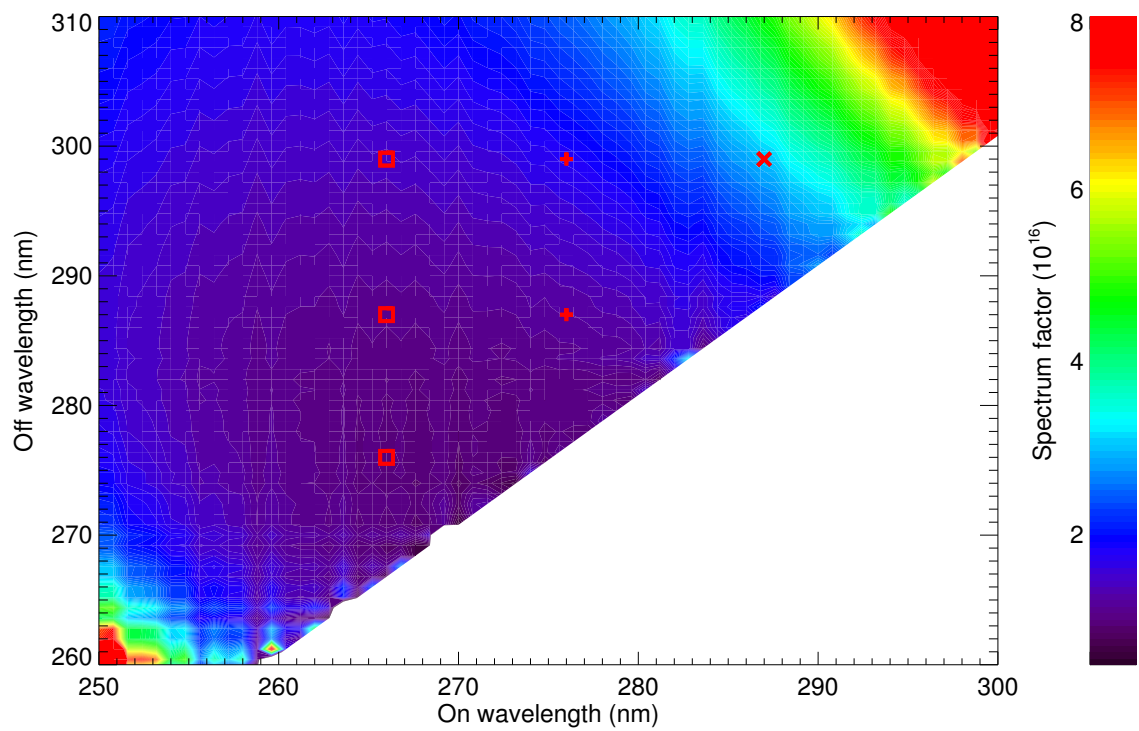
Figure 7.2: The spectrum factor B_λ as a function of the "on" and "off" DIAL wavelengths. A larger spectrum factor leads to a higher ozone retrieval error due to differential scattering. The red symbols indicate the six on/off wavelength pairs that are used with the York ozone DIAL.

7.2 Measurement Uncertainty

The detection of light via photon counting is a statistical process governed by Poisson statistics The statistical nature of Photon counting is described by the Poisson distribution in which the standard deviation is equal to the square root of the mean value. The statistical error can be written as follows (Megie et al. 1985).

Assuming a Poisson distribution governing the photon counting random noise, the signal to noise ratio (SNR) can be represented as

$$\text{SNR}_\lambda(r) = \frac{P_\lambda(r)}{\sqrt{(P_\lambda(r) + P_b + P_d)}} \tag{7.6}$$

where $P_\lambda(r)$ is the lidar signal (photon counts) from backscattered light at range r, P_b is the number of counts from background light and P_d is the number of counts resulting from dark current. With the appropriate discriminator settings, the dark current can be neglected, as can the background levels in most situations, this simplifies equation 7.6 to

$$\text{SNR}_\lambda(r) = \sqrt{P_\lambda(r)} \tag{7.7}$$

Propagation of the statistical error through the DIAL equation yields,

$$\Delta n(r) = \frac{1}{\Delta r \Delta \sigma \sqrt{N}} \sqrt{\sum_{r,\lambda} \frac{1}{(\text{SNR}_\lambda(r))^2}} \tag{7.8}$$

where Δr is the range resolution of the measurement and $\Delta \sigma$ is the differential absorption cross section for the wavelength pair being used and N is the number of averaged

129

shots. It is apparent that the primary means of reducing the statistical ozone retrieval error is increasing the integration time of the measurement to reduce the signal to noise ratio, averaging over a larger number of bins and reducing the range resolution, and choosing a wavelength pair that maximizes the differential absorption coefficient.

7.3 Interference from other atmospheric gasses

An important consideration, especially in urban environments, is absorption of the DIAL wavelengths by atmospheric pollutants. Ozone retrieval is dependent on the differential absorption of ozone between the "on" and "off" DIAL wavelengths. The choice of wavelength pairs used in the ozone retrieval has a significant impact on how much the presence of these UV absorbers will affect the accuracy of the ozone retrieval.

A comparison of the UV absorption cross sections of O_3, SO_2, NO_2 and H_2CO is shown in Figure 7.3. Also shown are the positions of the four UV wavelengths (266, 276.2, 287.2 and 299.1 nm) used for ozone retrieval by the CO_2 DIAL.

Table 7.1 outlines the effect of SO_2, NO_2 and H_2CO interference on ozone retrieval. The interference factor indicates how strongly the presence of these pollutants will affect the measured ozone. For example, the 287/299 nm pair has an interference factor of $\sim 38\%$, thus, the presence of 10 ppbv of SO_2 will result in an overestimation of the ozone retrieval in the affected regions by 3.8 ppbv. The 287 and 299 nm wavelengths lie on the tail end of the Hartley ozone absorption band, and consequently have the lowest
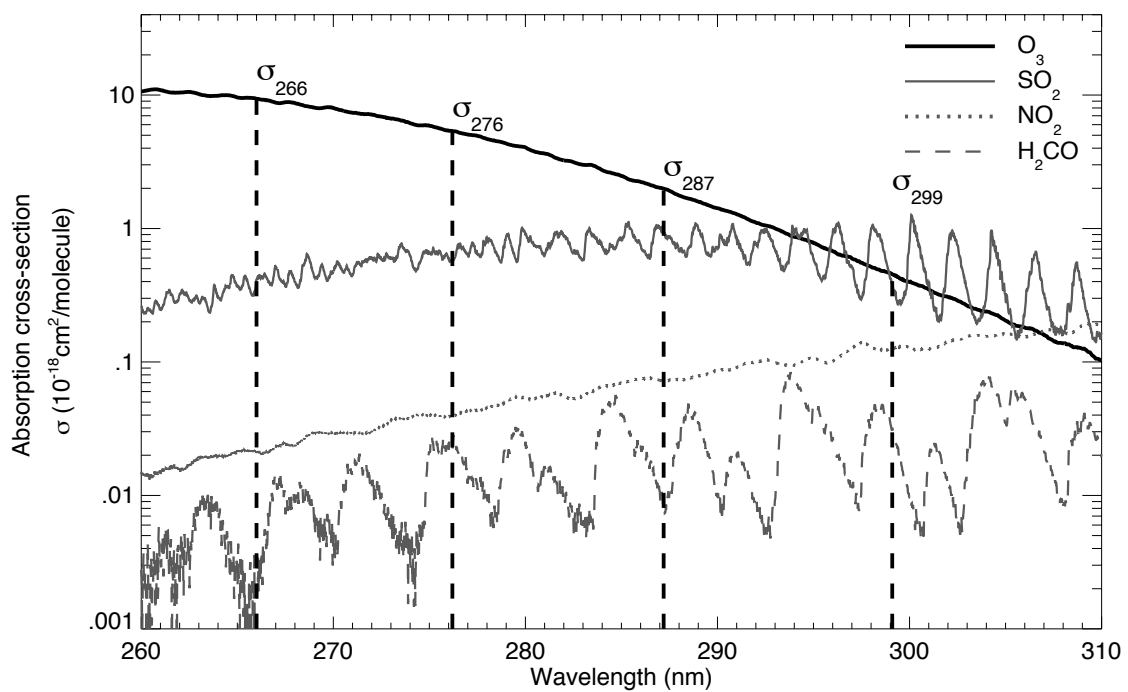
Figure 7.3: Ozone[1], SO$_2$[1] NO$_2$[1] and H$_2$CO[2] absorption cross sections in the UV near 300 K from the [1]HITRAN 2008 database (Rothman et al. 2009) and [2](Keller-Rudek et al. 2013, Rogers 1990).

On/Off pair	Differential cross section ($\Delta\sigma$)				Interference factor (%)		
	O_3	SO_2	NO_2	H_2CO	SO_2	NO_2	H_2CO
266/276 nm	4.008	-0.163	-0.018	-0.022	-4.1	-0.4	-0.5
266/287 nm	7.390	-0.557	-0.052	-0.008	-7.5	-0.7	-0.1
266/299 nm	8.929	0.025	-0.105	-0.030	0.3	-1.2	-0.3
276/287 nm	3.382	-0.394	-0.033	0.014	-11.6	-1.0	0.4
276/299 nm	4.921	0.188	-0.087	-0.008	3.9	-1.8	-0.2
287/299 nm	1.539	0.582	-0.053	-0.022	37.8	-3.5	-1.4

Table 7.1: Differential absorption cross-sections ($\Delta\sigma$) in terms of (10^{-18}cm^2/molecule) and calculated interference factor for ozone, sulfur dioxide, nitrogen dioxide and formaldehyde for the on/off DIAL wavelength pairs.

differential absorption cross-section, and least sensitivity to ozone out of all the possible DIAL wavelength pairs. This wavelength pair is the most sensitive to interference from other UV absorbing species with interference factors of 37.8 for SO_2, -3.5 for NO_2, and -1.4 for H_2CO.

Winter Arctic troposphere measurements made in 1987 in Northern Scandinavia (Möhler and Arnold (1992)) found tropospheric concentrations of SO_2 ranging between $50 - 400$ pptv, and measurements in the North American Arctic in 1985 (Thornton et al. (1989)) found that with the exception of an exceptionally hazy layer in Alaska, where SO_2 concentrations exceeded 10 ppbv, concentrations were typically between 74–134 pptv. An airborne study in 1979 investigating the vertical distribution of SO_2 in the atmosphere [Meixner (1984)] shows that levels of SO_2 generally decrease with increasing altitude in the troposphere (Figure 7.4) thus interference from this pollutant becomes less problematic at higher altitudes.

Ground based (de Serves 1994) and column measurements (Viatte et al. 2014) of H_2CO show a variability of 30–700 pptv in the Arctic troposphere while NO_2 tropospheric concentrations have been measured at concentrations between 20-40 pptv in the Arctic (Carroll et al. 1990, Merlaud et al. 2011). At these concentrations, the effect on ozone retrieval is negligible, in the worst case, the interference factor is -1.4 % and -3.5 % respectively for the $287/299$ nm wavelength pair leading to uncertainties in ozone concentration in the low ppt range.

In polluted urban environments these UV absorbers may need to be accounted for in order to extract accurate ozone concentrations from the DIAL measurements. But with Arctic tropospheric concentrations of these pollutants in the ppt range, the interference from these gasses for these Arctic DIAL measurements is negligible.
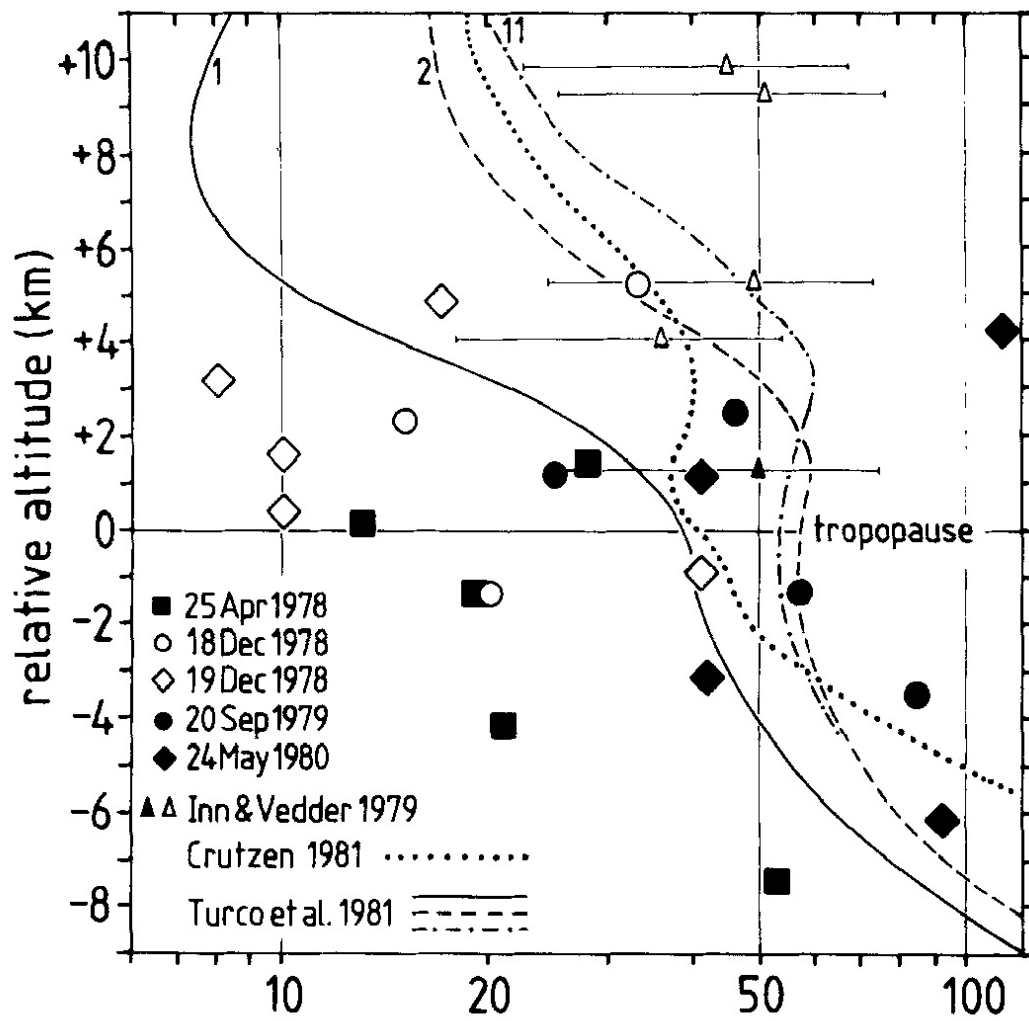
Figure 7.4: Vertical distribution of measured and calculated SO_2 mixing ratios (pptv) relative to the height of the tropopause (Meixner (1984)).

Bibliography

Anlauf, K., R. Mickle, and N. Trivett, 1994: Measurement of ozone during polar sunrise experiment 1992. *Journal of Geophysical Research*, **99**(D12), 25345–25.

Barber, D. G., M. G. Asplin, Y. Gratton, J. V. Lukovich, R. J. Galley, R. L. Raddatz, and D. Leitch, 2010: The International polar year (IPY) circumpolar flaw lead (CFL) system study: Overview and the physical system. *Atmosphere-Ocean*, **48**(4), 225–243.

Barrie, L., G. Hartog, J. Bottenheim, and S. Landsberger, 1989: Anthropogenic aerosols and gases in the lower troposphere at Alert Canada in April 1986. *Journal of Atmospheric Chemistry*, **9**(1), 101–127.

Bottenheim, J., J. Fuentes, D. Tarasick, and K. Anlauf, 2002: Ozone in the Arctic lower troposphere during winter and spring 2000 (ALERT2000). *Atmospheric Environment*, **36**(15-16), 2535–2544.

Bottenheim, J., A. Gallant, and K. Brice, 1986: Measurements of NO_y species and O_3 at $82°N$ latitude. *Geophysical Research Letters*, **13**(2), 113–116.

Bottenheim, W., S. Netcheva, S. Morin, and S. Nghiem, 2009: Ozone in the boundary layer air over the Arctic Ocean: measurements during the TARA transpolar drift 2006–2008. *Atmospheric Chemistry and Physics*, **9**(14), 4545–4557.

Carroll, M. A., D. D. Montzka, G. Hübler, K. K. Kelly, and G. L. Gregory, 1990: In situ measurements of NOx in the Airborne Arctic Stratospheric Expedition. *Geophysical Research Letters*, **17**(4), 493–496.

de Serves, C., 1994: Gas phase formaldehyde and peroxide measurements in the Arctic atmosphere. *Journal of Geophysical Research: Atmospheres*, **99**(D12), 25391–25398.

Draxler, R. and G. Hess, 1998: An overview of the HYSPLIT 4 modelling system for trajectories, dispersion, and deposition. *Australian Meteorological Magazine*, **47**(4), 295–308.

Fix, A., M. Wirth, A. Meister, G. Ehret, M. Pesch, and D. Weidauer, 2002: Tunable ultraviolet optical parametric oscillator for differential absorption lidar measurements of tropospheric ozone. *Applied Physics B*, **75**(2-3), 153–163.

Frieß U., J. Hollwedel, G. König-Langlo, T. Wagner, and U. Platt, 2004: Dynamics and chemistry of tropospheric bromine explosion events in the Antarctic coastal region. *Journal of Geophysical Research*, **109**(D6).

Güldner, J. and D. Spänkuch, 2001: Remote sensing of the thermodynamic state of the atmospheric boundary layer by ground-based microwave radiometry. *Journal of Atmospheric and Oceanic Technology*, **18**(6), 925–933.

Haas, C., 2012: Personal communication.

Haas, C., S. Hendricks, H. Eicken, and A. Herber, 2010: Synoptic airborne thickness surveys reveal state of Arctic sea ice cover. *Geophysical Research Letters*, **37**(9).

Hausmann, M. and U. Platt, 1994: Spectroscopic measurement of bromine oxide and ozone in the high arctic during polar sunrise experiment 1992. *Journal of Geophysical Research*, **99**(D12), 25399–25413.

Herber, A. B., C. Haas, R. S. Stone, J. W. Bottenheim, P. Liu, S.-M. Li, R. M. Staebler, J. W. Strapp, and K. Dethloff, 2012: Regular airborne surveys of Arctic sea ice and atmosphere. *Eos, Transactions American Geophysical Union*, **93**(4), 41–42.

Jones, A., P. Anderson, E. Wolff, H. Roscoe, G. Marshall, A. Richter, N. Brough, and S. Colwell, 2010: Vertical structure of Antarctic tropospheric ozone depletion events: characteristics and broader implications. *Atmospheric Chemistry and Physics*, **10**, 7775–7794.

Jones, A. E., P. S. Anderson, M. Begoin, N. Brough, M. A. Hutterli, G. J. Marshall, A. Richter, H. K. Roscoe, and E. W. Wolff, 2009: BrO, blizzards, and drivers of polar tropospheric ozone depletion events. *Atmospheric Chemistry and Physics*, **9**(14), 4639–4652.

Kahl, J. D., 1996: On the prediction of trajectory model error. *Atmospheric Environment*, **30**(17), 2945 – 2957.

Kahl, J. D., J. M. Harris, G. A. Herbert, and M. P. Olson, 1989: Intercomparison of three long-range trajectory models applied to arctic haze. *Tellus B*, **41B**(5), 524–536.

Keller-Rudek, H., G. K. Moortgat, R. Sander, and R. Sörensen, 2013: The MPI-Mainz UV/VIS spectral atlas of gaseous molecules of atmospheric interest. *Earth System Science Data*, **5**(2), 365–373.

Koo, J.-H., Y. Wang, T. P. Kurosu, K. Chance, A. Rozanov, A. Richter, S. J. Oltmans, A. M. Thompson, J. W. Hair, M. A. Fenn, A. J. Weinheimer, T. B. Ryerson, S. Solberg, L. G. Huey, J. Liao, J. E. Dibb, J. A. Neuman, J. B. Nowak, R. B. Pierce, M. Natarajan, and J. Al-Saadi, 2012: Characteristics of tropospheric ozone depletion events in the Arctic spring: analysis of the ARCTAS, ARCPAC, and ARCIONS measurements and satellite BrO observations. *Atmospheric Chemistry and Physics Discussions*, **12**(7), 16219–16257.

Liljegren, J. C., B. M. Lesht, S. Kato, E. E. Clothiaux, F. Solheim, and R. Ware, 2001: Initial evaluation of profiles of temperature, water vapor, and cloud liquid water from a new microwave profiling radiometer, paper presented at 11th symposium on meteorological observations and instrumentation. Am. Meteorol. Soc., Albuquerque, N.M.

McConnell, J. C., G. S. Henderson, L. Barrie, J. Bottenheim, H. Niki, C. H. Langford, and E. M. J. Templeton, 1992: Photochemical bromine production implicated in Arctic boundary-layer ozone depletion. *Nature*, **355**(6356), 150–152.

McElroy, C. T., C. A. McLinden, and J. C. McConnell, 1999: Evidence for bromine monoxide in the free troposphere during the Arctic polar sunrise. *Nature*, **397**(6717), 338–341.

Megie, G., J. Y. Allain, M. L. Chanin, and J. E. Blamont, 1977: Vertical profile of stratospheric ozone by lidar sounding from the ground. *Nature*, **270**(5635), 329–331.

Megie, G. J., G. Ancellet, and J. Pelon, 1985: Lidar measurements of ozone vertical profiles. *Appl. Opt.*, **24**(21), 3454–3463.

Meixner, F. X., 1984: The vertical sulfur dioxide distribution at the tropopause level. *Journal of Atmospheric Chemistry*, **2**(2), 175–189.

Merlaud, A., M. Van Roozendael, N. Theys, C. Fayt, C. Hermans, B. Quennehen, A. Schwarzenboeck, G. Ancellet, M. Pommier, J. Pelon, J. Burkhart, A. Stohl, and M. De Mazière, 2011: Airborne DOAS measurements in Arctic: vertical distributions of aerosol extinction coefficient and NO_2 concentration. *Atmospheric Chemistry and Physics*, **11**(17), 9219–9236.

Möhler, O. and F. Arnold, 1992: Gaseous sulfuric acid and sulfur dioxide measurements in the Arctic troposphere and lower stratosphere: Implications for hydroxyl radical abundances. *Berichte der Bunsengesellschaft für physikalische Chemie*, **96**(3), 280–283.

Nakazato, M., T. Nagai, T. Sakai, and Y. Hirose, 2007: Tropospheric ozone differential-absorption lidar using stimulated raman scattering in carbon dioxide. *Applied Optics*, **46**(12), 2269–2279.

Nehrir, A. R., K. S. Repasky, J. L. Carlsten, M. D. Obland, and J. A. Shaw, 2009: Water vapor profiling using a widely tunable, amplified diode-laser-based differential absorption lidar (DIAL). *Journal of Atmospheric and Oceanic Technology*, **26**(4), 733–745.

Nghiem, S. V., I. G. Rigor, A. Richter, J. P. Burrows, P. B. Shepson, J. Bottenheim, D. G. Barber, A. Steffen, J. Latonas, F. Wang, G. Stern, P. Clemente-Colón, S. Martin, D. K. Hall, L. Kaleschke, P. Tackett, G. Neumann, and M. G. Asplin, 2012: Field and satellite observations of the formation and distribution of Arctic atmospheric bromine above a rejuvenated sea ice cover. *Journal of Geophysical Research: Atmospheres*, **117**(D17).

Oltmans, S., 1981: Surface ozone measurements in clean air. *Journal of Geophysical Research*, **86**(C2), 1174–1180.

Oltmans, S. and W. Komhyr, 1986: Surface ozone distributions and variations from 1973–1984 measurements at the noaa geophysical monitoring for climatic change baseline observatories. *Journal of Geophysical Research*, **91**(D4), 5229–5236.

Oltmans, S. J., B. J. Johnson, and J. M. Harris, 2012: Springtime boundary layer ozone depletion at Barrow, Alaska: Meteorological influence, year-to-year variation, and long-term change. *Journal of Geophysical Research: Atmospheres*, **117**(D14), n/a–n/a.

Piot, M. and R. von Glasow, 2008: The potential importance of frost flowers, recycling on snow, and open leads for ozone depletion events. *Atmospheric Chemistry and Physics*, **8**(9), 2437–2467.

Pöhler, D., L. Vogel, U. Frieß, and U. Platt, 2010: Observation of halogen species in the Amundsen Gulf, Arctic, by active long-path differential optical absorption spectroscopy. *Proceedings of the National Academy of Sciences*, **107**(15), 6582–6587.

Pratt, K. A., K. D. Custard, P. B. Shepson, T. A. Douglas, D. Pohler, S. General, J. Zielcke, W. R. Simpson, U. Platt, D. J. Tanner, L. Gregory Huey, M. Carlsen, and B. H. Stirm, 2013: Photochemical production of molecular bromine in Arctic surface snowpacks. *Nature Geosci*, **6**(5), 351–356.

Ramacher, B., J. Rudolph, and R. Koppmann, 1999: Hydrocarbon measurements during tropospheric ozone depletion events: Evidence for halogen atom chemistry. *Journal of Geophysical Research*, **104**(D3), 3633–3653.

Reinecke, P. A. and D. R. Durran, 2008: Estimating topographic blocking using a Froude number when the static stability is nonuniform. *Journal of the Atmospheric Sciences*, **65**(3), 1035–1048.

Ridley, B. A., E. L. Atlas, D. D. Montzka, and E. V. Browell, 2003: Ozone depletion events observed in the high latitude surface layer during the TOPSE aircraft program. *Journal of Geophysical Research*, **108**(D4).

Rogers, J. D., 1990: Ultraviolet absorption cross sections and atmospheric photodissociation rate constants of formaldehyde. *The Journal of Physical Chemistry*, **94**(10), 4011–4015.

Rothman, L., I. Gordon, and A. Barbe, 2009: The HITRAN 2008 molecular spectroscopic database. *Journal of Quantitative Spectroscopy and Radiative Transfer*, **110**, 533–572.

Schotland, R., 1966: Some observations of the vertical profile of water vapor by a laser optical radar. In *Proceedings of the 4th Symposium on Remote Sensing of the Environment*, University of Michigan, 273-283.

Seabrook, J. A., J. Whiteway, R. M. Staebler, J. W. Bottenheim, L. Komguem, L. H. Gray, D. Barber, and M. Asplin, 2011: Lidar measurements of Arctic boundary layer ozone depletion events over the frozen Arctic Ocean. *Journal of Geophysical Research*, **116**.

Seabrook, J. A., J. A. Whiteway, L. H. Gray, R. Staebler, and A. Herber, 2013: Airborne lidar measurements of surface ozone depletion over Arctic sea ice. *Atmospheric Chemistry and Physics*, **13**(12), 6023–6029.

Shepson, P., P. Matrai, L. Barrie, and J. Bottenheim, 2003: Ocean-atmosphere-sea ice-snowpack interactions in the arctic, and global change. *Eos Transactions, American Geophysical Union*, **84**(36).

Shimanouchi, T., 1972: *Tables of Molecular Vibrational Frequencies*. Number v. 1 in NSRDS-NBS. National Bureau of Standards.

Smith, R. B., 1980: Linear theory of stratified hydrostatic flow past an isolated mountain. *Tellus*, **32**(4), 348–364.

Stohl, A., 1998: Computation, accuracy and applications of trajectories—a review and bibliography. *Atmospheric Environment*, **32**(6), 947 – 966.

Strong, C., J. Fuentes, R. Davis, and J. Bottenheim, 2002: Thermodynamic attributes of Arctic boundary layer ozone depletion. *Atmospheric Environment*, **36**(15-16), 2641–2652.

Stunder, B. J. B., 1996: An assessment of the quality of forecast trajectories. *Journal of Applied Meteorology*, **35**(8), 1319–1331.

Tarasick, D. and J. Bottenheim, 2002: Surface ozone depletion episodes in the Arctic and Antarctic from historical ozonesonde records. *Atmospheric Chemistry and Physics*, **2**(3), 197–205.

Thornton, D. C., A. R. Bandy, and A. R. Driedger, 1989: Sulfur dioxide in the North American Arctic. *Journal of Atmospheric Chemistry*, **9**, 331–346. 10.1007/BF00052841.

Viatte, C., K. Strong, K. A. Walker, and J. R. Drummond, 2014: Five years of CO, HCN, C_2H_6, C_2H_2, CH_3OH, HCOOH and H_2CO total columns measured in the Canadian high Arctic. *Atmospheric Measurement Techniques*, **7**(6), 1547–1570.

Wang, C.-C. and G. T.-J. Chen, 2003: On the formation of leeside mesolows under different Froude number flow regime in TAMEX. *Journal of the Meteorological Society of Japan. Ser. II*, **81**(2), 339–365.

Yang, X., J. A. Pyle, and R. A. Cox, 2008: Sea salt aerosol production and bromine release: Role of snow on sea ice. *Geophysical Research Letters*, **35**(16).

Yang, X., J. A. Pyle, R. A. Cox, N. Theys, and M. Van Roozendael, 2010: Snow-sourced bromine and its implications for polar tropospheric ozone. *Atmospheric Chemistry and Physics*, **10**(16), 7763–7773.

Zeng, T., Y. Wang, K. Chance, E. V. Browell, B. A. Ridley, and E. L. Atlas, 2003: Widespread persistent near-surface ozone depletion at northern high latitudes in spring. *Geophysical Research Letters*, **30**(24), 2298.